Design and Synthesis of

Organic Molecular Models of Artificial Photosynthetic Reaction Center

by

Jaro Arero

A Dissertation Presented in Partial Fulfillment
of the Requirements for the Degree
Doctor of Philosophy

Approved April 2014 by the
Graduate Supervisory Committee:

Devens Gust, Chair
Ana Moore
Ian Gould

ARIZONA STATE UNIVERSITY

May 2014

ABSTRACT

A clean and sustainable alternative to fossil fuels is solar energy. For efficient use of solar energy to be realized, artificial systems that can effectively capture and convert sunlight into a usable form of energy have to be developed. In natural photosynthesis, antenna chlorophylls and carotenoids capture sunlight and transfer the resulting excitation energy to the photosynthetic reaction center (PRC). Small reorganization energy, λ and well-balanced electronic coupling between donors and acceptors in the PRC favor formation of a highly efficient charge-separated (CS) state.

By covalently linking electron/energy donors to acceptors, organic molecular dyads and triads that mimic natural photosynthesis were synthesized and studied. Peripherally linked free base phthalocyanine (Pc)-fullerene (C_{60}) and a zinc (Zn) phthalocyanine-C_{60} dyads were synthesized. Photoexcitation of the Pc moiety resulted in singlet-singlet energy transfer to the attached C_{60}, followed by electron transfer. The lifetime of the CS state was 94 ps. Linking C_{60} axially to silicon (Si) Pc, a lifetime of the CS state of 4.5 ns was realized. The exceptionally long-lived CS state of the SiPc-C_{60} dyad qualifies it for applications in solar energy conversion devices. A secondary electron donor was linked to the dyad to obtain a carotenoid (Car)-SiPc-C_{60} triad and ferrocene (Fc)-SiPc-C_{60} triad. Excitation of the SiPc moiety resulted in fast electron transfer from the Car or Fc secondary electron donors to the C_{60}. The lifetime of the CS state was 17 ps and 1.2 ps in Car-SiPc-C_{60} and Fc-SiPc-C_{60}, respectively.

In Chapter 3, an efficient synthetic route that yielded regioselective oxidative porphyrin dimerization is presented. Using Cu^{2+} as the oxidant, *meso*-β doubly-connected fused porphyrin dimers were obtained in very high yields. Removal of the copper from the macrocycle affords a free base porphyrin dimer. This allows for exchange of metals and provides a route to a wider range of metallporphyrin dimers.

In Chapter 4, the development of an efficient and an expedient route to bacteriopurpurin synthesis is discussed. *Meso*-10,20- diformylation of porphyrin was achieved and one-pot porphyrin diacrylate synthesis and cyclization to afford bacteriopurpurin was realized. The bacteriopurpurin had a reduction potential of – 0.85 V vs SCE and λ_{max}, 845 nm.

DEDICATION

This dissertation is dedicated to my loving mum who despite all the challenges faced by an uneducated single mother in rural Northern Kenya ensured that I stayed in school and got a decent education.

ACKNOWLEDGMENTS

My research work and education would not have been possible without the support of a number of people. My first thanks goes to my advisor Prof. Devens Gust and collaborators Profs. Ana and Tom Moore. They kindly accepted me into their research group without reservation and guided me through the years of my graduate education and research. Also my research work would not have been possible if not for the talented and helpful members of Gust Moore^2 research group. In particular I would like to thank: Dr. Paul Liddell for providing me with porphyrin starting material for the bacteriopurpurin project and much invaluable advice and suggestions on synthetic procedures, Dr. Smitha Pillai for her advice on phthalocyanine synthesis and for providing me with the Wittig reagents for the carotene-phthalocyanine-fullerene triad project, Dr. Gerdenis Kodis and Robert Schmitz for their photophysical expertise, Dalvin Mendez, Dr. Ben Sherman and Dr. Maxime Fournier for their electrochemical work,. Dr. Mathieu Koepf, Dr. Yuichi Terrazono and Dr. Graeme Copley for many useful suggestions on synthesis and advice during my candidacy oral exam, Katie WongCarter for proof reading and editing my dissertation and many great suggestions. Many thanks to DOE and DARPA for funding.

Beyond my research, I would like to thank my family and friends, particularly my wife, Cholle and children, Liban and Mooti for all the encouragement and patience with my many years of absence from home. They are my source of inspiration

TABLE OF CONTENTS

CHAPTER Page

LIST OF SCHEMES

Scheme Page

Scheme Page

LIST OF TABLES

LIST OF FIGURES

Figure Page

LIST OF SYMBOLS AND ABBREVIATIONS

BAHA	Tris(4-bromophenyl)aminium hexachloroantimonate
BBr_3	Boron tribromide
$BF_3 \bullet OEt_2$	Boron trifluoride diethyl etherate
BINAP	2,2'-bis(diphenylphosphino)-1,1'-binaphthyl
C_{60}	Fullerene
Car	Carotene
$CDCl_3$	Deuterated chloroform
CH_2Cl_2	Dichloromethane
$CHCl_3$	Chloroform
CS	charge-separated
CS_2	Carbon disulfide
CR	charge recombination
$Cu(BF_4)_2$	Copper(II) tetrafluoroborate
Cu(II)	Copper (II)
CuI	Copper iodide
CV	Cyclic Voltammetry
d_8-THF	Deuterated tetradrofuran
DBU	1,8-Diazabicyclo[5.4.0]undec-7-ene
DDQ	2,3-Dichloro-5,6-dicyano-1,4-benzoquinone

List of Abbreviations

DMAE	2-(dimethylamino)ethanol
DMF	*N, N*-dimethylformamide
DMSO	Dimethylsulfoxide
DSCC	Dye Sensitized Solar Cells
Et_3N	Triethylamine
EtOAc	Ethyl acetate
Fc	Ferrrocene
fs	femtosecond
H_2Pc	Metal-free phthalocyanine
H_2SO_4	Sulfuric acid
HBr	Hydrobromic acid
HCl	Hydrochloric acid
HOMO	Highest Occupied Molecular Orbital
IBX	Iodoxybenzoic acid
$InCl_3$	Indium trichloride
K_3PO_4	Tripotassium phosphate
KOH	Potassium hydroxide
LUMO	Lowest Unoccupied Molecular Orbital
MALDI-TOF	Matrix Assisted Laser desorption Ionization- Time of flight
MeOH	Methanol

List of Abbreviations

mg	milligram
mL	milliliter
$NADPH^+$	Nicotinamide adenine dinucleotide phosphate
NaOMe	Sodium methoxide
NBS	*N*-Bromosuccinimide
NIR	Near infrared
nm	nanometer
NMR	Nuclear Magnetic Resonance
o-DCB	*o*-Dichlorobenzene
Pc	Phthalocyanine
$Pd(PPh_3)_2Cl$	Bis(triphenylphosphine)palladium(II) dichloride
$POCl_3$	Phosphorous oxychloride
ppm	parts per million
PRC	Photosynthetic Reaction Center
PS II	Photosystem II
Pt	Platinum
Q	Quinone
rpm	revolutions per minute
Ru	Ruthenium
SCE	Saturated calomel electrode

List of Abbreviations

SiO_2	Silica
$TBAPF_6$	Tetrabutylammonium hexafluorophosphate
TBPPM	Trans-2-[3-(4-tert-butylphenyl)-2-methyl-2-propenylidene]-malonitrile.
TFA	Trifluoroacetic acid
TiO_2	Titanium dioxide
TLC	Thin Layer Chromatography
TW	Terrawatt
UV	Ultraviolet
ΔG	Change in free energy
λ	Reorganization energy

1.1 INTRODUCTION

One of the biggest challenges facing mankind in this century is access to affordable and clean energy. With a very high population growth expected to reach 9.6 billion by 2050[1] and rapid industrialization being experienced in most parts of the world, the demand for energy will be astronomical and finding a reliable source of energy will be a matter of urgency. In the year 2012, the rate of global energy consumption was 16.3 TW.[2] Going by the current rate of energy consumption, the global annual energy demand will be at least 20 TW by 2030, doubled by mid-century, and tripled by the turn of the century.[3-5]

Currently 85% of the total global energy consumed comes from burning fossil fuels; for developing countries 90% of their energy comes from fossil fuels.[6] Over-reliance on fossil fuels presents energy security, national security, environmental security, and economic security issues which need to be addressed within the next 10-20 years.[5] At the current rate of fossil fuel consumption, the atmospheric CO_2 concentrations within the 21st century will be more than double the pre-anthropogenic values.[3,7] Against this backdrop of challenges associated with this energy source, there is an urgent need for energy rapid diversification away from fossil fuels and switching to carbon neutral energy sources.

Nuclear fission is a carbon-neutral alternative. It is estimated that existing terrestrial uranium (U) resources are capable of producing □100 TW of electricity using the conventional once-through U reactor technology. [5] At the present global energy consumption rate of 16.3 TW/year, these terrestrial U resources will be exhausted in six years. Besides, use of nuclear energy has associated safety concerns after accidents such as Fukushima in 2011 and Chernobyl

in 1986; in addition nuclear energy presents an additional challenge of waste disposal of used nuclear fuels.

A promising alternative to the fossil fuels that can meet a rapidly increasing global demand for energy is the nearly infinite and inexhaustible solar energy. The energy from the sun that reaches our planet is 100,000 TW/yr. This means that the energy from one hour of sunlight is equivalent to all the energy currently used by mankind in a year.[6] Photovoltaic technologies have been utilized to capture sunlight and produce electricity, and their efficiency and robustness are rapidly improving.[8,9] However, in terms of price, the photovoltaic system currently in use is more costly than fossil based fuels.[10] One approach to realizing a long-term solution to addressing the energy challenge lies in the development of solar conversion systems that are modeled on the principles of the natural photosynthetic systems.

Natural Photosynthesis

Natural photosynthesis is a process where sunlight energy is converted into organic molecules of biomass such as carbohydrates.[6]

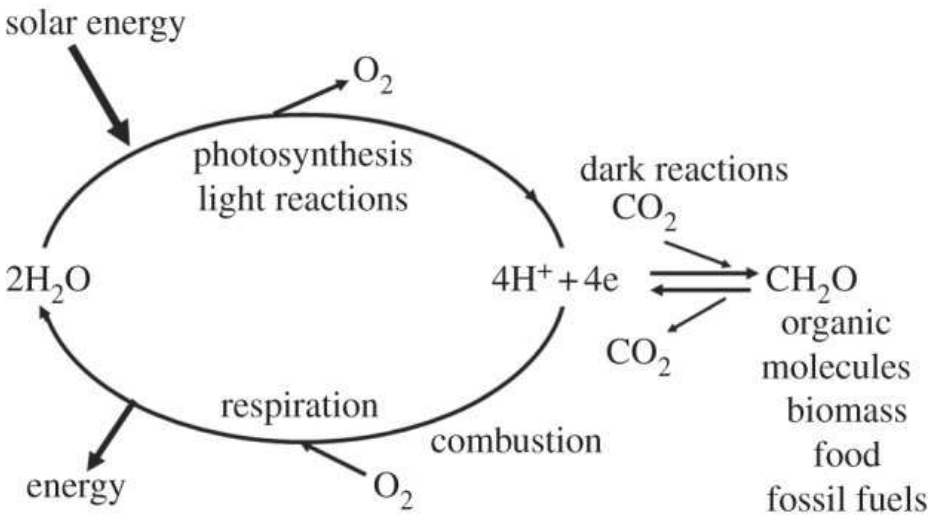

Figure 1: A diagrammatic representation of energy flow in nature.[6]

Figure 1 shows how solar energy is utilized in nature. At the light reactions part of photosynthesis, light absorption, charge separation, water splitting, and electron/proton transfer take place. The dark reaction uses these reducing equivalents from the light reactions in the form of energized electrons and a proton gradient to convert carbon dioxide into carbohydrates (CH_2O) and useful organic molecules which makes up biomass, including those that provide humanity with food. Fossil fuels that we burn to power our technology are a product of photosynthetic reactions that happened millions of years ago. Respiration and combustion of biomass are the reverse of photosynthesis, releasing CO_2, H_2O and energy. It can be concluded that photosynthesis is a way of storing solar energy in the form of chemical bonds.[6]

Natural photosynthesis utilizes two photosystems per electron to drive water splitting and carbon dioxide fixation. The energy of two 'red' photons is required for every electron/proton extracted from H_2O and used to reduce CO_2.[6] The two photosystems are: photosystem II (PSII)

where light is used to split water and release electrons and protons, and photosystem I (PSI), where light is used to provide additional reductive potential energy to the electrons from PSII so as to reduce carbon dioxide via NADPH.

Figure 2 is a schematic representation of how photosynthesis uses PSII and PSI to capture sunlight and convert it to chemical energy. PSII is a very powerful oxidant; in fact, $P680^+$ is the most oxidizing species in living systems and is capable of extracting electrons from water due to its potential at 1.2 V Vs SCE. [12] To produce one molecule of oxygen, PSII accumulates four oxidizing equivalents that are needed to abstract four reducing equivalents ($4e/4H^+$) from two water molecules (scheme 1).

$$2\ H_2O + 4h\lambda \rightarrow 4H^+ + 4e^- + O_2$$

Scheme 1: Overall water oxidation reaction by P680

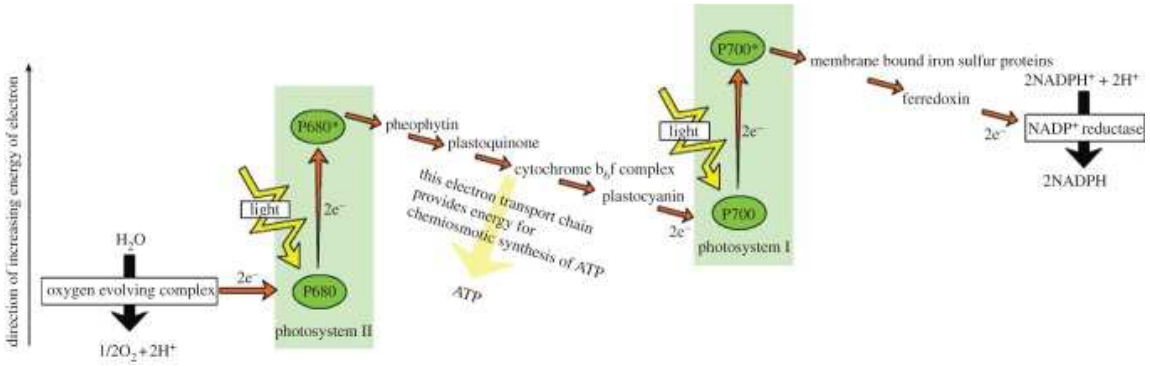

Figure 2: A simplified Z-scheme of the light reactions of photosynthesis.[11]

On the reducing side, PSII has pheophytin (Pheo) and quinone molecules as electron acceptors. The redox potential of $Pheo^{\bullet-}$ (-0.5 V[6]) is sufficiently negative and in turn it passes the reducing equivalent along an electron transfer chain to PSI (figure 2). In PSI, a second 'red' photon is absorbed by a chlorophyll molecule, P700, to attain a reducing potential of -1 V vs SCE or more.[6] The electron donated by the excited P700 (P700*) gets accepted by a 4Fe-4S center. The low-potential 4Fe-4S center reduces $NADP^+$ to NADPH through ferredoxin. The reduced 'hydrogen carrier' NADPH is the cofactor used by enzymes to drive fixation of CO_2. Natural photosynthesis can be used as a blueprint to design and develop highly efficient, artificial, molecular-based conversion of solar energy to chemical energy.

Artificial photosynthesis

Artificial photosynthesis refers to use of the underlying scientific principles of natural photosynthesis to harvest solar energy for electricity or fuel production. There are many

approaches that have been used to convert sunlight to another form of energy. For the purpose of this dissertation, we will restrict artificial photosynthesis to the use of molecular species to store energy from the sun in a charge separated state and eventually a useful fuel.[13]

Carotenoid (Car)-porphyrin (P)-fullerene (C_{60}) molecular triad (figure 3)[14] dissolved in 2-methyltetrahydrofuran yielded a long-lived charge separated state after excitation of the porphyrin followed by electron transfer and charge shift.[15]

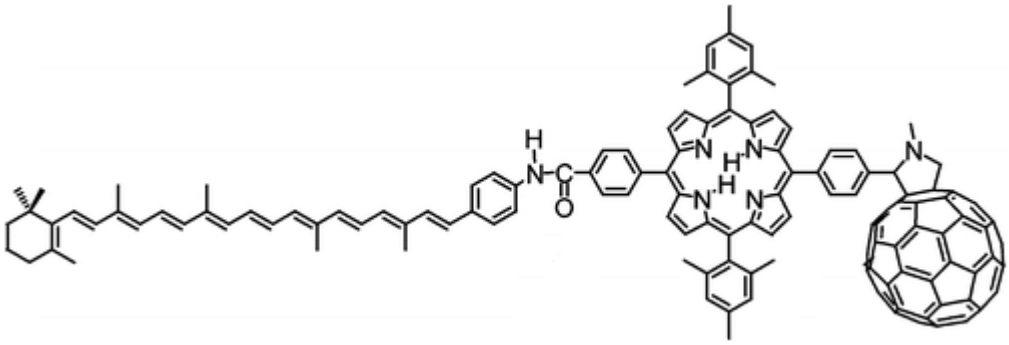

Figure 3: Structure of carotenoid-porphyrin-fullerene artificial reaction center.[14]

On excitation, the porphyrin moiety yields the first excited state Car-^{1}P-C_{60}, this decays by transferrring its electron to the fullerene with a lifetime τ of 32 ps and a quantum yield of 0.99 for Car-$P^{\bullet+}$-$C_{60}^{\bullet-}$. Here the molecule has converted the absorbed photon to electrochemical potential, but the back electron transfer to yield the ground state leading to energy wastage occurs with τ = 3.3 ns. This is a very short time making it difficult to accessing the redox potential. However, in the triad, a fast charge shift with rate constant of 125 ps competes favorably with charge recombination, yielding the long-lived charge separated state $Car^{\bullet+}$-P-$C_{60}^{\bullet-}$ with a lifetime of 57 ns and overall quantum yield of 0.95.[15] A lifetime of 170 ns at ambient temperature and 1 µs at 77 K has been observed for a similar Car-P-C_{60} triad.[16] In the

triad the electron transfer step is fast enough to compete with other alternative deexcitation pathways. The forward electron transfer is favored by sufficient thermodynamic driving force and a relatively strong electronic coupling between the initial and final states.[15] In the final state of the triad, $Car^{\bullet+}$-P-$C_{60}^{\bullet-}$, the charges are well separated and the coupling weak. This retards recombination even when the driving force is high. On the other hand, stepwise recombination is slow due to the endergonicity of the first step. Natural photosynthetic reaction centers also use a long-lived, energetic charge-separated state with a high quantum yield achieved by step-wise, short-range electron transfers.

Photosynthetic organisms use antennas to capture sunlight and transfer the resulting singlet excitation energy to reaction centres. Most natural systems use chlorophyll *a* (figure 4) to efficiently capture the photons from sunlight and funnel it to the special pair.

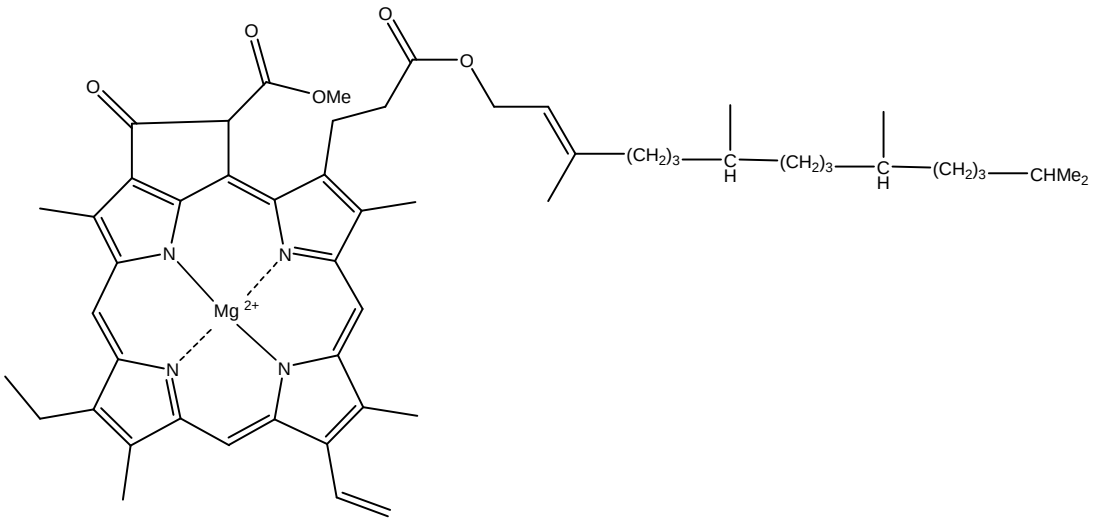

Figure 4: Molecular strucutre of chlorophyll *a*.[17]

The chlorin ring is the chromophore that absorbs light, and is responsible for the oxidation-reduction activity of chlorophyll *a* pigment. The side chain referred to as phytol tail of the molecule is used to properly orient the pigment molecule when it binds protein. About 99% of chlorophyll molecules in most photosynthetic membrane are involved in excitation energy-transfer reactions, serving the antennae role. Only 1% or less of the remaining chlorophyll molecules are involved in the redox-active catalytic site where electron transfer reactions are initiated.[18]

In artificial systems, porphyrins, analogues of chlorophyll, have been used as artificial antennae. Porphyrins are naturally occuring macrocylic heteroaromatic conjugated compounds and they are synthetically easy to prepare and also more photostable than chlorophylls. They exhibit very intense absorption in the visible region, with a Soret band at 400-500 nm and weak Q bands at 550-650 nm spectral regions.[19]

Chlorophyll *a* has very strong light absorption around 425 nm and 660 nm but exhibits weak absorption bands in the regions between these wavelengths. Natural photosynthetic systems use accessory antenna chromophores to harvest energy in regions where chlorophyll has poor light absorption. Carotenoid polyenes are examples of the some of the commonly used molecules.[15]

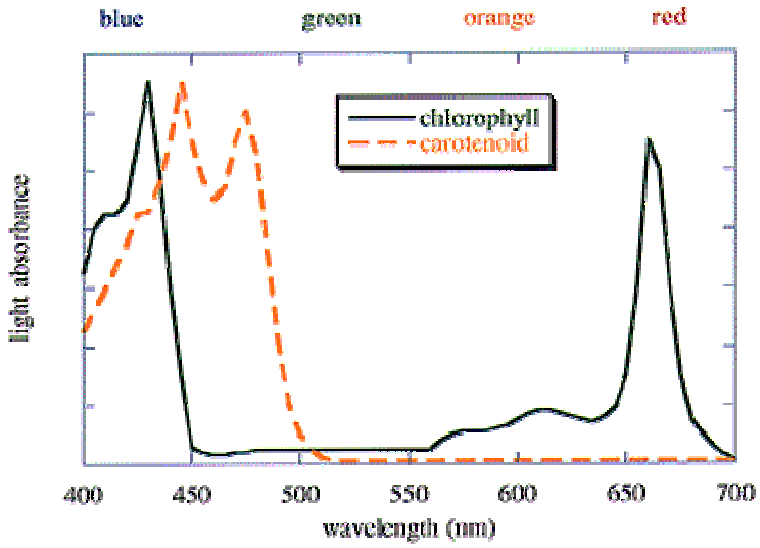

Figure 5: Absorption spectrum of Chlorophyll *a* and carotenoid species.[20]

As shown in figure 5, carotenoids absorb sunlight around 470 and 500 nm, the blue and the green part of the solar spectrum where chlorophyll doesn't absorb. Use of antennae can also benefit artificial photosynthetic systems. The primary electron donors in artificial reaction centers such as porphyrins and phthalocyanines do not absorb equally at all wavelengths and the overall efficiency of the solar radiation can be increased by incorporating antennas. Carotenoid antennas offer an additional benefit of photoprotection[21,22] to the artificial system just as it does in the natural systems.

An effective way of using artificial photosynthesis to generate sustainable energy is by efficient use of the renewable solar energy to produce H_2 and fuels; particularly those fuels obtained by conversion of carbon dioxide to safe and easily storable liquid fuels are the most useful.[23,24] A bio-inspired efficient and cost-effective artificial system such as solar fuel making

device should have the the key steps of natural photosynthesis; capture of sunlight, long-lived charge separated state and energy transduction into H_2 or another fuel.[25] Figure 6 shows the simplified general scheme of a solar fuel system.

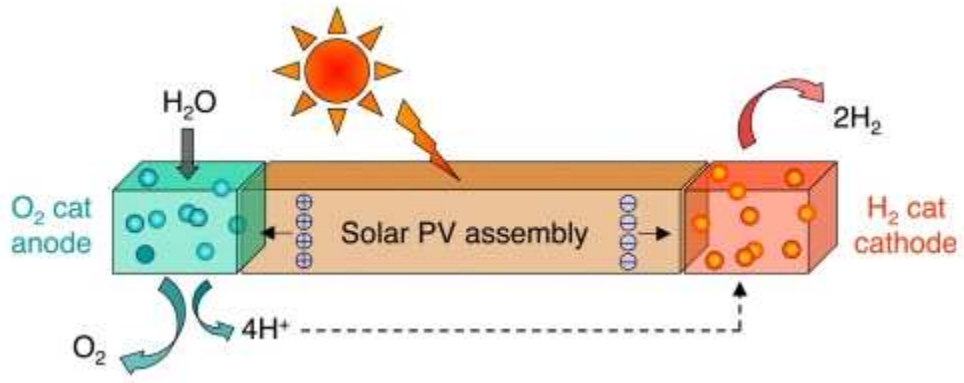

Figure 6: Simplified diagram of a general solar fuel system.[5]

The solar fuel assembly absorbs sunlight and a charge separated state is created. The resulting electrochemical potential is used by the photocatayst at the anode to oxidize water. The produced electrons and protons are transported to the cathodic side. At the cathode, proton and electron recombination to form H_2 takes place in presence of a reduction catalyst. An advanced system will have a cathode that can chemsorb CO_2 and in the presence of electrons and protons catalytically covert it to fuels or valuable chemicals.[26]

In a nutshell, an efficient artificial solar energy converting system must meet the following criteria: (i) light captured by antenna molecules and/or photosensitizers should result into excited state formation, (ii) the absorption of the sunlight must result in a fast transfer of electrons to the acceptor component, (iii) the transfer of electrons must be directional,[27] (iv) the charge separated state should be long-lived enough for charge-shift or electrochemical reaction

to occur, (v) photoprotection capability and/or repair mechanism should be included for long term usage.

1.2 Artificial Photosynthetic Reaction center models

When covalently linked, supramolecular systems such as donor-linker-acceptor (D-L-A) are often used as photosynthetic models. In these systems, D is the light absorbing molecular unit, L is a covalent linker, and A is the component of the supramolecule that accepts light or electrons from D in the light induced process. After the donor absorbs light (scheme 2.1), the singlet excited state of the donor (^{1}D) is formed, and this excited state can relax back to the ground state through different relaxation pathways. Among them is the transfer of energy to the acceptor (scheme 2.2) or transfer of the excited electron to the acceptor to form a charge separated state (scheme 2.3). A schematic representation of these relaxation pathways is shown in Scheme 2.

D-L-A + hν→ ^{1}D-L-A	photoexcitation	(2.1)
^{1}D-L-A → D-L-^{1}A	electronic energy transfer	(2.2)
^{1}D-L-A → $D^{\bullet+}$-L-$A^{\bullet-}$	electron transfer	(2.3)

Scheme 2: Energy transfer and electron transfer pathways of de-excitation of the excited state.

Energy transfer processes

There are two energy transfer mechanisms through which transfer of excitation energy from the donor to the acceptor can occur**.**

Coulombic Mechanism

The coulombic mechanism also referred to as resonance, Förster[28,29] or through space mechanism is a long range mechanism that can occur without presence of physical contact between donor and acceptor. This mechanism of energy transfer is efficient in systems in which the radiative transitions connecting the ground state and the excited state of each partner have high oscillator strength.[30] The rate of energy transfer (k_{EnT}) in coulombic mechanism is given by the Förster equation (1)[31]

$$k_{EnT} = 0.529\kappa^2\Phi_D J / n^4 N\tau_D R^6 \qquad (1)$$

Where κ is the orientation factor which takes into account the directional nature of the dipole-dipole interaction, and κ^2 is 2/3 for random orientation, Φ is the quantum yield of fluorescence of the donor, τ is the lifetime of the excited state of the donor, R is the distance in cm between donor and the acceptor, *J* is the Förster overlap integral between the emission spectrum of the donor and the absorption spectrum of the acceptor, n is the dielectric constant of the medium, and N is the Avogadro's number.

When a good spectral overlap integral is present and the photophysical properties are right, the energy transfer by this mechanism occurs efficiently over distances that exceed the molecular diameter.[30] Large aromatic molecules can exhibit an efficient singlet-singlet energy transfer; this process is analogous to the one used by nature in the photosynthetic antenna system.[32]

Exchange Mechanism

The rate constant for energy transfer by the exchange mechanism, also referred to as Dexter mechanism, is given by equation (2).[33]

$$k_{EnT}=KJ \exp(-2R/L) \qquad (2)$$

Where K is related to the specific orbital interactions between the donor and the acceptor, *J* is the overlap intergral between the emission spectrum of the donor and the absorption spectrum of the acceptor, and R is the distance between the donor and the acceptor relative to their Van der Waals radii, L.

The exchange mechanism is a double electron transfer process; it involves the transfer of one-electron from the LUMO of the excited donor to the LUMO of the acceptor, and the remaining electron moves from the acceptor HOMO to the donor HOMO.[30] This mechanism allows electrons to be transferred in the cases where excited states involved are spin forbidden in the usual spectroscopic sense. An example of an efficient exchange mechanism is that of triplet-triplet energy transfer in metal complexes from the lowest spin state.[34]

Electron transfer processes

Photoinduced electron transfer is one of the pathways through which deexcitation of the excited state donor occurs via transfer of electrons to the acceptor. It's in competition with other deactivation pathways such as fluorescence, intersystem crossing (ISC) to the triplet state, and internal conversion to the ground state. Electron transfer leads to a decrease in the lifetime of the excited singlet state of the donor and the fluorescence quantum yield.

Electron transfer processes is described by Marcus, Levich, Hush and Jortner theory.[35-39] The rate of the electron transfer process is given by equation (3)

$$k_{eT} = (\pi/\hbar^2\lambda\kappa_B T)^{1/2}|V|^2\exp[-(\Delta G^0 + \lambda)^2/4\lambda\kappa_B T) \quad (3)$$

where ħ is the Planck's constant, λ is the nuclear reorganization energy, κ_B is the Boltzmann's constant, *V* is the electronic coupling matrix element between the donor and the acceptor of the supramolecule, and ΔG^0 is the standard free energy of the reaction. For a homogenous series of reactions a log k_{eT} versus ΔG^0 forms a bell-shaped curve.[30] Figure 7 shows the relationship between log k_{eT} verse ΔG.[40]

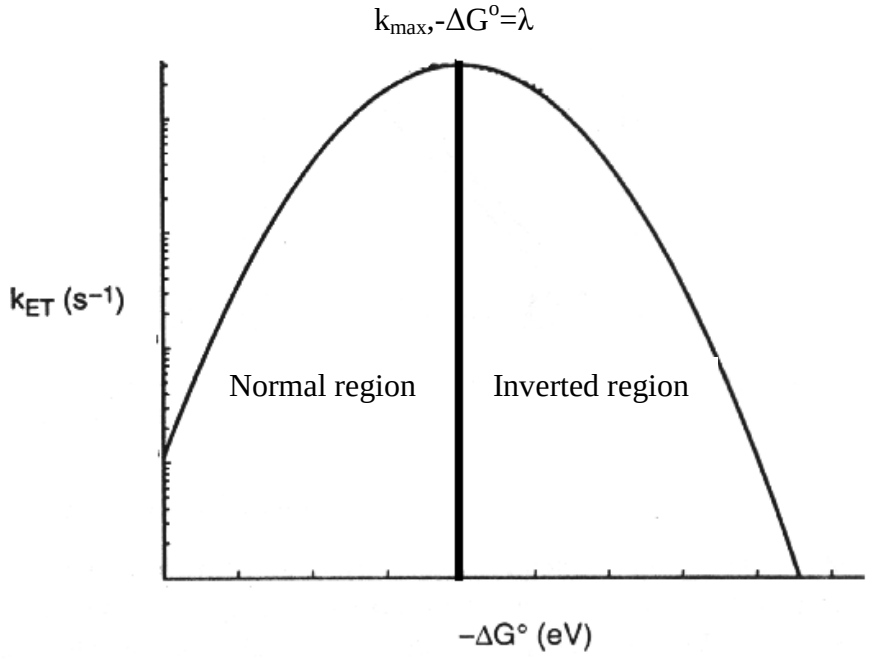

Figure 7: An example of a Marcus curve showing the normal and the inverted region

As shown in figure 7 above, there are three distinct scenarios in the bell-shaped curve. In the normal region, -ΔG □ λ , the rate of electron transfer increases with increasing driving force.

At the activationless region, the rate of electron transfer is optimum (- λ= ΔG), in this region increase or decrease in the driving force does not cause much changes in the rate of the electron transfer. In the "inverted region," the reaction is strongly exergonic (-ΔG > λ) and increasing the driving forces leads to a decrease in the electron transfer rate.[41]

The reorganization energy, λ, is the sum of two independent reorganization energies: there are the "inner" (bond lengths and angles with the donor and acceptor partners) and "outer" (solvent reorientation around the reacting pair) nuclear modes. The outer reorganization energy is the predominat term in the electron transfer processes.[30]

From figure 7 it can be deduced that the electron transfer rate in donor-acceptor systems with smaller λ is faster (small $-\Delta G^0$) and slower recombination (large - ΔG^0) compared to those having larger λ values.[42] The early events of natural photosynthetic centers (PRC) have near 100% efficiency and reduced energy-wasting recombination. This is achieved by shuttling electrons away a long distance from its point of origin and kinetically by employing a low reorganization energy (λ~0.3 eV) which forces back electron transfer into the Marcus "inverted" region.[43] Artificial donor-acceptor systems that replicate these important properties has been the focus of research to design mimics of PRC.[44] In artificial systems, fullerene has been used as an electron acceptor due to its superior electron accepting ability and low reorganization energy.

Fullerenes

Buckminsterfullerene, C_{60} was discovered by Kroto and co-workers in 1985.[45] Owing to the high degree of symmetry and the arrangement of its molecular orbitals, C_{60} has a number of

interesting chemical and physical properties.[46] C_{60} is a superior electron acceptor, and its triply-degenerate low-lying LUMOs (1.5-2.0 eV above the HOMO) allow it to reversibly accept up to six electrons.[47] Due to the remarkably small reorganization energies associated with reductions of C_{60} and its derivatives, donor-acceptor systems containing fullerenes have been proposed as models for photosynthesis and as energy conversion systems.[48-50]

Imahori and co-workers compared the electron transfer rate (k_s) and the charge recombination rate (k_{CR}) of the dyads shown in structure **1a** and structure **1b**. In structure **1a**, benzoquinone (Q), a commonly used acceptor, was replaced with the C_{60} as both of them have similar reduction potentials, the reduction potential for Q = -0.45 V vs. Ag/AgCl while that of C_{60} = -0.65 V vs. Ag/AgCl. Also the semi-rigid amide bond between the electron acceptor and the porphyrin ensures a similar separation distance and nature of the linker between the redox pair.

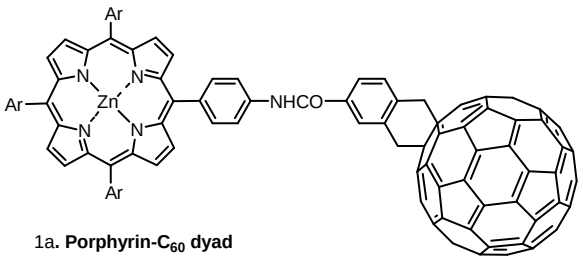

1a. **Porphyrin-C_{60} dyad**

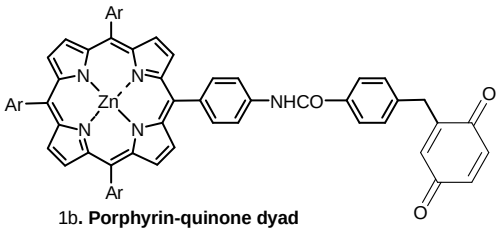

1b. **Porphyrin-quinone dyad**

Structures **1a** and **1b** above shows molecular structures of two D-L-A systems with a zinc porphyrin as the donor and it was observed that the rate of charge separation was faster using a fullerene than Q by a factor of six. However, the charge recombination rate in **1a** was smaller by a factor of less than 1/25 compared with that of **1b**. This superior property of C_{60} over the two-dimensional acceptors has been attributed to the smaller reorganization energy of the C_{60}

compared to those of their two-dimensional counterparts. The small reorganization energy of C_{60} pushes the photoinduced charge separated state to the top of the Marcus parabolic curve (figure 7) in the normal region, but forces the charge recombination downward into the inverted region. This phenomenon favors photoinduced electron transfer while retarding charge recombination. [48]

2.1 Design and synthesis of phenylethynyl-bridged phthalocyanine-fullerene dyads

Phthalocyanines (Pcs) are structural analogues of porphyrins which have strong absorption in the visible and near-infrared regions. The stronger absorption at longer wavelengths is as a result of extended conjugation afforded by the peripheral benzene rings. Figure 8 shows the structure of a simple unsubstituted metal free phthalocyanine (H_2Pc) and the nomenclature of the positions on the fused benzene ring.

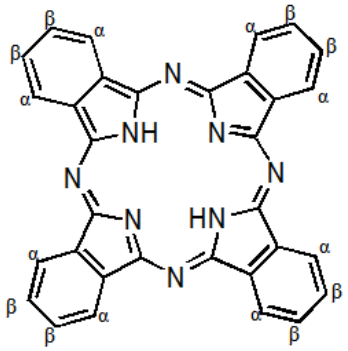

Figure 8 : Phthalocyanine (Pc) core structure and position nomenclature

Pcs have very versatile macrocycles which makes it possible to place seventy different elemental ions in the central cavity, which can be used to tune the physical properties.[51] Phthalocyanine solutions have a characteristic strong absorption between 670 and 690 nm (Q-

band) (Figure 9). There is also a strong absorption band in the UV region between 320 and 370 nm (B-band or Soret band).

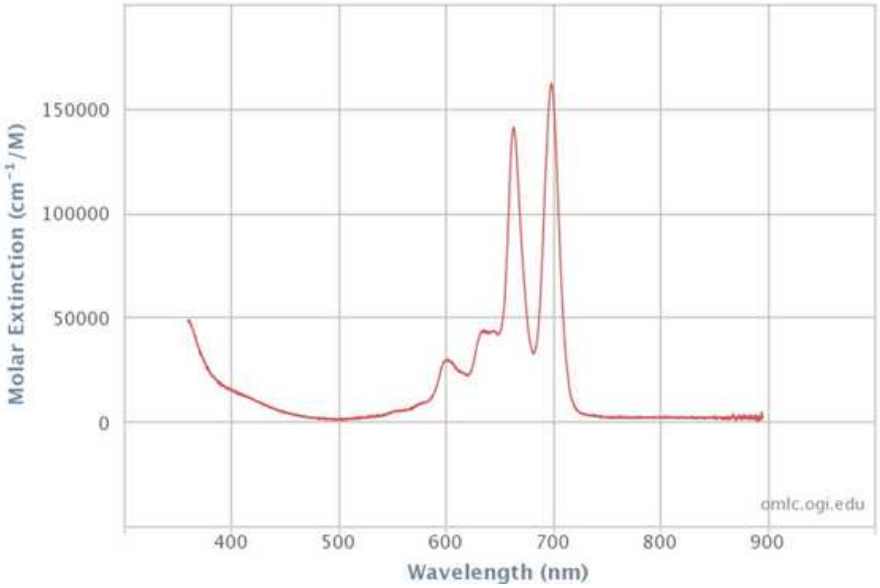

Figure 9: UV/Vis spectrum of H_2Pc in chloronapthalene.[52]

It is the Q-band that is responsible for the characteristic intense blue or sometimes blue-green color of the compound and also it is the one that is susceptible to substitution and to the Pc macrocycle environment.[53] The Q-band absorption is due to π-π^* transition from the HOMO of a_{1u} symmetry, to the LUMO of e_g symmetry.[54] This leads to a doubly degenerate first excited state of ^1E_u symmetry. The split in the Q-band usually observed in H_2Pc is as a result of lower symmetry (D_{2h}) compared with those of planar metal Pcs (D_{4h}) which leads to the loss of degeneracy of the LUMO orbital to produce Q_y and Q_x.[53] Also, the position of the Q-band in the absorption spectrum of Pcs is sensitive to the central metal ion. Distinct metal-ligand charge

transfer (MLCT) bands arising from excitation from the atomic orbitals of the metal ion to the ligand's molecular orbitals or *vica versa* have been observed.[55] The effect on the optical properties of Pcs by substitution on the fused benzene ring depends on the position of substituents. α- Substitution greatly influences the energy levels of the molecular orbitals and hence the absorption spectrum. For example, it has been shown that electron-donating groups such as alkoxyl moieties cause a 70 nm red-shift of the Q-band of CuPc substituted at the α-position by raising the energy level of the HOMO.[56] On the other hand, with exception of substitutions that results in an extension of the π-orbital, most β-substitution has very little effect on the Q-band's position.[57] Due to these interesting properties phthalocyanines have been extensively investigated for their promising electrical, optoelectronics, photochemical and catalytic properties.[53]

Pc-fullerene dyads with the electron donor and the electron acceptor covalently linked is an important approach to artificial photosynthesis and molecular electronic devices.[58] Donor-fullerene dyad systems that exhibit a fast photoinduced charge separation (CS) with a fairly long lifetime of the charge separated state was initially observed in porphyrin-fullerene dyads and several of those types of dyads has been prepared.[48] However, connecting Pc donor and fullerene acceptor has several advantages over porphyrin-fullerene dyads. Unlike porphyrins, which have poor absorption in the red part of the visible light, Pcs have strong light absorption in the red region of the solar spectrum (figure 9) and this allows for efficient conversion of solar energy in organic solar cells by collecting a larger section of the available sunlight. In addition, the

relatively large driving force for photoinduced electron transfer favors charge-separated state even in non-polar solvents.[59]

A number of peripherally connected Pc-fullerene dyads have been synthesized in the last few years.[60-63] These dyads are known to have an open conformation where the fullerene is located aside the Pc macrocycle rather than on top of it [59] and it has been concluded that the electron transfer in these dyads take place through space rather than through bonds.[60,61] The general trend in these type of donor-acceptor units are that the alignment is edge-to-edge and the charge recombination is faster than those that are face-to-face.[59] The shorter the donor-acceptor linkage, the shorter the recombination time. Quintiliani and co-workers observed that the lifetime of charge-separated state is shorter in the dyads that lack a linker between the ZnPc and the C_{60} moiety (figure 10).[64]

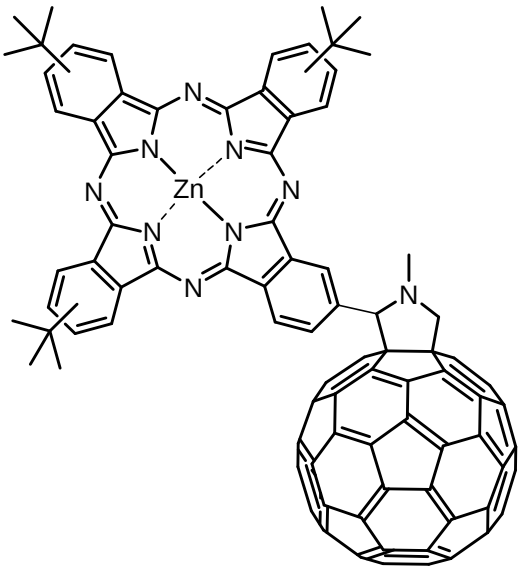

Figure 10: ZnPc-C_{60} dyad

The role of the donor-acceptor spacer in dyads are not only structural, it is also involved in the electronic communication between the terminal units. The modular composition of the spacer is also important as it allows one to alter the separation without affecting the electronic nature of the linkage.[64] Of the linkers studied, acetylene linkers have shown the longest lifetime of the radical ion-pair state.[64] It is postulated that a longer linker that has phenyl-ethynyl spacer can lead to fast charge separation and slower recombination. Towards this goal phthalocyanine-C_{60} dyads separated by phenyl-ethynyl linkers were synthesized and the electrochemical and photochemical properties studied.

Results and Discussion

Synthesis

Phthalonitrile **2** was synthesized by Sonogashira coupling of 4-iodophthalonitrile with 4-ethynylbenzyl alcohol in the presence of $[Pd(PPh_3)_2Cl]$ and CuI as the catalyst (scheme 3).[65] Silica column purification of the crude using ethyl acetate/dichloromethane (1:9) solvent afforded compound **2** in 93% yields. It was observed that higher yield is favored by use of increased amount of catalyst.

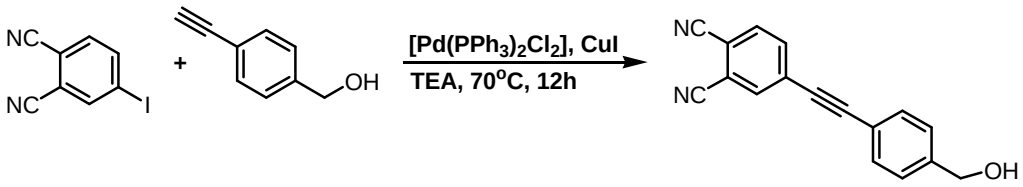

Scheme 3: Synthesis of 4-(2-(4-(Hydroxymethyl)phenyl)ethynylpthalonitrile **2**

As shown in scheme 4 below, unsymmetrical Pc **3** was obtained by a statistical condensation reaction between phthalonitrile **2** and a commercially obtained 4-*tert*-butylphthalonitrile in N, N-dimethylaminoethanol (DMAE) heated to reflux in the presence of $Zn(OAc)_2.2H_2O$. Thin-layer chromatography (TLC) of the crude product showed two main products: the less polar symmetrically substituted tetra(*tert*)butylphthalocyaninatozinc (II) side product and the desired asymmetrically substituted Pc **3**. Due to the significant polarity difference between the two products separation was easily achieved by using silica column chromatography to yield Pc **3**, 17%. This approach was preferred over the alternative method where tri-*tert*-butyl-iodophthalocyanine get reacted in a Sonogashira coupling reaction with 4-ethynylbenzyl alcohol to afford compound **3**, because the condensation reaction to prepare tri-*tert*-butyl-iodophthalocyanine yields three products which are all very similar in polarity hence difficult to separate, and also the target product was recovered at a lower yield of 10 %.

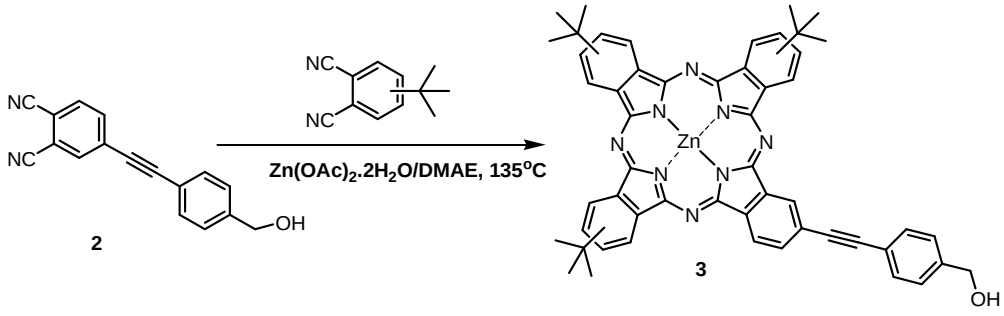

Scheme 4: Synthesis of Tri(tert)butyl(benzylalcohol-4-ethynyl)phthalocyaninatozinc (II) **3**

The hydroxyl functionality on the unsymmetrically substituted Pc **3** was oxidized to a formyl group by use of 2-iodoxybenzoic acid (IBX) in dimethyl sulfoxide/tetrahydrofuran

mixture as the reaction solvent at room temperature to yield Pc **4**, 79% (scheme 5). MALDI-TOF (terthiophene): *m/z*: 874.49

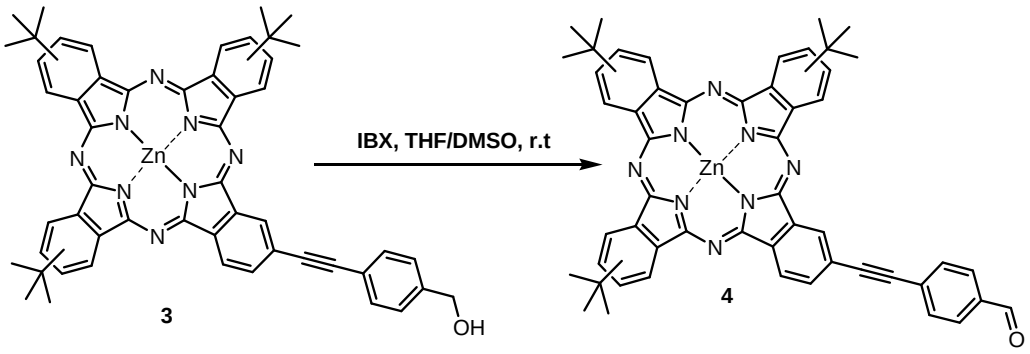

Scheme 5: Tri (tert)butyl(benzaldehyde-4-ethynyl)phthalocyaninato (II) **4**

Synthesis of ZnPc-C_{60} dyad **5** from ZnPc **4** was achieved by a 1, 3-dipolar cycloaddition of azomethine ylide generated *in situ* in a Prato reaction. Scheme 6 shows the reaction between ZnPc **4** and fullerene, C_{60} in the presence of sarcosine in refluxing toluene to yield a 53% of dyad **5** after silica column purification with toluene/THF (49:1). MALDI-TOF MS (dithranol): $[M]^+$: *m/z*: 1620.48.

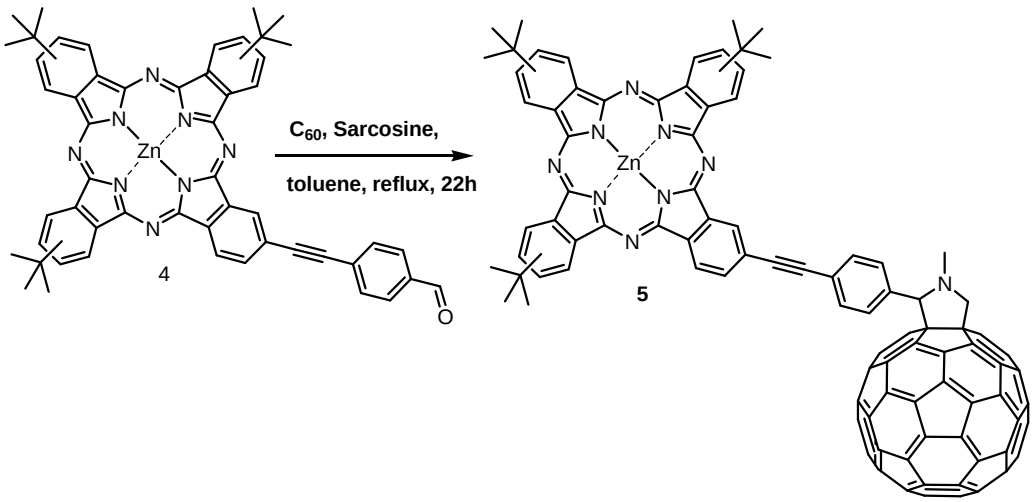

Scheme 6: Synthesis of ZnPhthalocyanine-C_{60} dyad **5**

Scheme 7 below shows the synthesis of H_2Pc-C_{60} dyad **7** and its precursor, H_2Pc **6.** Heating Pc **4** in HCl-Pyridine/pyridine mixture at 120 ^oC for 24 hours afforded H_2Pc **6** in a quantitative yield of 98% without the need for a column purification.

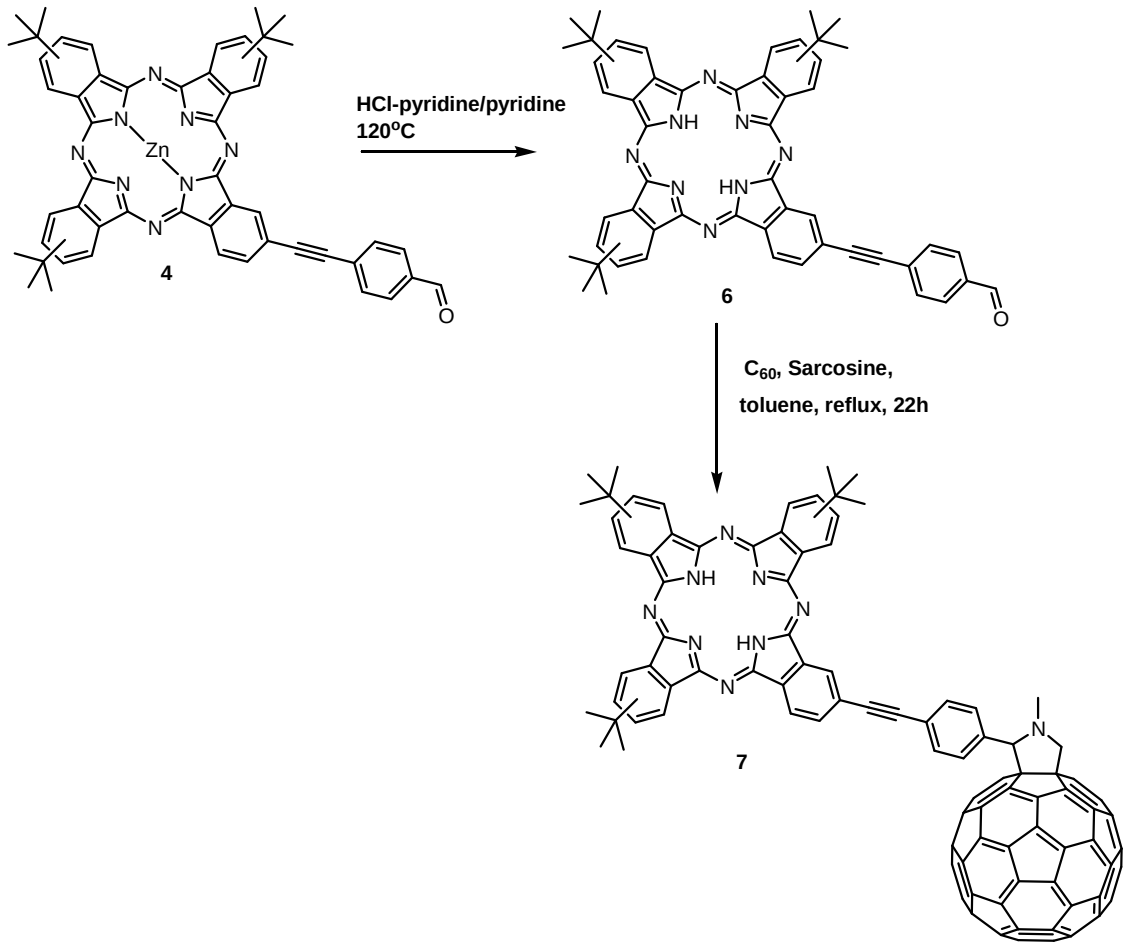

Scheme 7: Synthesis of Tri (*tert*)butyl(benzaldehyde-4-ethynyl)phthalocyanine **6** and H_2Phthalocyanine-C_{60} dyad **7**

Then, a 1,3-dipolar cycloaddition (Prato reaction) between H_2Pc **6** and fullerene C_{60} in the presence of sarcosine was carried out to obtain H_2Pc-C_{60} dyad **7**, 69% yield, after silica gel column purification with toluene/carbon disulphide (1/1) as the solvent. MALDI-TOF (dithranol matrix) showed a single peak, $[M]^+$: *m/z*: 1558.8.

De-zincation of hydroxyl substituted unsymmetrical ZnPc **3** model was achieved by heating it in pyridine-HCl/Pyridine at 120 ^{o}C for 21 hours (scheme 8) followed by adding water to the reaction mixture, then cooling, centrifugation and filtration to obtain a pure hydroxyl substituted unsymmetrical H_2Pc model **8,** 38% yield. The yield here was far lower than the one obtained during dezincation of ZnPc **4**; this may be attributed to the presence of the hydroxyl functionality on ZnPc **3** which may be interfering with the effectiveness of the pyridine-HCl reagent.

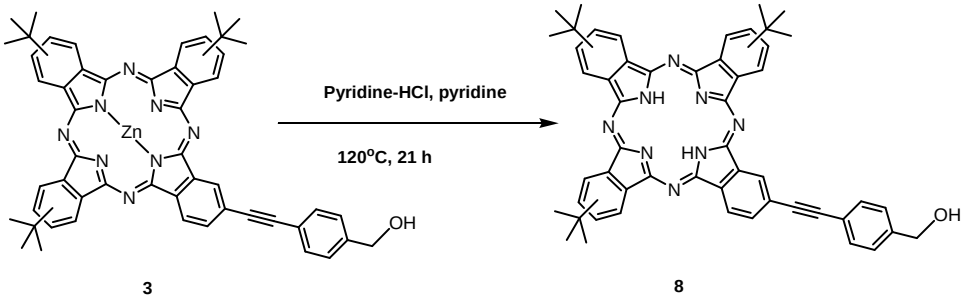

3 8

Scheme 8: Synthesis of Tri (*tert*)butyl(benzylalcohol-4-ethynyl)phthalocyanine **8**

Scheme 9 shows the synthesis of fulleropyrrolidine phenol model **9** and its precursor, fulleropyrrolidine methoxyphenyl **10**. A Prato reaction between 4-anisaldeyde and fullerene C_{60} in the presence of sarcosine in refluxing toluene afforded compound **9**, 60% after silica column purification with toluene/ethyl acetate solvent.

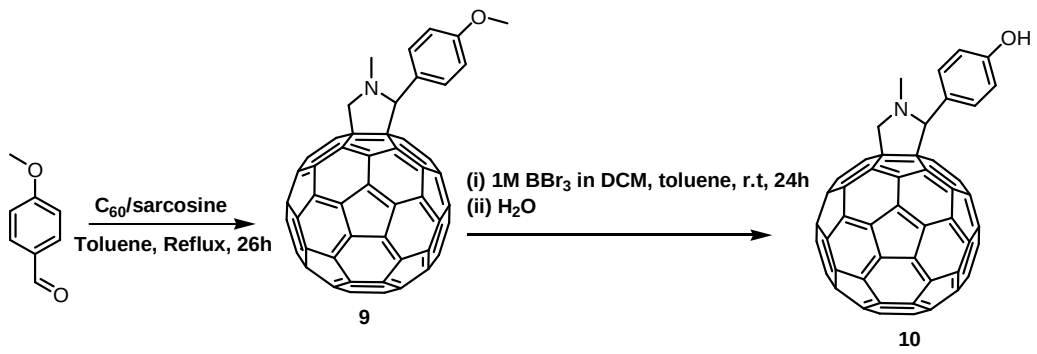

Scheme 9: Synthesis of N-methyl-2-(p-methoxyphenyl)-3, 4-fulleropyrrolidine **9** and N-methyl-2-(p-phenylalcohol)-3, 4-fulleropyrrolidine **10**

Demethylation of compound **9** was done by reacting it with boron tribromide (BBr_3) at room temperature and the reaction crude was quenched by washing with water. The crude was purified by silica column chromatography with toluene/methanol (19/1) solvent system to afford N-methyl-2-(*p*-phenylalcohol)-3, 4-fulleropyrrolidine **10**, 65% yield.

The structures of the molecules were confirmed by ^1H NMR ($CDCl_3$), the precursor, hydroxyl substituted phthalonitrile **2** showed all the expected signals. All the 10 protons were accounted for, the single aromatic proton between cyano group and the alkynyl group appeared down field at 7.83 ppm, the two benzylic protons appeared at 4.68 ppm while the hydroxyl proton was a broad signal at 1.85 ppm. Due to the poor solubility of the phthalocyanines in chloroform, all the NMR measurements for all the phthalocyanine molecules were taken in d_8-THF. On condensation to form phthalocyanine **3**, the hydroxyl proton was down field shifted to 4.35 ppm an indication that it is experiencing deshielding from the phthalocyanine aromatic system. Due to the presence of the regioisomers all the Pc aromatic protons appeared as broad signals. The single proton between the Pc macrocycle and alkynyl group was further shifted

downfield to 10.02 ppm, an indication that being sandwiched between the macrocycle and the triple bond deshields it more than the other Pc aromatic protons. The *tert*-butyl protons appeared up field between 1.73 and 1.85 ppm. Oxidizing Pc **3** to formyl-derivative phthalocyanine **4**, a slight up field shift of most protons was observed. Formyl proton could be seen as a sharp singlet at 10.00 ppm. All the Pc and the phenyl aromatic protons appeared as poorly resolved multiplets. In the ZnPc-C_{60} dyad **5**, the signals of the Pc protons were not significantly impacted, while those on the functionalized fullerene were when compared to those of fullerene model compound **10**. The pyrolidine protons signals were shifted down field from 4.97-4.23 ppm in the model compound **10** to 5.06-5.01 ppm in dyad **5**, while the N-CH_3 protons in the dyad **5** were up field shifted from 2.97 ppm in the model compound **10** to 2.86 ppm in the dyad **5**. Generally the signals in the dyad were broad and poorly resolved which could be attributed to poor solubility of the dyad in d_8-THF, addition of few drops of carbon disulphide to the NMR solvent did not yield much improvement in signal resolutions.

In the free base dyad, H_2Pc-C_{60} dyad **7,** the same pattern as dyad **5** was observed where the Pc signals did not change much from those observed in the model compounds. However, notable differences were observed in the functionalized fullerene components, in H_2Pc-C_{60} dyad **7,** the N-CH_3 signals broadened and were shifted upfield to 2.29 ppm from 2.97 ppm in the model fullerene **10**.

Steady-state Absorption

Figure 11 shows the UV/vis spectrum in THF of H_2Pc-C_{60} dyad **7** and shows Q-band at 694, 672, 644 and 613 nm and a Soret band at 331 nm, while the Q-band of the H_2Pc model compound **8** was at 694, 667, 644, 611 nm and Soret band at 344 nm. For the ZnPc-C_{60} dyad **5** the most red Q-band appeared at 685 nm and the Soret band at 350 nm and the Q-band of the ZnPc model compound **3** was at 683 nm and its Soret band at 350 nm (figure 12). These observations where the Q-bands in both Zn and metal free dyads were not significantly shifted compared to those of the respective models is an indicator that there is no significant ground state interactions between the electronic systems of the two chromophores.

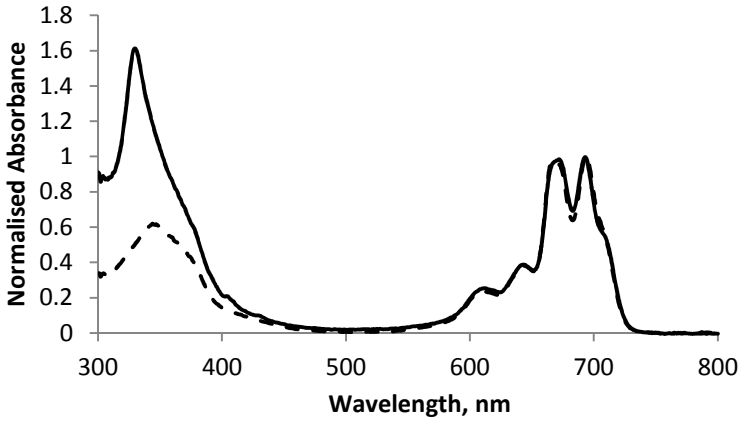

Figure 11: UV/Vis spectra of H_2Pc-C_{60} **7** (solid line) and H_2Pc model **8** (dashed line), normalized at Q-band in THF.

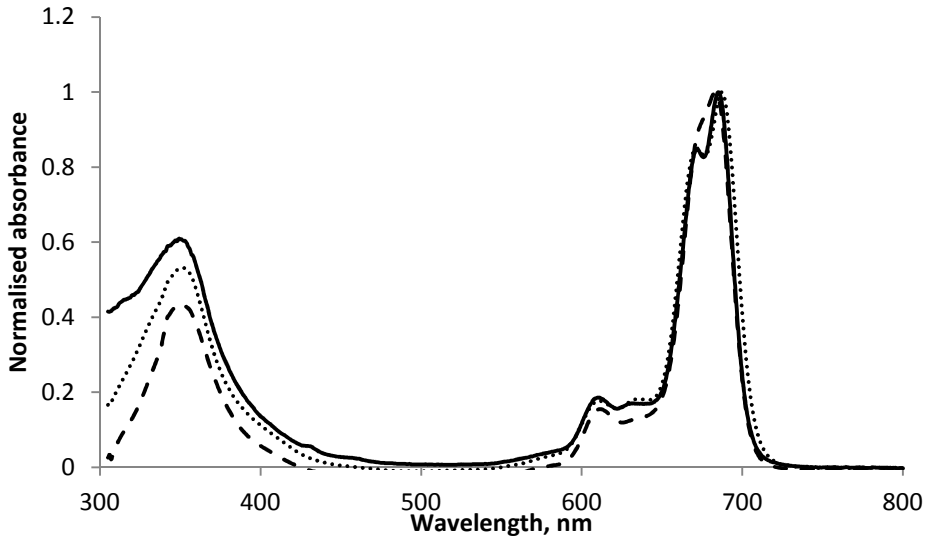

Figure 12: UV/Vis spectra of ZnPc model **3** (dashed line, - - -), ZnPc aldehyde **4** (dotted line, ····), and ZnPc-C_{60} **5** (solid line, —) normalized at Pc Q-band in THF.

As shown in figure 12 above, the dyad **5** shows a weak absorption at 432 nm and this is a characteristic of the [6, 6] mono-adduct of C_{60}. The bands for H_2Pc **3** model and the H_2Pc-C_{60} dyad **7** are broader than those of their zinc counterparts, this can be attributed to the poor solubility of the metal free compounds and this causes aggregation. The better solubility of the zinc containing molecules can be attributed to the ability of the central metal to bind a fifth ligand[66], such as the solvent. This binding affects both the optical and electronic transfer properties[67], and could be useful in sensor applications.[66] Both the dyads show higher absorption in the UV region than their respective models; this is because of the additional absorption by the fullerene moiety. The fulleropyrrolidine component has a high extinction coefficient at 310 nm, seen from the fullerene model **10** (spectrum not shown). The weak absorption at 703 nm of the

fullerene component was not seen in the dyads as it gets eclipsed by the strong Q-bands of the Pcs.

The Q-band of the metal free compounds are red-shifted by 7-8 nm when compared to those of their Zn counterparts, this observation is in agreement with HOMO-LUMO gap differences in these molecules as supported by the electrochemistry data (table 1). Using the oxidation and the reduction potential values the HOMO-LUMO gap were found to be 1.4 eV and 1.6 eV for the H_2Pc model **8** and ZnPc model **3** respectively. Oxidizing Pc alcohol **3** to the corresponding aldehyde **4**, the Q-band was shifted from 683 nm to 687 nm, this red-shift can be attributed to the extended conjugation due to the additional formyl double bond which raises the HOMO and consequently reduce the HOMO-LUMO gap.

Electrochemistry

Table 1: Redox potentials of Pc-fullerene dyads and their respective models (Electrochemistry measurements were done by Dalvin Mendez)

Molecule	**Oxidation (V vs SCE)**	**Reduction (V vs SCE)**
H_2Pc model **8**	0.62 (160)	-0.78 (54)
H_2Pc-C_{60} 7	0.74 (irr)	-0.46 (90)
C_{60} model **10**	-	-0.63 (80)
ZnPc-C_{60} 5	0.54 (210)	-0.66 (74)
ZnPc model **3**	0.59 (145)	-0.99 (90)

The first oxidation potential of the free base Pc model **8** is 0.62 V vs SCE as measured by cyclic voltammetry in benzonitrile solution. A model for ZnPc model **3** is oxidized at 0.54 V vs

SCE whereas the first reduction potential for a model fullerene **10** is -0.63 V vs SCE (table 1). Using these data, the energies of the charge separated states of dyads **5** and **7** in benzonitrile are as follows: $H_2Pc^{\bullet+}$-$C_{60}^{\bullet-}$ and $ZnPc^{\bullet+}$-$C_{60}^{\bullet-}$ are 1.25 eV and 1.17 eV, respectively. The free base Pc dyad retains higher energy of the absorbed photons.

The electrochemistry data are approximately a linear combination of the oxidation and reduction potentials of the model phthalocyanines and fullerene. This observation agrees with the absorption spectra and these are evidences that there is no strong perturbation of the chromophores due to the covalent linkages.

The energies of the excited singlet states are calculated using the frequency-domain average of the most red wavelength absorption and most blue wavelength emission. They were calculated for the free base phthalocyanine **8** (1.79 eV), the zinc phthalocyanine **3** (1.82 eV), and the fullerene **10** (1.76 eV) (figure 13).

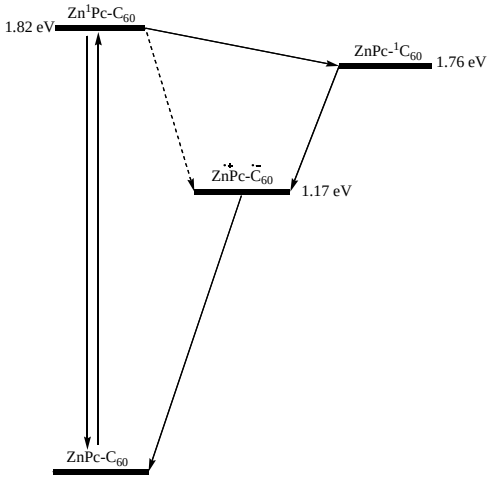

Figure 13: High energy states and possible interconversion pathways for ZnPc-C_{60} dyad **5** following photoexcitation of the ZnPc chromophore.

The energy of the charge-separated state is estimated from the cyclic voltammetric data of model compounds in benzonitrile. Solid arrow represents the main pathway while the dashed arrow represents a minor pathway.

From the spectroscopic and cyclic voltammetric measurements in benzonitrile, a polar solvent, the thermodynamic driving forces for photoinduced electron transfer from $H_2{}^1Pc\text{-}C_{60}$ to $H_2Pc^{\bullet+}\text{-}C_{60}^{\bullet-}$ and $Zn^1Pc\text{-}C_{60}$ to $ZnPc^{\bullet+}\text{-}C_{60}^{\bullet-}$ are -0.54 eV and -0.65 eV respectively. The rate constant for most electron transfer processes such as this one is expected to be dependent on the thermodynamic driving force, the electronic coupling, and the nature of the linker. For the ZnPc-C_{60} dyad **5** and the free base Pc-C_{60} dyad **7** under study here, the last two factors are not different. However, from the thermodynamic argument, it is expected that the rate of electron transfer is faster in dyad **5** as long as the process is in the normal region of the Marcus curve.

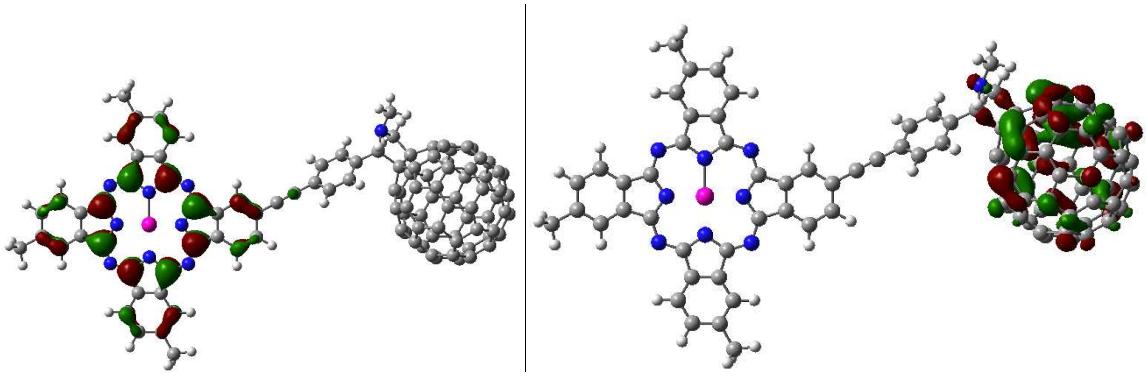

Figure 14: DFT calculated (gaseous phase) molecular orbitals of the ZnPc-C_{60} dyad **5**, the HOMO is localized on the Pc (top) moiety and the LUMO on the C_{60} (bottom).

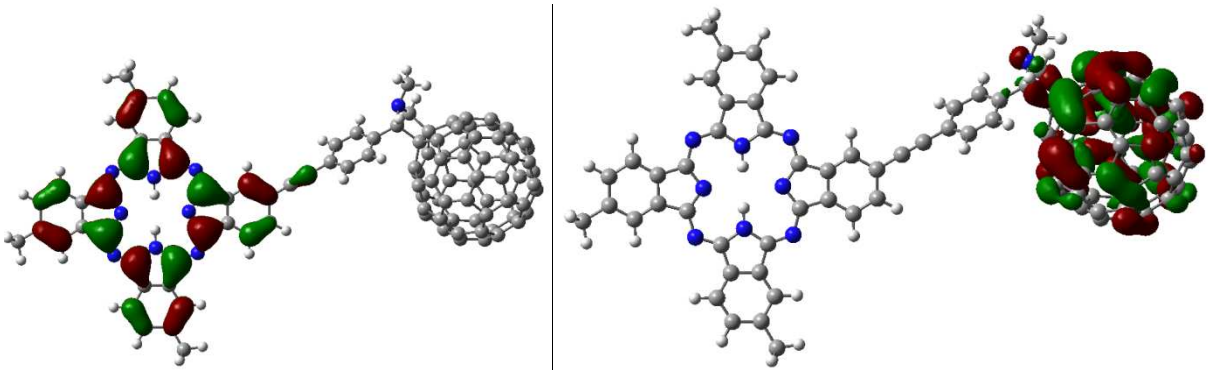

Figure 15: DFT-calculated (gaseous phase) molecular orbitals of the H_2Pc-C_{60} dyad **7**, the HOMO is localized on the Pc moiety (top) and the LUMO on the C_{60} (bottom).

As shown in figures 14 and 15 above, the HOMO is exclusively on the Pc and the LUMO is on the C_{60} in both dyads, this gives a further support to the conclusion that in the Pc-C_{60} conjugates under study, Pc is the electron donor and the C_{60} is the electron acceptor and that the molecular orbitals of the components of the dyads retain their individual properties.

Stead-state emission

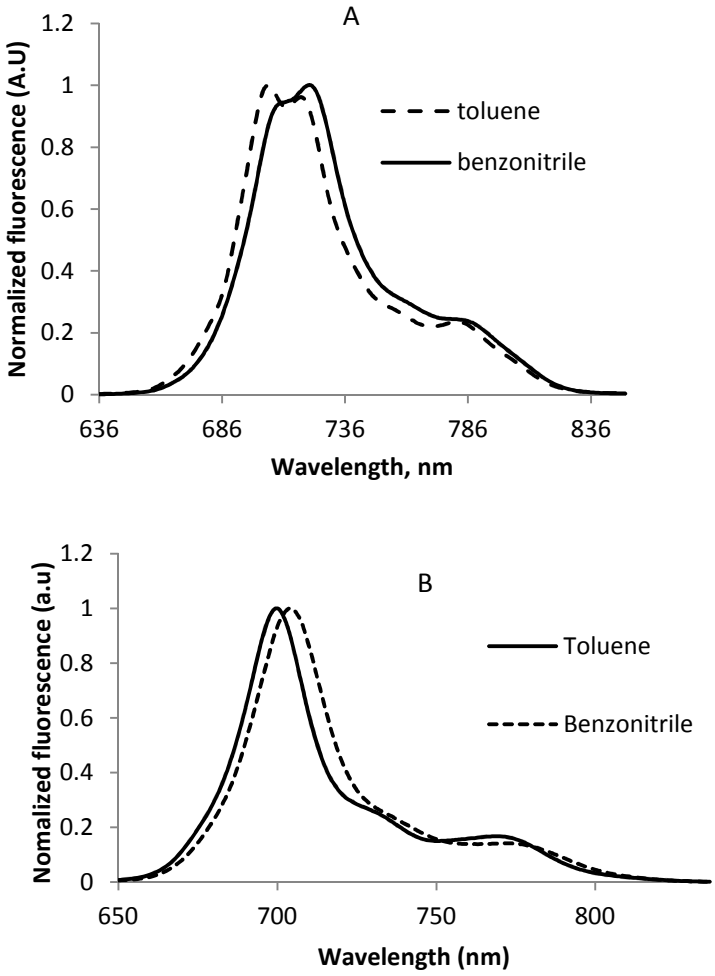

Figure 16: Steady state emission spectra for H_2Pc model **7** (figure 16A) and ZnPc model **3** (figure 16B), excitation at 330 nm.

The emission wavelength for the models are, H_2Pc (figure 16A): 705, 719 and 781 nm (toluene) and 709, 721 and 784 nm (benzonitrile) and ZnPc (figure 16B): 704 and773 nm (toluene) and 700 and 770 (benzonitrile). Just like as been observed in the absorption spectra, the emission spectra of the models also show that the free base Pc model emits at a longer wavelength.

Supporting the conclusion that free base Pc model has a smaller HOMO-LUMO gap than the ZnPc model. The emission spectra are mirror images of the absorption spectra, an indication that fluorescence is the major deactivation pathway for the excited singlet state Pc

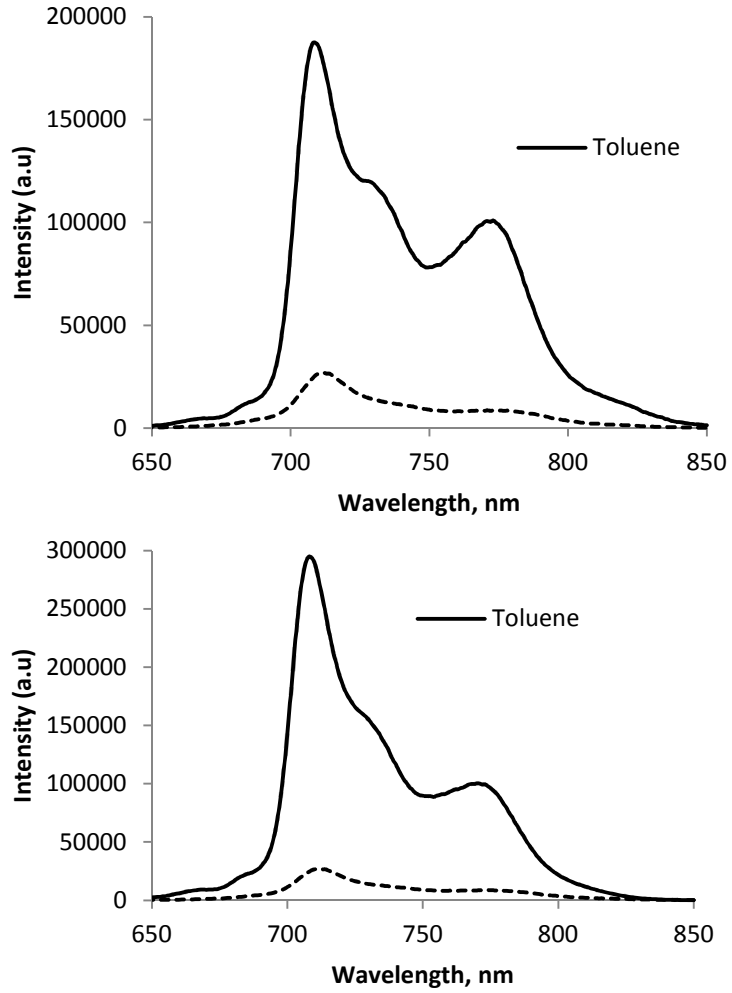

Figure 17: Emission spectra of the H_2Pc-C_{60} dyad **7** (top) and ZnPc-C_{60} dyad **5** (bottom) in toluene and benzonitrile after excitation at 345 nm wavelength.

In figure 17 the fluorescence intensity is quenched several orders of magnitude in the polar solvent, benzonitrile, compared to the fluorescence intensity in the non-polar solvent,

toluene. The solvent dependent quenching in the dyads means that electron-donor acceptor interactions are involved in the excited-state deactivation of the photoexcited singlet state Pc. This observation is a preliminary evidence that electron transfer from the excited state Pc to C_{60} is the predominant deexcitation pathway in polar solvents. Polar solvents are able to stabilize the charge separated state and hence lowering its energy, thus, thermodynamically favoring charge separation as can be seen from the respective $-\Delta G_{CS}$ values of the dyads in table 2.

Energetics

Table 2: Energies (eV) of the dyads in benzonitrile

Feature	ZnPc-C_{60} **5**	H_2Pc-C_{60} **7**
^{1*}Pc	1.82	1.79
$Pc^{\bullet+}$-$C_{60}^{\bullet-}$	1.17	1.25
$-\Delta G_{CS}$	0.65	0.54
$-\Delta G_{CR}$	1.17	1.25

As shown in the table 2 above, the energies of the charge-separated states lie well below those of the three singlet excited states in benzonitrile, ^{1*}ZnPc (**3**) (1.82 eV), $^{1*}H_2$Pc (**8**) (1.79 eV) and $^{1*}C_{60}$ (1.76 eV)[68]. This favorable driving force ($-\Delta G_{CS}$)suggests a strongly exothermic electron transfer in both cases to form $ZnPc^{+}$-$C_{60}^{\bullet-}$ and $H_2Pc^{\bullet+}$-$C_{60}^{\bullet-}$.

Time-resolved studies

To investigate the dominant pathways of the deactivations in the Pc-C_{60} as a result of electron-donor-acceptor interactions time-resolved studies were conducted.

Transient Emission

Table 3: Fluorescence lifetimes (ns) measurements of Pc models and Pc-C_{60} dyads after excitation at 330 in toluene and benzonitrile. (Measurements were taken by Robert Schimtz)

Molecule	**Toluene**	**Benzonitrile**
ZnPc (**3**)	2.4	2.3
H_2Pc (**8**)	6.5	6.3
ZnPc-C_{60} (**5**)	0.11 (51%)	□ 0.020 (90%)
	1.7 (22%)	0.1 (9%)
	2.18 (27%)	2.3 (1%)
H_2Pc-C_{60} (**7**)	0.22 (59%)	0.08 (55%)
	2.0 (39%)	0.2 (44%)
	6.5 (2%)	2.3 (1%)

As shown by data in table 3 above, both ZnPc **3** and H_2Pc **8** models have solvent independent fluorescence lifetime. The lifetimes of Pc excited state in both dyads were significantly reduced, although the reduction is much greater in benzonitrile than in toluene. In the non-polar solvent, toluene, there is a presence of a characteristic emission of the $^1C_{60}$, in dyad **5** it is 1.7 ns (22 %) and in **7** it is 2.0 ns (39 %). In benzonitrile, for

both dyads there is no evidence of $^1C_{60}$ emission, it appears if does exist, it get quenched very fast.

In both solvents, the lifetime of the excited state Pc is shorter in ZnPc-C_{60} **5** than in H_2Pc-C_{60} **7**. These observations in addition to the solvent dependent quenching of dyads observed in steady fluorescence can be used to conclude the existence of energetically favorable fast intramolecular electron transfer processes from locally excited Pc to the C_{60}. The long-lived minor component in the free base dyad **7** which makes up 2% and 1% of the decay in toluene and benzonitrile respectively is most likely an impurity

Transient absorption

To test the nature and dynamics of the charge-separated radical ion-pair state of ZnPc-C_{60} conjugate, femtosecond-resolved transient absorption spectroscopy was utilized. Due to the observed aggregation phenomenon H_2Pc-C_{60} dyad **7** was not studied. In figure 18 transient absorption spectra for ZnPc-C_{60} **5** are gathered.

There is a competing energy transfer from Pc singlet excited state to C_{60} singlet excited state and formation of $ZnPc^{\bullet+}$-$C_{60}^{\bullet-}$ CS state with 1.3 ps. After that there is slower (with 10 ps) formation of $ZnPc^{\bullet+}$-$C_{60}^{\bullet-}$ CS state. The CS state due to $ZnPc^{\bullet+}$-$C_{60}^{\bullet-}$ decays in 94 ps. The longer-lived CS state is attributed to the presence of the phenylethynyl linker.

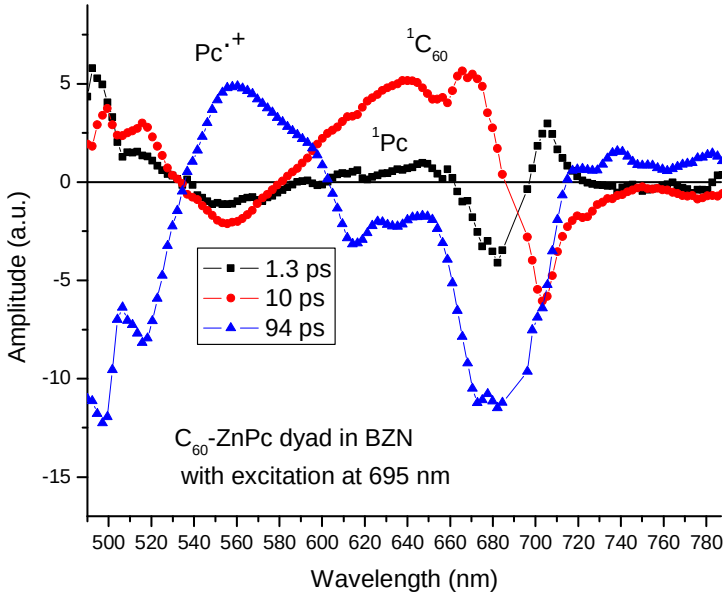

Figure 18: differential absorption spectra (visible) obtained upon femtosecond flash photolysis (695 nm) of **5** in benzonitrile with several time delays at RT (Experiment was done by Dr. Gerdenis Kodis)

Torres and co-workers reported shorter CS state lifetime for ZnPc-C_{60} conjugates with no linker (figure 10) or with just an ethynyl linker (figure 19).

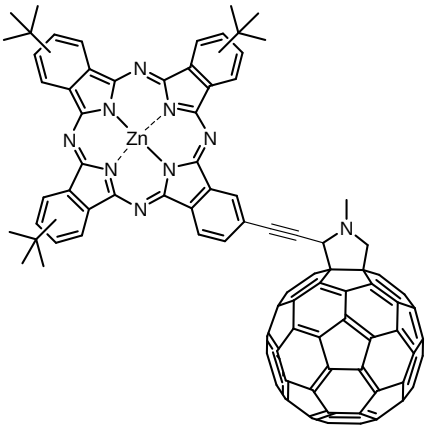

Figure 19: Ethynyl-linked ZnPc-C_{60} dyad

The lifetime (τ) of the CS state for the structure in figure 10 was reported to be 32 ps and that of the structure in figure 19 was 36 ps.[69] The driving force ($-\Delta G_{CR}$) for the CS for **5** and for the structure in figure 10 is 1.19 eV and 1.17 eV respectively, therefore it cannot be the main factor favoring the longer lifetime of the CS state of **5**. It can be concluded that for ZnPc-C_{60} conjugates with similar charge-recombination (CR) driving force, the lifetime of CS state is significantly influenced by the linker.

Experimental section

Synthesis

4-(2-(4-(Hydroxymethyl)phenyl)ethynylpthalonitrile 2

Thirty mL of Et_3N was placed in a round-bottom flask immersed in ice-water and degassed with argon for 40 min. A mixture of 4-ethynylbenzyl alcohol (126 mg, 0.953 mmol) and 4-iodophthalonitrile (219 mg, 0.862 mmol) was dissolved in the degassed and cold Et_3N (30 mL). This was followed by addition of [$Pd(PPh_3)_2Cl_2$) (63 mg, 0.0898 mmol) and CuI (21 mg, 0.11 mmol). The reaction mixture was stirred for 15 hrs at 70^{o}C under argon atmosphere. The solvent was removed under reduced pressured and the crude product purified by flash column chromatography on silica gel CH_2Cl_2/EtOAc (9:1) to yield 207 mg (93%) of **2** as a white solid.

^{1}H-NMR ($CDCl_3$, 400 MHz) δ_H 7.83 (s, 1H), 7.75-7.69 (m, 2H), 7.48- 7.46 (d, *J*=8, 2H), 7.35-7.33 (d, *J*=8, 2H), 4.68 (s, 2H), 1.85 (br s, 1H)

Tri (*tert*)butyl(benzylalcohol-4-ethynyl)phthalocyaninatozinc (II) 3

A mixture of 4-tertbutylphthalonitrile (715 mg, 3.88 mmol), phthalonitrile **2** (200 mg, 0.775 mmol), and $Zn(OAc)_2.2H_2O$ (825 mg, 3.76 mmol) in 30 mL DMAE was stirred and heated at 130^oC for 24 hrs. Then the mixture was cooled to room temperature, the solvent was removed and the residue was washed with $MeOH/H_2O$ (5:1) and the dark green crude obtained was purified by flash column chromatography on silica gel, toluene/THF (9:1). The blue symmetrical Pc was eluted first, followed by the greenish blue Pc **3** 119 mg, 17%

^{1}H-NMR (d_8-THF, 400 MHz) δ_H , ppm 10.02 (s, 1H), 9.45-9.20 (m, 8H), 8.33-8.27 (m, 3H), 7.86-7.72 (m, 4H), 4.71 (s, 2H), 4.35 (br s, 1H), 1.85-1.73 (m, 27H)

UV/Vis (THF): λ_{max} 683, 611 and 350 nm

MALDI-TOF (terthiophene): calc. for $C_{53}H_{46}N_8OZn$: $[M]^+$: *m/z*: 874.37, found 874.75.

Tri (*tert*)butyl(benzaldehyde-4-ethynyl)phthalocyaninato (II) 4

A mixture of Pc **3** (20 mg, 0.0229 mmol), IBX (20 mg, 0.0714 mmol) in THF (3 mL)/DMSO (3 mL) was stirred under argon atmosphere at room temperature for 48 hrs. Stirring was stopped and 10 mL of brine was added to the mixture followed by extraction with ether. Solvent was removed from the organic layer under reduced pressure and crude purified by column chromatography toluene/THF (19:1) to yield a green Pc **4,** 16 mg, 79%.

^{1}H-NMR (d_8-THF, 400 MHz) δ_H , ppm 9.99 (s, 1H), 9.40-9.28 (m, 4H), 9.22-911 (m, 4H), 8.22-8.15 (m, 4H), 7.96-7.86 (m, 4H), 1.75-1.62 (m, 27H)

UV/Vis (THF): λ_{max} 687, 672, 611, 352 nm

MALDI-TOF (terthiophene): calc. for $C_{53}H_{44}N_8OZn$: $[M]^+$: *m/z*: 872.29, found 874.49.

Phthalocyanine-C_{60} dyad 5

A mixture of Pc **4** (15 mg, 0.0172 mmol), C_{60} (41 mg, 0.0569 mmol), sarcosine (11 mg, 0.123 mmol) in an anhydrous toluene (25 mL) was stirred at reflux temperature for 22 hrs under argon atmosphere. After this time the mixture was cooled and solvent removed under reduced pressure. The crude was purified by a column chromatography in silica gel, toluene/THF (49:1) to obtain the ZnPc-C_{60} dyad **5** as a dark-blue powder 15 mg, 53%.

^{1}H-NMR (d_8-THF, 400 MHz) δ_H , ppm 9.41-9.49 (m, 4H), 9.31-9.23 (m, 4H), 8.31-8.22 (m,4H), 7.98 (br s, 2H), 7.87 (br s, 2H), 5.06-5.01 (m, 3H), 4.28-4.25 (d, *J=12*, 2H), 2.86 (s, 3H, N-CH_3), 1.94-1.76 (m, 27H)

UV/Vis (THF): λ_{max} 685, 672, 632,610, 350 nm

MALDI-TOF MS (dithranol): calc. for $C_{115}H_{49}N_9Zn$: $[M]^+$: *m/z*: 1620.34, found 1620.48

Tri (*tert*)butyl(benzaldehyde-4-ethynyl)phthalocyanine 6

Tri(*tert*)butyl(benzaldeyde-4-ethynyl) phthalocyaninatozinc(II) **4** (100 mg, 0.115 mmol), pyridine (10 mL) and pyridine-HCl (0.3 g) were stirred under argon for 24 hrs. After this time, stirring and heating was stopped and to the hot mixture H_2O (10 mL) was added. The mixture was allowed to cool and resulting precipitate was collected by centrifugation at 3,250 rpm. The bluish green precipitate was washed several times with water, MeOH followed by drying on high vacuum to obtain 91 mg of Pc **5**, a 98% yield.

^{1}H-NMR (d_8-THF, 400 MHz) δ_H , ppm 10. 05 (s, 1H), 8.70-7.19 (m, 16H), 1.71-1.88 (m, 27H)

UV/Vis (CH_2Cl_2): λ_{max} 693, 677, 646, 620, 338 nm

MALDI-TOF MS (terthiophene): calc. for $C_{53}H_{46}N_8$: $[M]^+$: *m/z*: 810.38, found 810.55

Phthalocyanine-C_{60} dyad 7

A solution of tri(*tert*)butyl(benzaldeyde-4-ethynyl) Pc **6** (20 mg, 0.0247 mmol), C_{60} (59 mg, 0.0819 mmol), sarcosine (15.8 mg, 0.177 mmol) in an anhydrous toluene (25 mL) was heated to reflux with stirring under argon atmosphere for 22 hrs. After this time, solvent was removed under reduced pressure and the crude product purified by column chromatography toluene/CS_2 (1:1) to obtain a green product 26.7 mg, 69 %.

^{1}H-NMR (d_8-toluene, 400 MHz) δ_H , ppm 9.14-8.65 (m, 9H), 7.96-7.68 (m, 7H), 4.77 (s, 1H), 4.67-4.64 (d, *J*=12, 1H), 3.99-3.97 (d, *J*=8, 1H), 2.62 (s, 3H, N-CH_3), 1.66-1.63 (m, 27 H), 2.29 (br s, 2H)

UV/Vis (THF): λ_{max} 694, 672, 644, 613, 343 nm

MALDI-TOF MS (dithranol): calc. for $C_{115}H_{51}N_9$: $[M]^+$: *m/z*: 1558.43 found 1558.79

Tri (*tert*)butyl(benzylalcohol-4-ethynyl)phthalocyaninato 8

Tri(*tert*)butyl(benzylalcohol-4-ethynyl) phthalocyaninatozinc(II) **3** (36 mg, 0.412 mmol), pyridine (10 ml) and pyridine-HCl (0.089 g) were heated at 120 ^{o}C while stirring under argon for 21 hrs after which to the hot mixture H_2O (5 mL) was added. The mixture was allowed to cool and resulting precipitate was collected by centrifugation at 3,250 rpm. The green precipitate was washed several times with water, MeOH followed by drying on high vacuum to obtain 12.7 mg of Pc **6**, a 38% yield.

^{1}H-NMR (d_8-toluene, 400 MHz) δ_H , ppm

UV/Vis (THF): λ_{max} 694, 667, 644, 611, 344 nm

MALDI-TOF MS (terthiophene): calc. for $C_{53}H_{48}N_8O$: $[M]^+$: *m/z*: 812.39 found 812.44

N-methyl-2-(*p*-methoxyphenyl)-3, 4-fulleropyrrolidine 9

A mixture of C_{60} (216 mg, 0.3 mmol), 4-anisaldeyde (20 mg, 0.15 mmol), and sarcosine (136 mg, 1.5 mmol) in toluene (60 mL) was warmed to reflux under argon environment while stirring for 26 hrs. Solvent was removed under reduced pressure. The crude was purified on silica column chromatography, toluene/EtOAc (99:1) to obtain a brown powder fullerene **9** (78.8 mg, 60% yield).

^{1}H-NMR ($CDCl_3$, 400 MHz) δ_H , ppm 7.69 (br, s, 2H), 6.95-6.93 (d, *J*=8, 2H), 4.97-4.95 (d, *J*=8, 2H), 4.87 (s, 1H), 4.25-4.21 (d, *J*=12, 2H), 3.80 (s, 3H, N-CH_3), 2.77 (s, 3H, O-CH_3)

MALDI-TOF MS (terthiophene): calc. for $C_{53}H_{48}N_8O$: $[M]^+$: *m/z*: 883.10 found 883.18

N-methyl-2-(*p*-benzylalcohol)-3, 4-fulleropyrrolidine 10

To a solution of fullerene **9** (32 mg, 0.0362 mmol) in toluene (20 mL) immersed in ice-cold water, 1.5 mL of 1M BBr_3 (1.5 mmol) in dichloromethane was added drop wise. The mixture was stirred at room temperature for 24 hrs under an argon atmosphere. The mixture was transferred to a separating funnel and washed with water (30 mL×3) and then the solvent was removed under a reduced pressure. The crude was purified by a column chromatography on silica gel, toluene/MeOH (19:1) to obtain a brown fullerene **10** (20 mg, 65%). ^{1}H-NMR ($CDCl_3$, 400 MHz) δ_H , ppm 7.65 (br, s, 2H), 6.85-6.83 (d, *J*=8, 2H), 4.97-4.95 (d, *J*=8, 1H), 4. 86 (s, 1H), 4.25-4.23 (d, *J*=8, 2H), 2. 973 (s, 3H)

UV/Vis (Toluene): λ_{max} 704, 433, 310 nm

MALDI-TOF MS (terthiophene): calc. for $C_{69}H_{11}NO$: $[M]^+$: *m/z*: 869.08 found 869.15

2.2 Synthesis and photophysical studies of a novel carotenoid silicon Pc-C_{60} triad

Due to the presence of 18 π-electron aromatic cloud, most Pcs have cofacial intermolecular π-π interactions, even at low concentrations, and this causes aggregation which leads to fluorescence quenching and poor solubility.[70] The steric effect of the axial substituents on silicon phthalocyanines (SiPc) have been shown to exhibit a non-aggregation characteristics and increased solubility in common organic solvents. [71]

Phthalocyanines with two symmetrical fullerene substituents connected axially through central silicon have been reported in the last few years. [72-75] In addition to improving the solubility by diminishing intermolecular interactions, fullerenes bring additional properties to the phthalocyanine molecule. As mentioned earlier, fullerenes (C_{60}) are good electron acceptors and have low reorganization energy; λ. [46]

C_{60}-SiPc-C_{60} triads are good models for artificial photosynthetic reaction centers. However, to develop a better mimic of natural photosynthesis, artificial photosynthesis will require a system with two electron donors and one acceptor where a long-lived charge separation can be achieved via a step wise electron transfer.[76]

In natural photosynthesis the roles of carotenoids includes acting as an antennae by transferring excitation energy to the photosynthetic reaction center[77] and protection by quenching chlorophyll triplet states to prevent generation of the cell damaging reactive singlet oxygen species.[49,77] Excited state carotene has a high energy (~1.9 eV)[78] and this allows it to act as antenna via singlet-singlet energy transfer, but the triplet state is much lower in energy (0.63 eV) than singlet oxygen (0.98 eV)[79] and triplet chlorophyll (~1.3 eV)[80] and these properties allow it

to be a good energy acceptor as well. Figure 20 shows some of the naturally occurring carotenoids that play a light-harvesting role in photosynthesis.

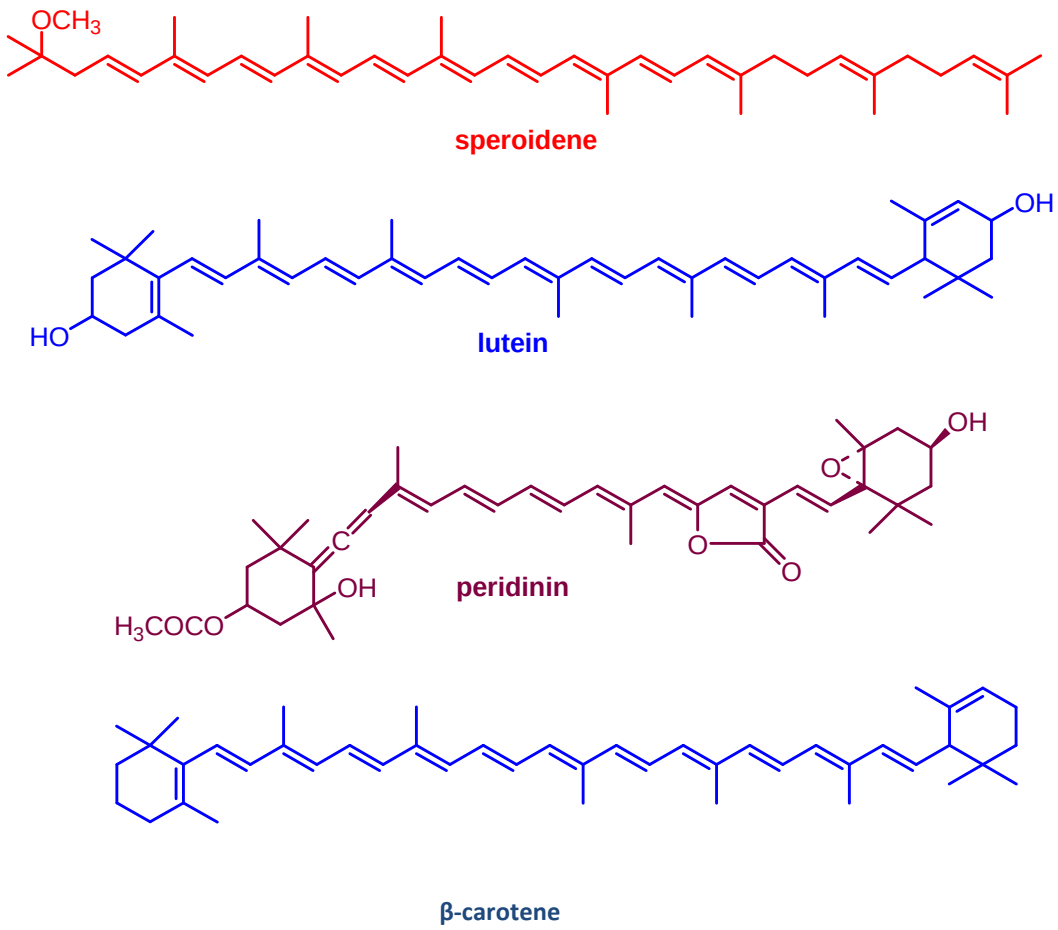

Figure 20: Molecular structures of four important carotenoids.[81]

In addition, under stress conditions, for example in Mn-depleted PSII or at low temperature, β-carotene has been observed to be an electron donor to the highly oxidizing $P680^{+}$.[82]

Incorporating carotenoids into artificial photosynthetic reaction center may lead to a long-lived charge separated state by charge shift and provide photoprotection. Also use of carotenoids and phthalocyanines together will ensure access to a wider spectral window of solar radiation. Hence an asymmetrical axial linkage on SiPc with potential electron donor on one side and a potential electron acceptor on the other side will be a good mimic for natural photosynthesis. To this end, synthesis of carotene and fullerene axially connected to a SiPc was achieved. Electron transfer and energy transfer processes in the triad were investigated by use of spectroscopic and electrochemical methods.

Results and Discussions

Synthesis

Axially substituted phthalocyanine **11** was afforded by a reaction between a commercially available silicon phthalocyanine dihydroxide with 4-iodobenzoate and 4-formylbenzoate (1:1) as shown in scheme 10. The crude product contained a statistical mixture of diformylbenzoate, diiodobenzoate, and the target asymmetrically linked 4-formylbenzoate-4-iodobenzoate SiPc products. By column purification, the bluish green phthalocyanine **11** was obtained in 30% yield. MALDI-TOF (terthiophene matrix) showed the molecular ion peak at m/z=1160.3 as the 100 % peak, fragments were also observed at m/z=1011.33 (target molecule with the formylbenzoate cleaved off) and m/z=913.45 (target molecule with the iodobenzoate cleaved off). Jesse Bergkamp and co-workers reported a similar kind of fragmentation pattern with axial ether linkages on SiPc.[83]

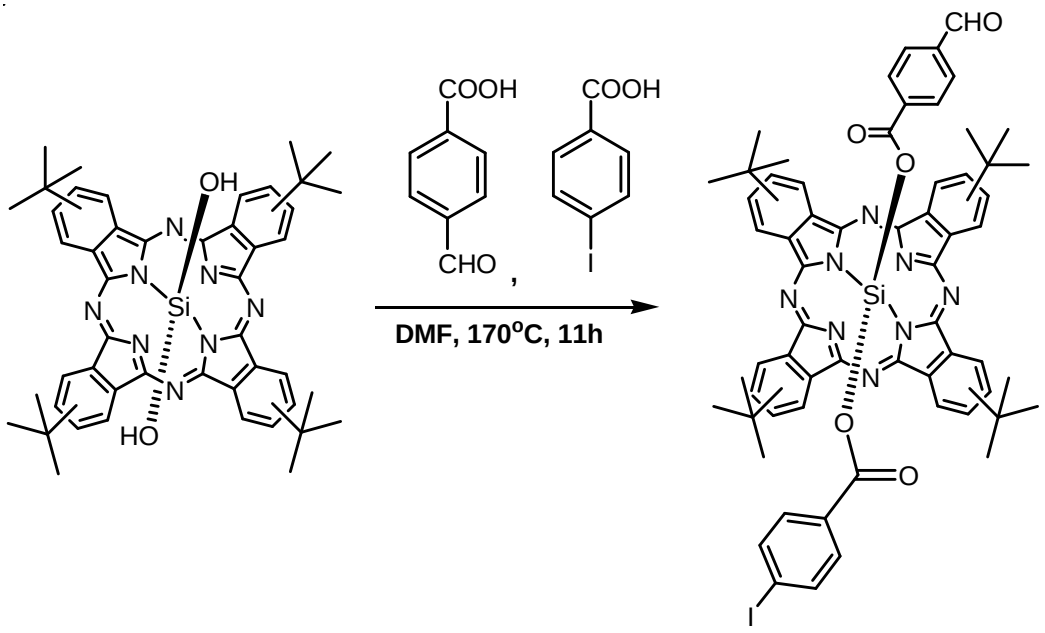

11

Scheme 10: Synthesis of (*p*-iodobenzoate)-(*p*-formylbenzoate)(2,9,16,23-tetra-*ter*t-butylphthalocyaninato)silicon **11**.

Heating a mixture of phthalocyanine **11**, sarcosine and C_{60} in *o*-dichlorobenzene at 140^{o}C afforded SiPc-C_{60} dyad **12** as shown in scheme 11. Column purification gave a non-fluorescent green compound dyad **2**, 40 % yield. MALDI-TOF (TBPPM matrix, mode-reflector 6000) showed the molecular ion peak at m/z=1909.2 as the only peak, no fragments beside the peak at m/z=720 for the unfunctionalized C_{60} was observed.

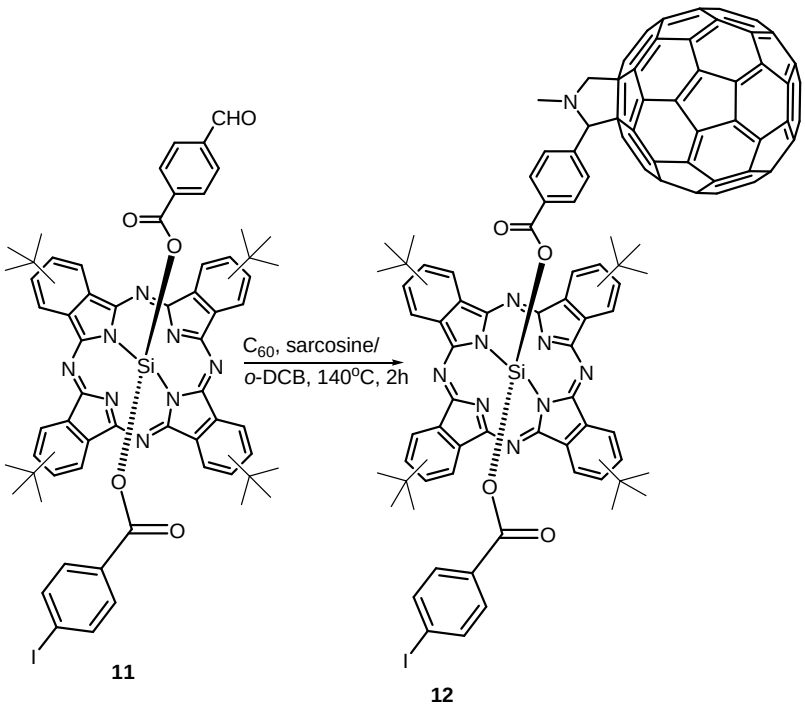

Scheme 11: (*p*-iodobenzoate)-[*p*-(N-methyl-3', 4'-fulleropyrrodin-2'-yl) benzoate] (2, 9, 16, 23-tetra-*ter*t-butylphthalocyaninato) silicon **12**.

Compounds **13** and **14** shown in scheme 12 were synthesized following a literature method.[84] Reacting commercially obtained β-apocarotenal with 4-(N-acetylamino)benzyltriphenylphosphonium bromide (kindly donated by Dr. Smitha Pillai) in a Wittig type reaction in presence of sodium methoxide in dimethyl sulfoxide solvent gave 4-amidophenyl-β-carotene **13**, 30% yield after column purification and crystallization over hexane/dichloromethane to remove the *cis* isomer.

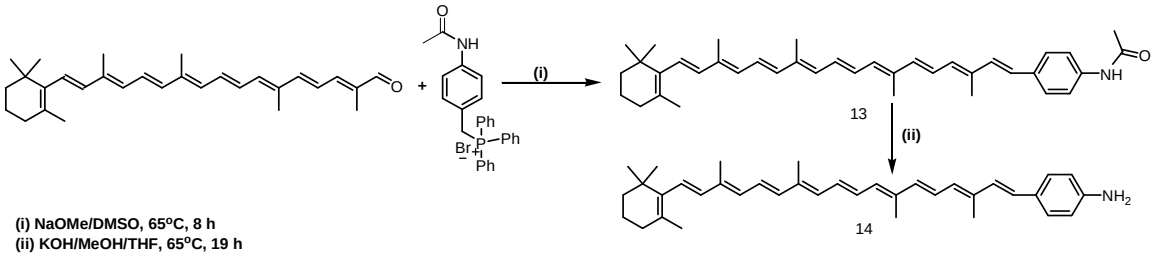

Schemes 12: synthesis of (*p*-7'-apo-7'-(4-aminophenyl)-β-carotene **14**.

4-Amidophenyl-β-carotene **13** was hydrolyzed using methanolic potassium hydroxide in THF at 65 ^{o}C to obtain 4-aminophenyl-β-carotene **14** in near quantitative yield of 94% after column purification.

Synthesis of carotene-SiPc-C_{60} triad **15** was attempted by stirring a mixture of SiPc-C_{60} dyad **12**, 4-amino-β-carotene **14** in presence of a new commercially acquired tris(dibenzylidene acetone) dipalladium (0)/BINAP/sodium *tert*-butoxide (1:3:4) in freshly distilled and degassed toluene and heated at 80^{o}C under argon environment (scheme 13). No product was realized after 7 hours of stirring. Increasing the temperature to 110 ^{o}C, addition of more catalysts and increase of the reaction time to 45 hours did not help to form a product. After stirring was stopped and the mixture cooled to room temperature, the reactants were partially recovered. It appears that the presence of C_{60} may have interfered with the effectiveness of the palladium (0) catalyst.

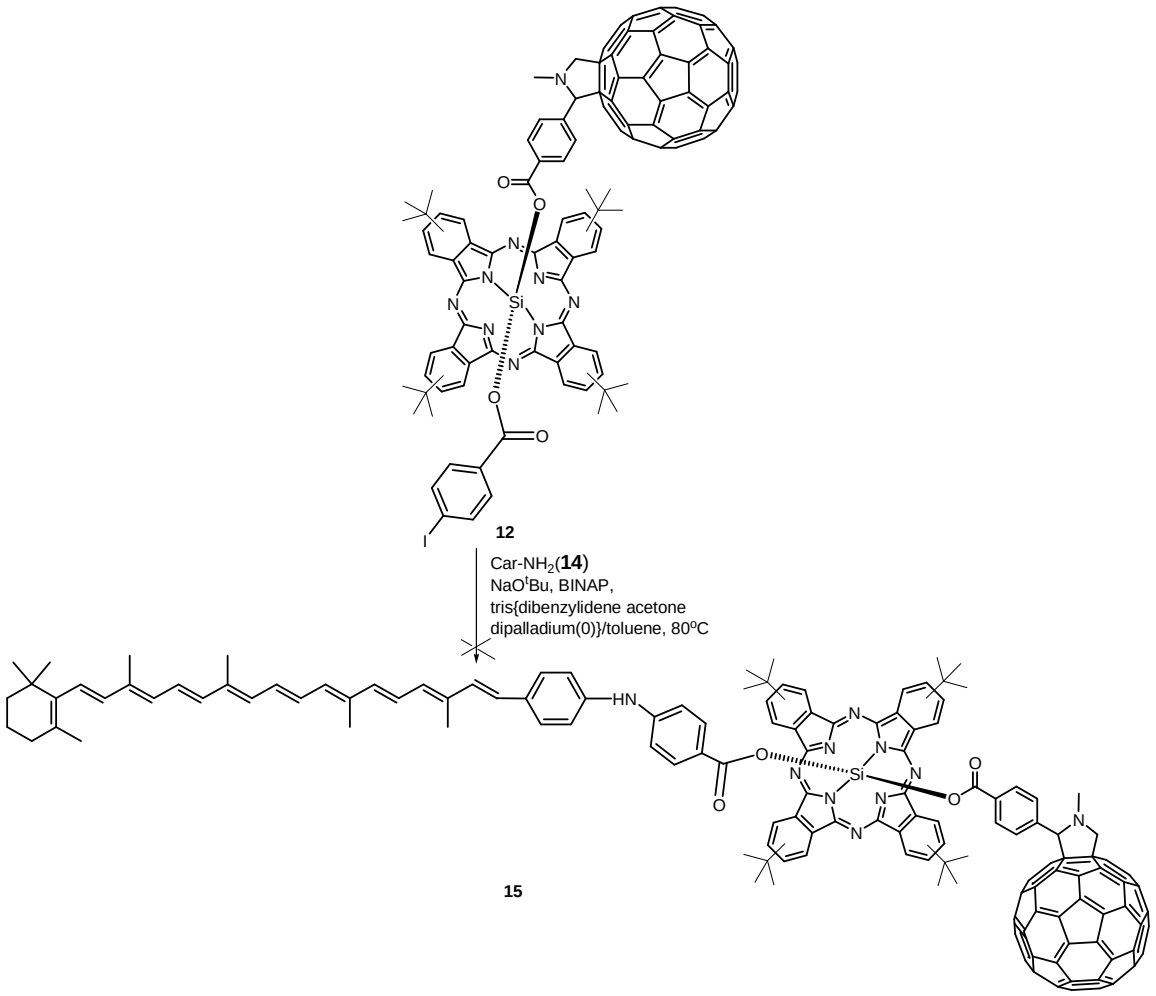

Scheme 13: Attempted synthesis of [*p*-7'-apo-7'-(4-aminophenyl)-β-carotenobenzoate]-[*p*--(N-methyl-3', 4'-fulleropyrrodin-2'-yl) benzoate] (2, 9, 16, 23-tetra-*ter*t-butylphthalocyaninato) silicon **15**.

Carotene-SiPc dyad **16** was synthesized by reacting SiPc **11** with 4-aminophenyl-β-carotene **14** in presence of a new commercially obtained catalyst/ligand/base mixture of tris(dibenzylidene acetone) dipalladium (0)/BINAP/sodium t*er*t-butoxide-1:3:4 in freshly distilled and degassed toluene at 80 ^{o}C (scheme 14), on column purification a yellowish green product, compound **16** was obtained, 33% yield. It was observed the yield was inversely

dependent on the temperature; lowering the temperature increases the yield. Increasing the temperature to 90^{o}C, the yield decreased to 12%, at 95^{o}C and the yield was 4% at 100^{o}C there was no detectable product formed. This is thought to be as a result of decomposition of the reaction intermediates, this conclusion is supported by the presence of multiple unaccounted for spots on the analytical TLC of the reaction crude and it was also observed that the number of spots increased with increasing temperature.

MALDI-TOF (Tertiophene matrix) showed only a tiny peak of the molecular ion, m/z=1537, the major peaks observed were the fragments, m/z=913.6, 100% intensity (target product with 4-aminophenyl-β-carotenobenzoate cleaved off) and m/z=1389.0, 20% intensity (target product with 4-formylbenzoate cleaved off).

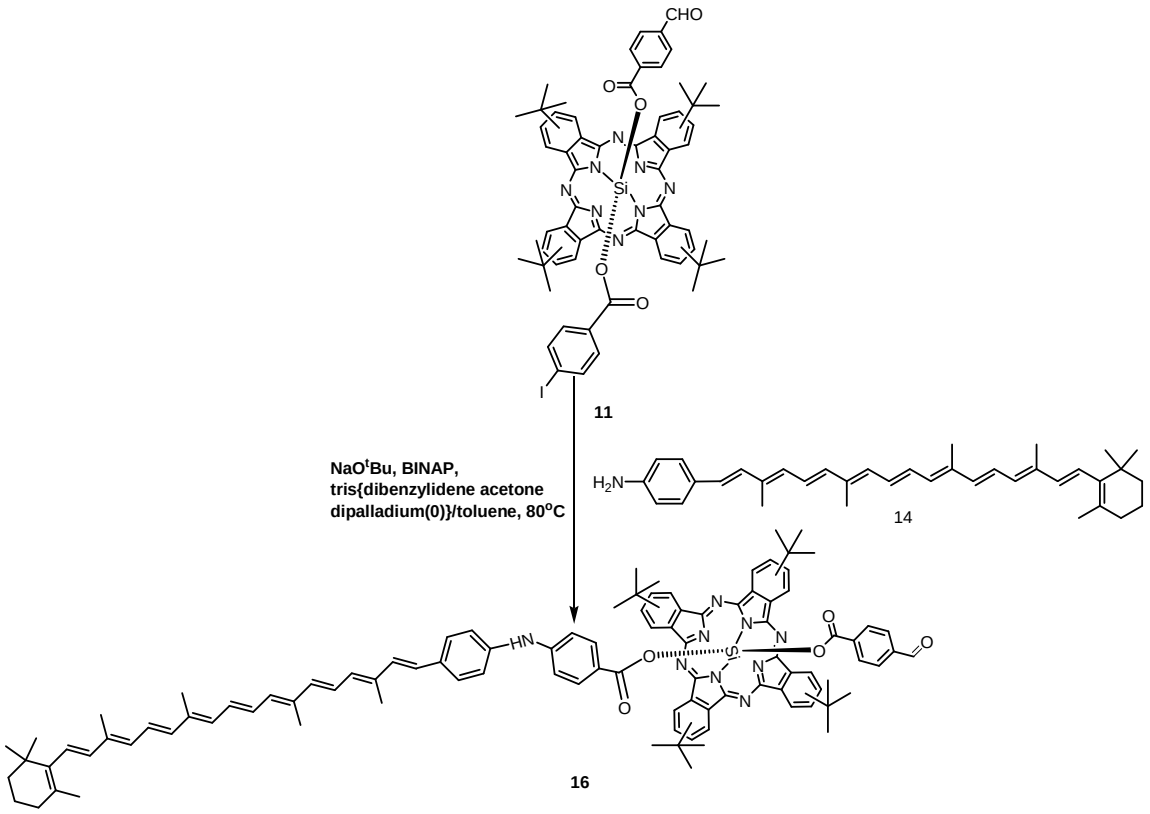

Scheme 14: Synthesis of (*p*-7'-apo-7'-(4-aminophenyl)-β-carotenobenzoate)-(*p*-formylbenzoate)(2,9,16,23-tetra-*ter*t-butylphthalocyaninato)silicon **16**.

As shown by scheme 15, carotene-SiPc-C_{60} triad **17** was afforded by a single Prato reaction from (*p*-7'-apo-7'-(4-aminophenyl)-β-carotenobenzoate)-(*p*-formylbenzoate)(2,9,16,23-tetra-*ter*t-butylphthalocyaninato)silicon **16** in 62% yield after purification by silica column chromatography.

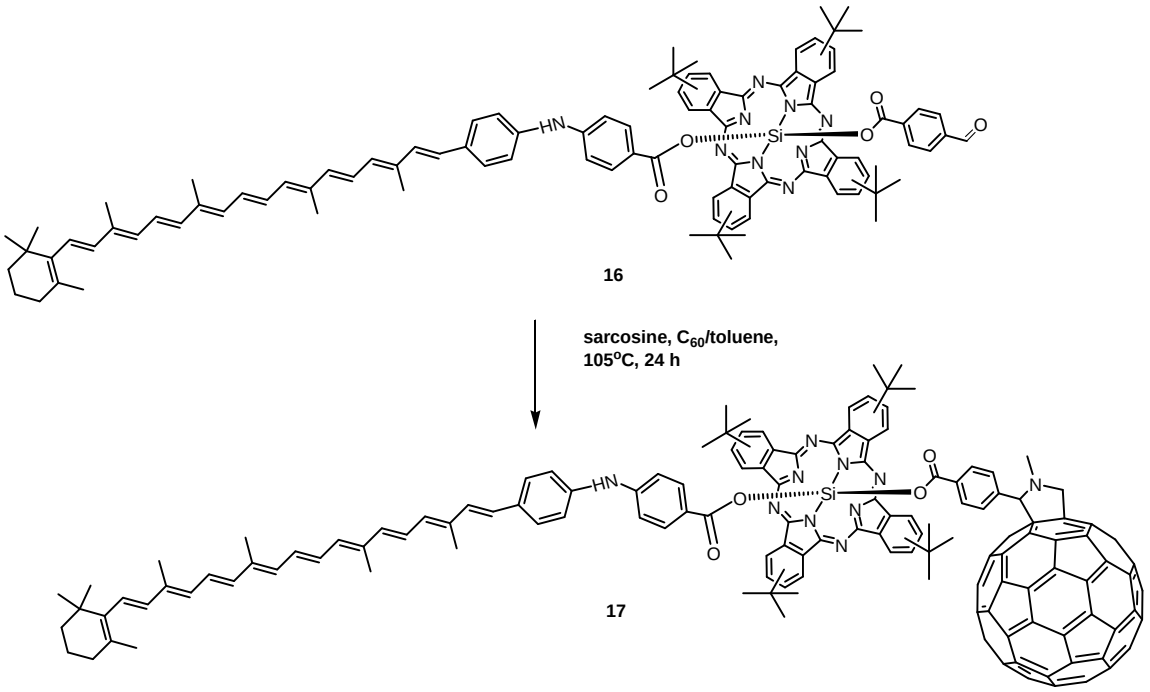

Scheme 15: Synthesis of [*p*-7'-apo-7'-(4-aminophenyl)-β-carotenobenzoate]-[*p*--(N-methyl-3', 4'-fulleropyrrodin-2'-yl) benzoate] (2, 9, 16, 23-tetra-*tert*-butylphthalocyaninato) silicon **17**.

MALDI-TOF (TBPPM matrix) showed the molecular ion peak at m/z=2284.5 as the only peak, no fragments beside the peak at m/z=720 for the unfunctionalized C_{60} was observed.

The model compound, SiPc **18** and compound **19** were prepared as shown in scheme 16. Reacting commercially obtained silicon phthalocyanine dihydroxide with 4-toluic acid/4-formyl benzoic acid mixture (1:1) gave SiPc **18** and SiPc **19** after column purification in 17% and 27% yield, respectively. MALDI-TOF (Tertiophene matrix) showed both the molecular ion peaks and the fragments peaks. For Pc **18**, peaks were observed at m/z=1048.5, which was the molecular ion peak, m/z=913.4 (target molecule with the 4-methylbenzoate cleaved off) and m/z=899.5 (target molecule with the 4-formylbenzoate cleaved off). For Pc **19,** peaks were observed at

m/z=1034.5, which was the molecular ion peak and m/z=899.4 (target molecule with the 4-methylbenzoate cleaved off).

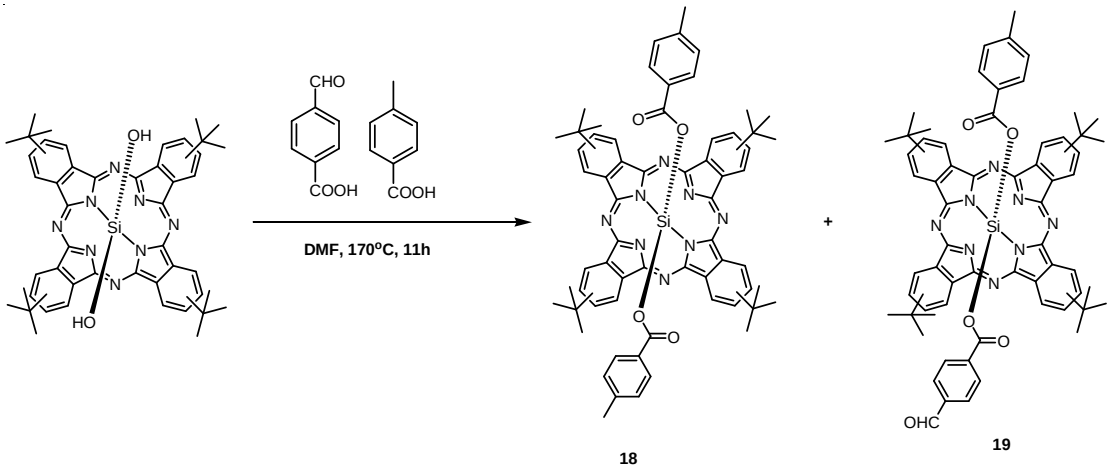

Scheme 16: Bis(*p*-methylbenzoate)(2,9,16,23-tetra-*ter*t-butylphthalocyaninato)silicon **18** and (*p*-formylbenzoate)-(*p*-methylbenzoate)(2,9,16,23-tetra-*ter*t-butylphthalocyaninato)silicon **19**.

To obtain SiPc-C_{60} dyad **20**, Pc **19** was reacted with C_{60} and sarcosine in *o*-dichlorobenzene (scheme 17). Column purification afforded a near quantitative yield of dyad **10**, 94%.

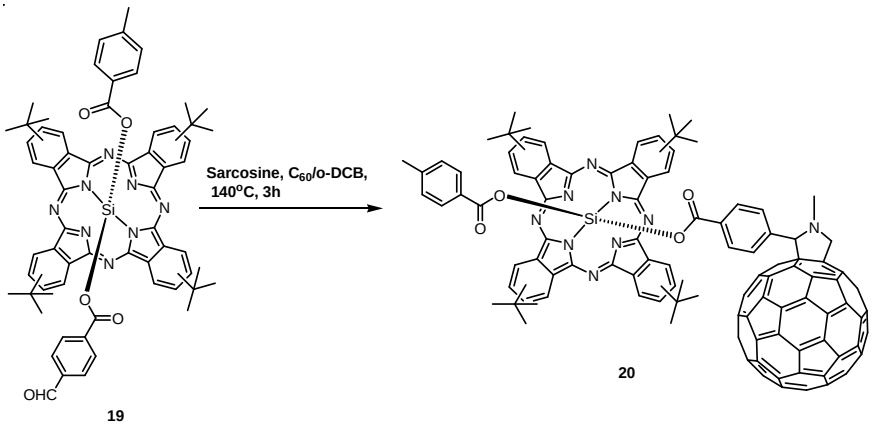

Scheme 17: (*p*-methylbenzoate)-[*p*-(N-methyl-3', 4'-fulleropyrrodin-2'-yl) benzoate] (2, 9, 16, 23-tetra-*ter*t-butylphthalocyaninato) silicon **20**.

MALDI-TOF (terthiophene matrix) showed the molecular ion peak at m/z=1795.4 as the only peak, no fragments beside the peak at m/z=720 for the unfunctionalised C_{60} was observed.

As shown in scheme 18, C_{60} model **21** was prepared by a Prato type reaction of 4-methylester benzaldeyde, C_{60} and sarcosine in refluxing toluene. On column purification a yield of 14% of C_{60} **21** was obtained. It was observed that no detectable product was obtained when the reaction was carried out in *o*-dichlorobenzene (*o*-DCB), this may be attributed to solubility difference of the reactants in toluene and *o*-DCB. Better solubility in the former may be favoring product formation.

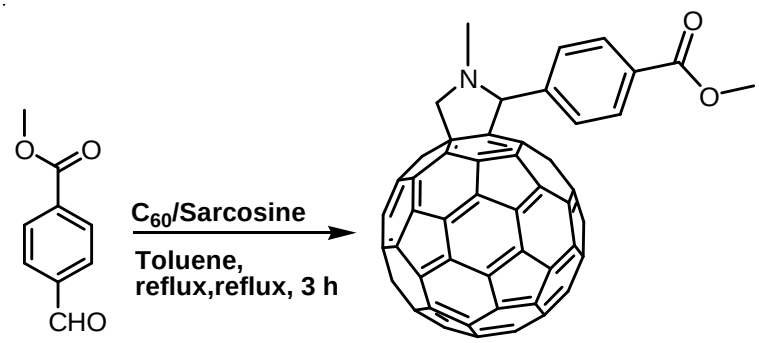

21

Scheme 18: N-Methyl-2-(*p*-methylbenzoate)-3, 4-fulleropyrrolidine **21**.

The ^1H NMR ($CDCl_3$) spectrum of phthalocyanine **11** showed an up field shift of the signals of benzoate protons to the range 6.67-4.83 ppm as opposed to the expected region of around 8 ppm for phenyl aromatic protons. This observation confirms the influence of the shielding effect of the phthalocyanine π cloud. In addition, the presence of four distinct benzoate signals at 6.73, 4.58, 5.26 and 4.83 ppm gives further support to the presence of an asymmetric axial linkage on the phthalocyanine. On the other hand, attachment of the carotene to the

phthalocyanine to form dyad **16** had no effect on the resonance of either of the components, i.e. phthalocyanine and carotene. The ^{1}H NMR ($CDCl_3$) spectrum of carotene-phthalocyanine dyad **16** was a sum of the spectrum of the two parts. This could be attributed to the presence of the two phenyl rings that separate the two components and hence protect the carotene from the shielding effect of the phthalocyanine aromatic electron cloud. In contrast, earlier work by our group showed that when a carotenoid is directly, axially attached to SiPc there was a very significant shift in the resonance of the carotene protons.[85] On attaching the C_{60} to form the triad **17**, the up field shift of the benzoate protons and those protons of the pyrrolidine linker between the C_{60} and the phthalocyanine were similar to the one reported by Martin-Gomis and co-workers. [73] The signal of the benzoate protons adjacent to C_{60}, pyrrolidine protons and N-CH_3 protons were all shifted up field when compared to the corresponding protons of the C_{60} model **21**. Benzoate protons were shifted from 7.84 ppm to 5.17 ppm, the pyrrolidine protons from 4.97, 4.96, and 4.25 ppm were moved to 4.63, 4.28, and 3.84 ppm; and the N-CH_3 protons were shifted from 2.78 to 2.17 ppm. This observation suggests that the attached C_{60} is in the range of the strong aromatic current of the Pc.

Steady-state Absorption

The UV/Vis absorption spectrum of the triad **17** and model compounds were taken in dichloromethane. It was observed that the absorption spectrum of triad **17** showed that the Q-band of the phthalocyanine is unperturbed on formation of the triad (figure 21); the addition of the carotenoid pigment causes a larger increase in absorption in the middle of the spectrum. Figure 22 shows that the carotenoid moiety band at 480 nm in carotene-Si Pc dyad **16** is red-

shifted compared to model 4-aminophenyl-β-carotene, which has a maximum absorbance at 475 nm. The carotene moiety absorption maximum is at 479 nm in triad **17**, not a significant change from that observed in the carotene-Pc **16** dyad. However, the absorption spectrum of the SiPc-C_{60} dyad **20** in dichloromethane is a close superposition of the spectra of the component chromophores making up the dyad. This is an indication that there is not much electronic interaction between the individual chromophores at the ground state. In addition, the sharp Q-bands are indications that the silicon phthalocyanine is not aggregating. C_{60} has its intense absorption at 220, 265 and 330 nm[42] and these bands are buried under the stronger Soret transition of the phthalocyanine and are only seen as an overall intensification of the absorption in the UV/Vis region.

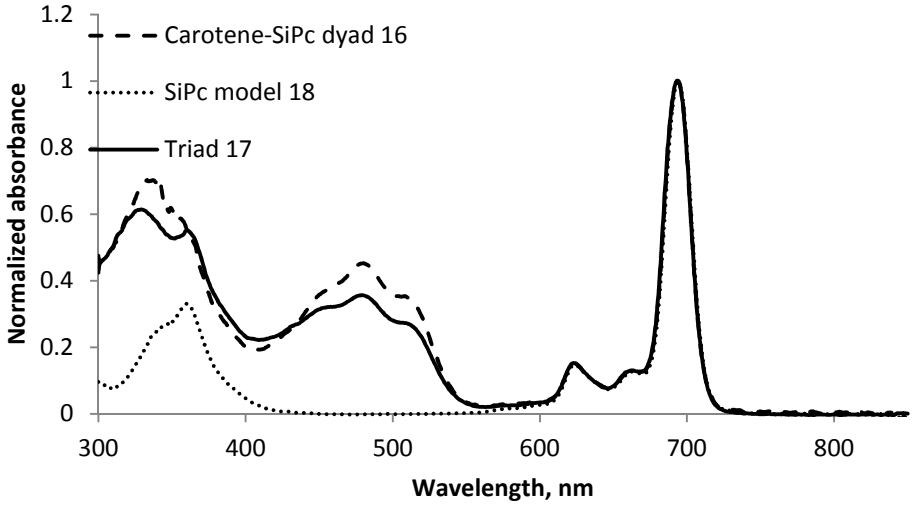

Figure 21: Normalized UV/Vis absorption spectrum of triad **17** (—), carotene-SiPc dyad **16** (- - -) and SiPc model **18** (…..) .

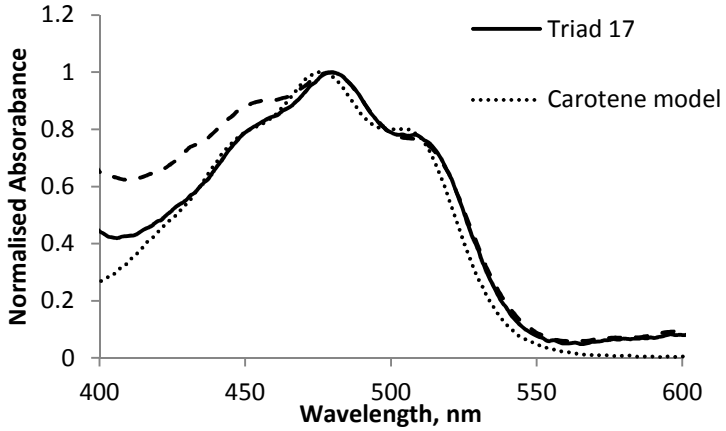

Figure 22: Normalized (λ=480 nm) uv/vis absorption spectrum of triad **17** (—), carotene-sipc dyad **16** (- - - -) and carotene model (…..)

The UV/Vis spectrum of SiPc **18** and SiPc **19** were exactly the same and yet at the *para*-position of the phenyl moiety on SiPc **18,** is the electron donating methyl group while on one of the *para*-position of the phenyl moiety of SiPc **19** there is the electron withdrawing formyl group. Based on this observation it can be concluded that the functional group on the *para*-position of the axial phenyl substituent does not have any influence on the conjugation of the Pc core.

Electrochemistry

Electrochemistry measurements were performed by Dr. Maxime Fournier

Table 4: First reduction potentials of C_{60} model **21** and C_{60}-SiPc dyad **20**.

Molecule	E_{red}^{1}
18	-0.47
21	-0.56
20	-0.64

Table 5: Oxidation potentials of carotene model, carotene-SiPc dyad **16**, SiPc model **18**, C_{60}-SiPc dyad **20**.

Molecule	Eox^1	Eox^2
Carotene model	0.49	
16	0.47	0.93
18	0.93	
20	1.10	

The first charge separated state, Car-SiPc$^{\bullet+}$-$C_{60}^{\bullet-}$ lies at 1.48 eV (figure 25) above the ground state, therefore the charge recombination to reform the ground state is likely to lie in the inverted region of the Marcus curve, where an increase in the driving force past the optimum leads to a decrease in electron transfer rate.[35,86,87] This phenomenon is expected to favor the charge shift towards the carotene moiety.

Electron transfer rates are determined by thermodynamics, steric and electronic effects. In the present triad, an initial electron transfer from excited singlet SiPc to C_{60}, followed by a charge shift to the carotenoid moiety to form a long-living charge separated state ($C^{\bullet+}$-SiPc-$C_{60}^{\bullet-}$) is thermodynamically favorable.

Steady-State Emission

Figure 23 shows the steady-state emission spectra of Car-SiPc-C_{60} triad **17** taken in toluene and benzonitrile after excitation at 363 nm.

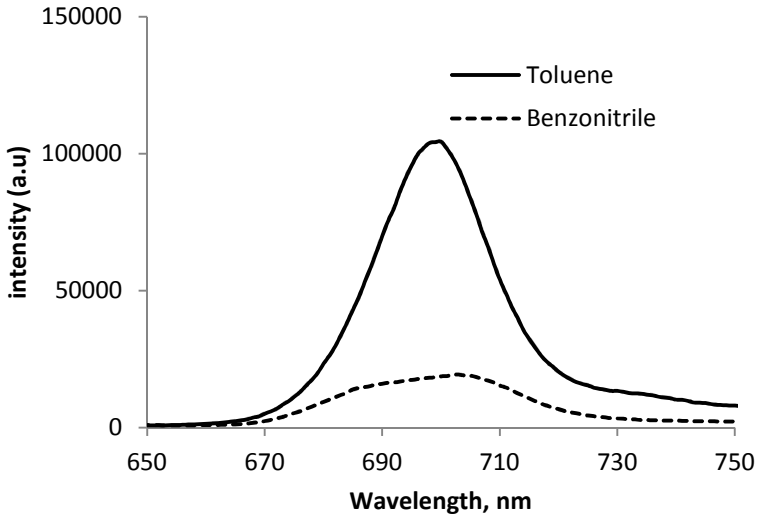

Figure 23: Emission spectra of Car-SiPc-C_{60} triad **17** in toluene and benzonitrile after excitation at 363 nm

Time-resolved Emission

The steady-state emission spectra of triad **17** shown in figure 23 indicate that there is solvent-dependence quenching, an indirect indication of existence of electron transfer in polar solvent. To get an insight into the nature of fluorescence, time resolved fluorescence experiments were carried out using single-photon-counting technique (Experiments were done by Robert Schimtz). The results are summarized in Table 6

Compound	Toluene	Benzonitrile
SiPc **18**	7.4	6.43
SiPc-C_{60} **20**	0.035 (65%)	~0.035 (52%)
	1.69 (26%)	0.490 (46%)
	2.62 (9%)	4.84 (2%)
Car-SiPc-C_{60} **17**	0.030 (74%)	0.020 (84%)
	0.303 (8%)	0.430 (13%)
	1.32 (14%)	5.56 (3%)
	3.66 (4%)	

Table 6: Lifetimes (ns) of excited singlet states of Pc moieties as determined from time-resolved fluorescence studies in toluene and benzonitrile. The excitation wavelength was 635 nm.

As was observed with peripheral ZnPc **3** and H_2Pc **8** models, SiPc **18** model also shows similar lifetime of excited state in both toluene and benzonitrile. The fluorescence lifetimes of model SiPc **18** in toluene and benzonitrile were 7.4 and 6.43 ns respectively. The lifetime of excited Pc is significantly reduced in dyad **20** in both solvents but roughly by the same magnitude, this solvent independent quenching may be due to energy transfer from the locally excited SiPc to C_{60}. In toluene for dyad **20**, there is presence of characteristic $^1C_{60}$ emission (1.69 ns, 26 %) and this is missing in benzonitrile. The same phenomenon was observed in the triad

17, where the characteristic $^1C_{60}$ emission occurs with 1.32 ns (14%) lifetime and this is again absent in benzonitrile, and it can be concluded that in benzonitrile, either $^1C_{60}$ doesn't form or it get quenched very fast as soon as it forms.

Time-resolved absorption studies

Pump-probe transient absorption experiments were carried out to characterize the various excited species in the dyad models and the triad and to allow detection of nonemissive species such as charge-separated states. Experiments were performed by Dr. Gerdenis Kodis.

The occurrence of electron transfer from the excited state Pc to the C_{60} acceptor in the SiPc-C_{60} dyad **20** was confirmed by femtosecond laser flash photolysis experiment. A degassed benzonitrile solution containing SiPc-C_{60} dyad **20** was subjected to 100 fs at 800 nm laser pulses. The resulting transients were monitored in the visible and the near-IR region (figure 24). Distinct characteristic absorption bands due to $SiPc^{\bullet+}$ (555 nm and 880 nm)[88,89] and $C_{60}^{\bullet-}$ (1000 nm)[90,91] were observed. This data is in agreement with that reported by Martin-Gomis and co-workers for C_{60}-SiPc-C_{60}.[73] This is a clear evidence of formation of charge-separated (CS) state. A long-lived band at λ=530 nm is a characteristic of $^3SiPc^*$.[88]

The presence of the long-lived $^3SiPc^*$ is an evidence that the back electron transfer from the CS state forms the excited SiPc triplet state instead of the ground state because of the lower triplet energy (1.26 eV)[70]) compared to the CS state (1.48 eV) determined from the redox potentials of the model compounds as shown in figure 25.

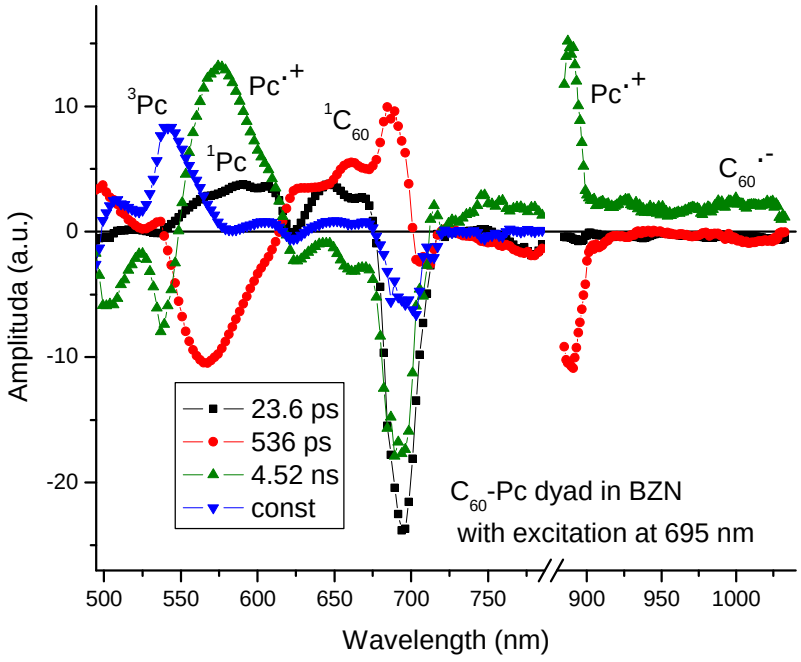

Figure 24: Differential absorption spectra (visible and near-infrared) of SiPc-C_{60} dyad **20** upon femtosecond photolysis (695 nm) in deaerated benzonitrile.

Overall, there is energy transfer from Pc singlet excited state to form C_{60} singlet excited state with ~24 ps. After that there is slow (with ~540 ps) formation of $Pc^{\bullet+}$-$C_{60}^{\bullet-}$ CS state, which is expected due to closeness in energy between Pc-$^1C_{60}$ (1.75 eV) and $Pc^{\bullet+}$-$C_{60}^{\bullet-}$ (1.48 eV) (figure 25).

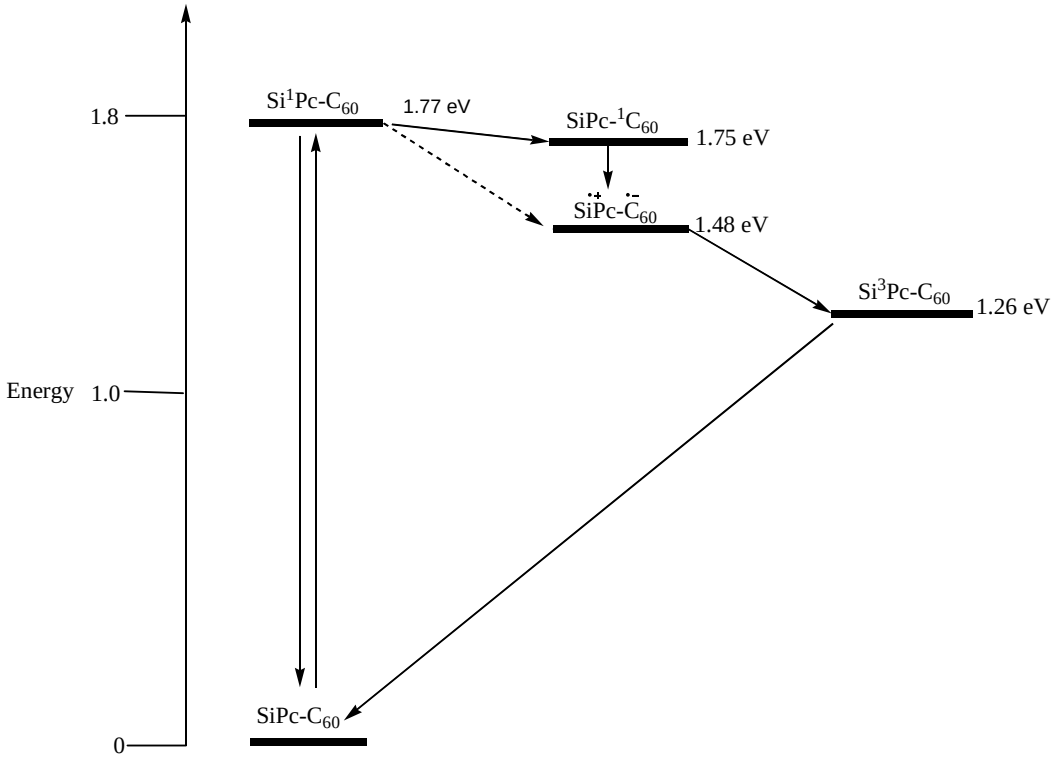

Figure 25: High energy states and possible interconversion pathways for SiPc-C_{60} dyad **20** following photoexcitation of the SiPc chromophore.

The energy of the charge-separated state is estimated from the cyclic voltammetric data of model compounds in benzonitrile.

The CS state decays in ~4.5 ns. Because of the slow formation of CS state there is substantial formation of C_{60} triplet excited state which decays to Pc triplet excited state.

The charge recombination (CR) of the CS state to directly regenerate the ground state has a driving force of , $-\Delta G_{CR}$=1.48 eV and this must be lying in the inverted region of the Marcus curve and this explains the long lifetime of the CS state and the decay first to the long-lived $^3SiPc^*$ and then to the ground state.

The decay associated spectrum of Car-SiPc dyad **16** dissolved in benzonitrile and excited at 695 nm is shown in figure 26. The excitation light at 695 nm is exclusively absorbed by the Pc moiety leading to a fast (with 3.3 ps) formation of $Car^{\cdot+}$-$Pc^{\cdot-}$ CS state. This is evidenced by the presence of a near-IR (~980 nm) band, a characteristic absorption of a carotenoid radical species. Previous work from our group on carotene-SiPc-carotene triad where the carotene lacked the aminophenyl linker showed a carotenoid radical at 860 nm.[92] The bathochromic shift in the carotenoid radical transient of the current may be attributed to the extended conjugation which makes it a better electron donor by raising the HOMO.

The transient in the 550-640 nm range also rises and decays with same time constant as the carotenoid radical. The huge negative amplitude at ~690 nm also recovers in the same time constant and is associated with the ground state bleaching of SiPc moiety. The match of the rise of the carotenoid radical cation transient with the decay of SiPc S_1 level (3.3 ps) is an evidence of electron transfer from the carotenoid to the excited $^1SiPc^*$ state as a dominant fluorescence quenching mechanism.

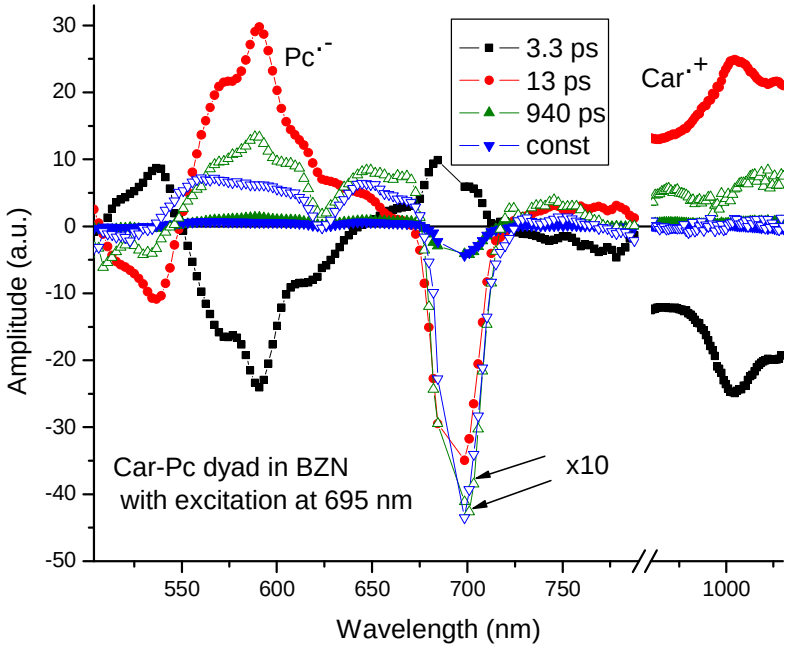

Figure 26: Decay associated spectra of the transient absorption of Car-SiPc dyad **16** in benzonitrile after a 100 fs laser pulse at 695 nm.

As shown on figure 26, the CS state forms after 3.3 ps and decays in 13 ps. There is some minor dyad conformation which shows much slower CS state recombination lifetime of ~940 ps. There is small impurity of SiPc that has a singlet excited state that does not decay on time scale measured. The fast CS and CR is in agreement with the large driving force for both processes, $-\Delta G_{CS} = 0.81$ and the $-\Delta G_{CR} = 0.96$ (figure 27).

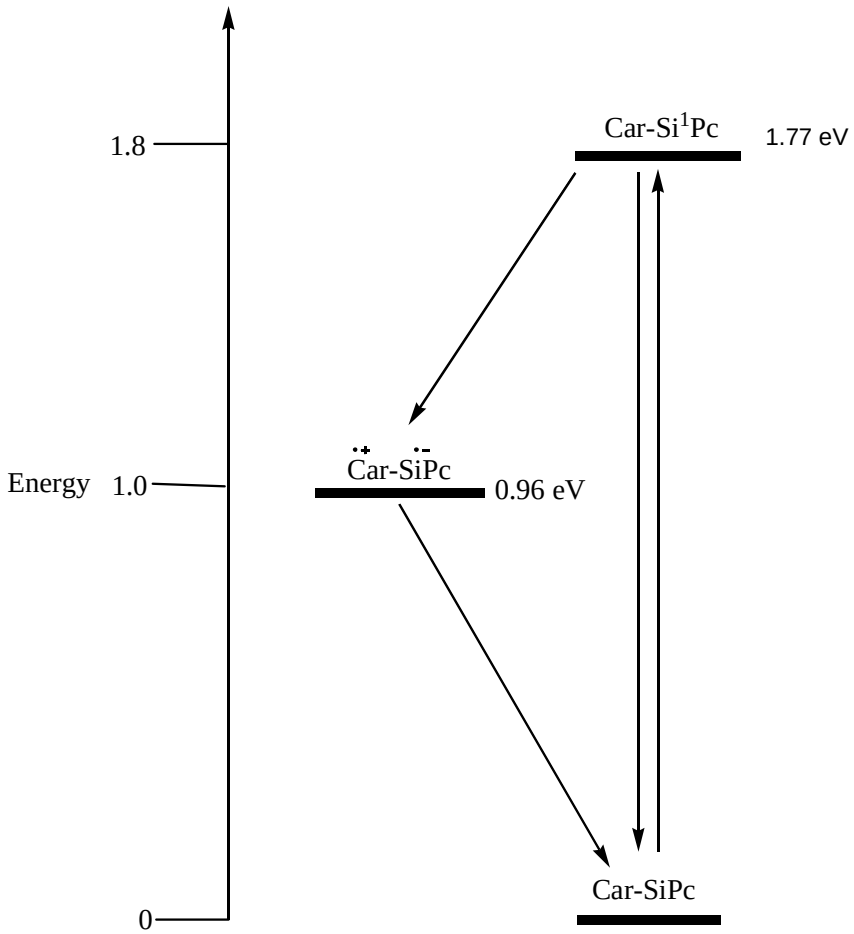

Figure 27: Deexcitation pathways for Car-SiPc dyad **16** following photoexcitation of the SiPc chromophore.

The energy of the charge-separated state is estimated from the cyclic voltammetric data of model compounds in benzonitrile. The ultrafast formation of $Car^{\bullet+}$-$Pc^{\bullet-}$ CS state is in agreement with previous studies on Car-SiPc-Car triad which gave a value of 2.5 ps and 10.5 ps as the rate of CS formation and the lifetime of the CS respectively.[85]

Figure 28 shows the decay associated spectrum (DAS) of Car-SiPc-C_{60} triad **17** dissolved in benzonitrile and excited at 695 nm.

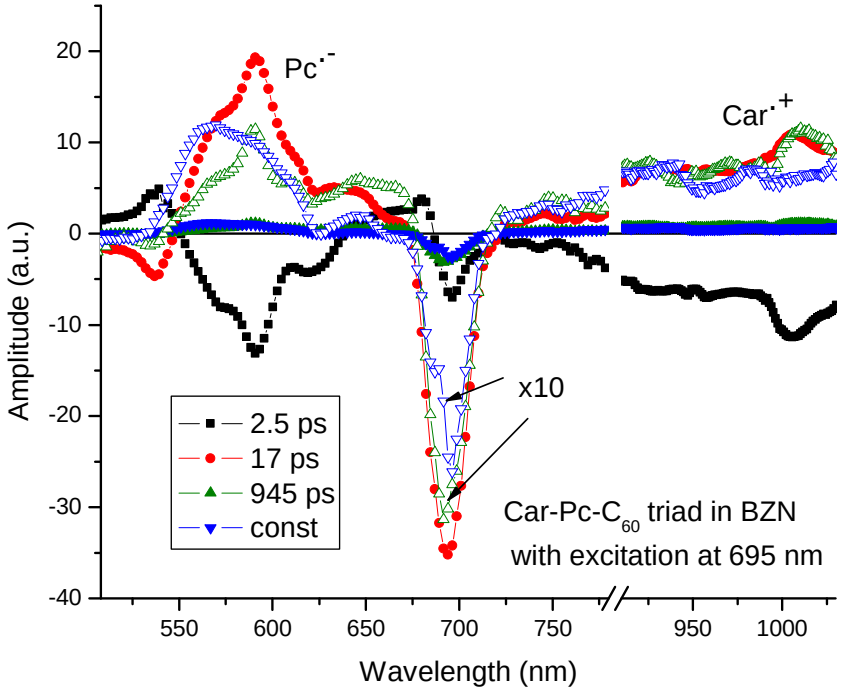

Figure 28: Decay-associated spectra of the transient absorption of Car-SiPc-C_{60} **17** in benzonitrile of 100 fs laser pulse at 695 nm

There is a fast (with ~2.5 ps) dominating formation of $Car^{\bullet+}$-$Pc^{\bullet-}$ CS state. There is also possible minor pathway of energy transfer from Pc singlet excited state to C_{60} singlet excited which competes with formation of $Car^{\bullet+}$-$Pc^{\bullet-}$ CS. The $Car^{\bullet+}$-$Pc^{\bullet-}$ CS state decays in ~17 ps. There is some minor triad conformation which shows much slower CS state recombination lifetime of ~945 ps. Since a $C_{60}^{\bullet-}$ transient has not been observed, this slowly decaying CS state is not likely to be $car^{\bullet+}$-SiPc-$C_{60}^{\bullet-}$. There is small impurity of Pc whose singlet excited state does

not decay on time scale measured. The DAS spectra are mixed; it possibly contains a few transient species and corresponds to a few processes. There is no long living Car radical cation signal in the IR, so there is no significant $Car^{\bullet+}$-Pc- $C_{60}^{\bullet-}$ final CS state forming in benzonitrile.

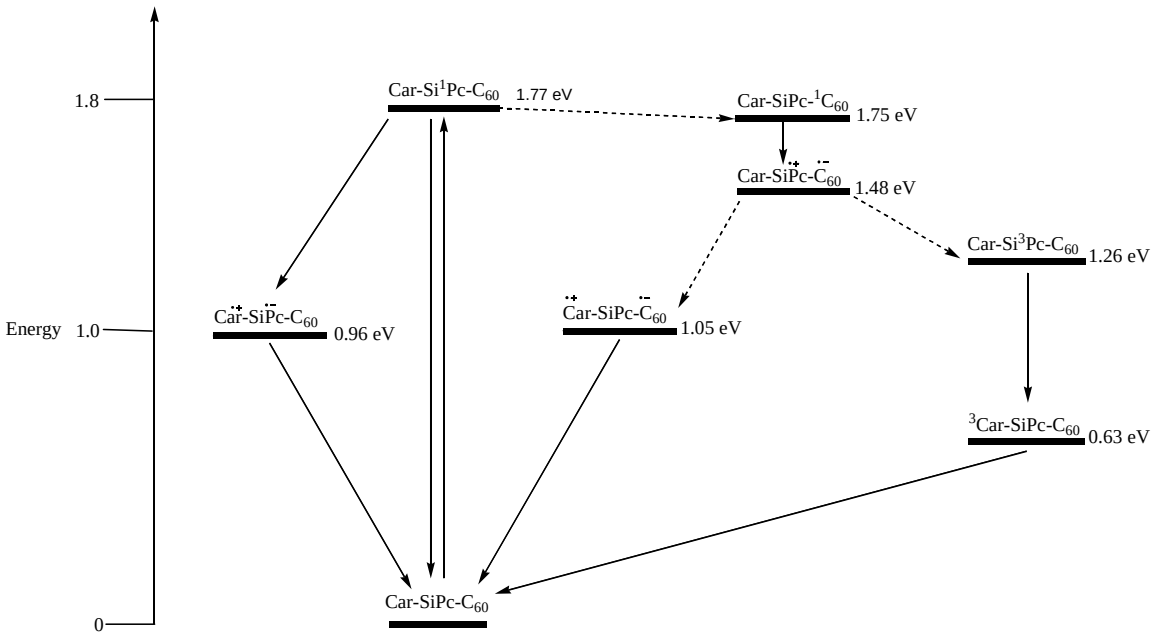

Figure 29: Deexcitation pathways for Car-SiPc-C_{60} dyad **17** following photoexcitation of the SiPc chromophore.

Dominant pathways are represented by full arrows and minor pathways are represented by broken arrows. The energy of the charge-separated state is estimated from the cyclic voltammetric data of model compounds in benzonitrile.

As shown in figure 29, the fast CS and CR involving $Car^{\bullet+}$-$SiPc^{\bullet-}$-C_{60} is the most favored thermodynamically and this supports the data obtained from the transient absorption. The other possible explanation for the fast intramolecular transfer in the Car-SiPc components of the triad is the enhanced coupling that exists between the carotenoid and the phthalocyanine as evidenced

by the 5 nm red shift observed in λ_{max} of carotene moiety after it was attached to the phthalocyanine.

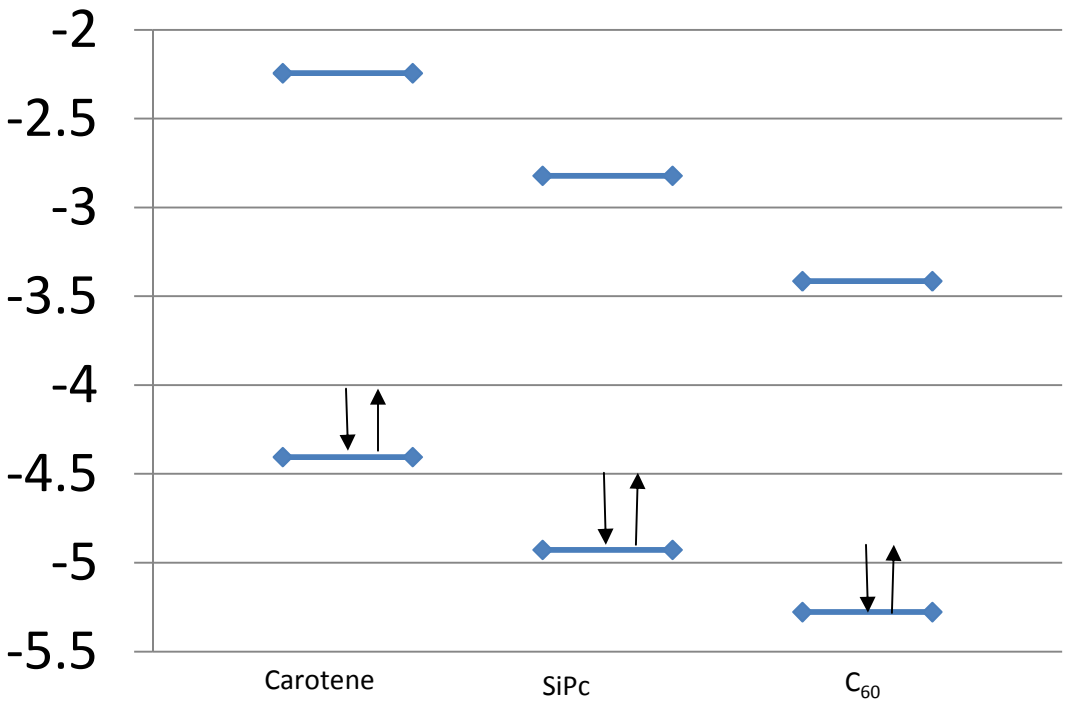

Figure 30: DFT calculated HOMO-LUMO energies of the components of the Car-SiPc-C_{60} triad **17**.

Figure 30 shows the HOMO-LUMO energies (calculation done by Dalvin Mendez) of the components making up the triad **17**, the HOMO-LUMO gaps are: C_{60} (1.86 eV), SiPc (2.11 eV) and carotene (2.16 eV). The calculations are in agreement with the experimental observations. Because of the relatively lowest level of the HOMO of the C_{60}, an alternative approach to realizing a long-lived $Car^{\bullet+}$-SiPc-$C_{60}^{\bullet-}$ CS state is by exclusive excitation of the C_{60} chromophore which will in turn result into a flow of electrons by gradient.

Experimental Section

Synthesis of (*p*-iodobenzoate)-(*p*-formylbenzoate)(2,9,16,23-tetra-*ter*t-butylphthalocyaninato)silicon 11

4-Iodobenzoic acid (242 mg, 1.0 mmol), 4-formylbenzoic acid (150 mg, 1.0 mmol), and $(^tBu)_4SiPc(OH)_2$ (92 mg, 0.115 mmol) in 25 mL anhydrous DMF were stirred at 165 ^oC under argon atmosphere for 10 hrs. The mixture was cooled to room temperature and solvent removed under reduced pressure and the crude purified by flash chromatography (SiO_2, dichloromethane/hexane 7:3) to yield 39 mg (30%) of SiPc **11** as a blue-green solid. ^1H NMR (400 MHz, $CDCl_3$) δ 9.74-9.56 (8H,m, Pc-Ar-H), 9.37 (1H, s, CHO), 8.45-8.43 (4H, m, Pc-Ar-H), 6.73 (2H, d, J=8 Hz, Ph-Ar-H), 6.58 (2H, d, J=8 Hz, Ph-Ar-H), 5.26 (2H, d, J=8 Hz, Ph-Ar-H), 4.83 (2H, d, J=8 Hz, Ph-Ar-H), 1.80-1.79 (36H, m, $4\times(CH_3)_3$). UV/Vis ($\lambda_{max/}$nm, CH_2Cl_2): 694, 662, 624, 360. MALDI-TOF-MS (Terthiophene matrix) m/z calcd for $C_{63}H_{57}IN_8O_5Si$ 1160.33 obsd 1160.35

Synthesis of (*p*-7'-apo-7'-(4-aminophenyl)-β-carotenobenzoate)-(*p*-formylbenzoate)(2,9,16,23-tetra-*ter*t-butylphthalocyaninato)silicon 16

SiPc **11** (53 mg, 0.053 mmol), *p*-7'-apo-7'-(4-aminophenyl)-β-carotene (31 mg, 0.0608 mmol) **14,** and 41 mg of a commercially obtained mixture of tris(dibenzylidene acetone) dipalladium (0): BINAP: sodium *tert*-butoxide (1:3:4) were stirred in a freshly distilled and degassed toluene (28 mL) at 80^oC under argon atmosphere for 48 hrs until almost all of the starting material have been consumed. The solution was then allowed to cool to room temperature. The solvent was evaporated at reduced pressure and the crude purified by column

chromatography (SiO_2, hexane/dichloromethane/EtOAc 8:1.5:0.5) to obtain 17.6 mg (31%) of the dyad **16.** ^{1}H NMR (400 MHz, $CDCl_3$) δ 9.68-9.51 (8H, m, Pc-Ar-H), 9.32 (IH, s, CHO), 8.39-8.37 (4H, m, Pc-Ar-H), 7.01-6.99 (2H, m, Ph-Ar-H), 6.68-6.66 (2H, m, Ph-Ar-H), 6.62-6.44 (8H, m), 6.30-625 (2H, m), 6.19-6.08 (6H, m), 5.75 (2H, d, J=8 Hz, Ph-Ar-H), 5.20 (2H, d, J=8 Hz, Ph-Ar-H), 5.13 (1H, br s, NH), 4.98 (2H, d, J=9 Hz, Ph-Ar-H),1.97-1.87 (m, 14H), 1.74-1.64 (m, 36H), 1.58-1.53 (m, 4H), 1.41-1.38 (m, 3H), 0.97-0.96 (m, 6H). UV/Vis (λ_{max}/nm, CH_2Cl_2): 694, 661, 623, 508 (sh), 480, 450 (sh), 341. MALDI-TOF-MS (Terthiophene matrix) m/z calcd for $C_{100}H_{103}N_9O_5Si$ 1538.79 obsd 1538.60

Bis(*p*-methylbenzoate)(2,9,16,23-tetra-*ter*t-butylphthalocyaninato)silicon 18 and (*p*-formylbenzoate)-(*p*-methylbenzoate)(2,9,16,23-tetra-*ter*t-butylphthalocyaninato)silicon 19

A portion of 4-toluic acid (136 mg, 1.0 mmol), 4-formylbenzoic acid (150 mg, 1.0 mmol), and (^{t}Bu)$_4$SiPc(OH)$_2$ (92 mg, 0.115 mmol) in 25 mL anhydrous DMF were stirred at 170 ^{o}C under argon atmosphere for 10 hrs. The mixture was cooled to room temperature and solvent removed under reduced pressure and the crude purified by flash chromatography (SiO_2, dichloromethane/hexane 8:2). The symmetrical SiPc **18** was eluted first, yielding 20.5 mg (17%), followed by asymmetrical SiPc **19** (32. 7 mg, 27 %).

SiPc **18** ^{1}H NMR (400 MHz, $CDCl_3$) δ 9.75-9.48 (8H, m, Pc-Ar-H), 8.35-8.33 (4H, m, Pc-Ar-H), 5.95 (4H, d, J= 8 Hz, Ph-Ar-H), 4.96 (4H, d, J= 8 Hz, Ph-Ar-H), 1.73-1.72 (36H, m, 4× $(CH_3)_3$), 1.60 (3H, s, 2×CH_3). UV/Vis (λ_{max}/nm, CH_2Cl_2): 693, 662, 623, 361. MALDI-TOF-MS (Terthiophene) m/z calcd for $C_{64}H_{62}N_8O_4Si$ 1034.47 obsd 1034.45.

SiPc **19** ^{1}H NMR (400 MHz, $CDCl_3$) δ 9.69-9.50 (8H, m, Pc-Ar-H), 9.30 (1H, s, CHO), 8.37-8.35 (4H, m, Pc-Ar-H), 6.67 (2H, d, J= 8 Hz, Ph-Ar-H), 5.95 (2H, d, J= 8 Hz, Ph-Ar-H), 5.20 (2H, d, J= 8 Hz, Ph-Ar-H), 4.97 (2H, d, J= 8 Hz, Ph-Ar-H), 1.73-1.72 (36H, m, 4×$(CH_3)_3$), 1.60 (3H, s, CH_3) . UV/Vis ($\lambda_{max/}$nm, CH_2Cl_2): 693, 662, 623, 361. MALDI-TOF-MS (Terthiophene) m/z calcd for $C_{64}H_{60}N_8O_5Si$ 1048.45 obsd 1048.46

(*p*-methylbenzoate)-[*p*-(N-methyl-3',4'-fulleropyrrodin-2'-yl)benzoate](2,9,16,23-tetra-*tert*-butylphthalocyaninato)silicon 20

SiPc **19** (32 mg, 0.0305 mmol), C_{60} (55 mg, 0.0764 mmol), and sarcosine (30 mg, 0.337 mmol) in *o*-dichlorobenzene (12 mL) were stirred at 140 ^{o}C under argon atmosphere for 2 hrs. The mixture was cooled and solvent removed under reduced pressure. The crude was purified on silica gel (toluene) yielding 52 mg (94%) of SiPc-C_{60} dyad **20** as green solid. ^{1}H NMR (400 MHz, $CDCl_3$) δ 9.73-9.55 (8H, m, Pc-Ar-H), 8.42-8.40 (4H, m, Pc-Ar-H), 6.68 (2H, br s, Ph-Ar-H), 6.01 (2H, d, J=8 Hz, Ph-Ar-H), 5.23 (2H, br s, Ph-Ar-H), 4.59 (2H, d, J=8 Hz, Ph-Ar-H), 4.59 (1H, d, J=8 Hz, CH*H*N), 4.25 (1H, s, CHN), 3.83 (1H, d, J=8 Hz, C*H*HN), 2.17 (3H, s, N-CH_3), 1.79-1.78 (36H, m, 4×$(CH_3)_3$), 1.66 (3H, s, CH_3). (λmax/nm, CH_2Cl_2):694, 663, 623, 360, 331. MALDI-TOF-MS (Terthiophene) m/z calcd for $C_{126}H_{65}N_9O_4Si$ 1795.49 obsd 1795.35

N-Methyl-2-(*p*-methylbenzoate)-3, 4-fulleropyrrolidine 21

A mixture of C_{60} (50 mg, 0.0694 mmol), methyl-4-formylbenzoate (30 mg, 0.183 mmol), and sarcosine (28 mg, 0.314 mmol) in toluene (10 mL) were heated to reflux under argon atmosphere for 3 hrs. The mixture was then cooled to room temperature and solvent removed and crude purified by flash chromatography (SiO_2, toluene:/EtOAc-19:1) yielding 9 mg (14%) of

21 as a brown solid. ^{1}H NMR (400 MHz, $CDCl_3/CS_2$ 1:1) δ 8.03 (2H,d,J=8 Hz, Ar-H), 7.83 (2H, br s, Ar-H), 4.96-4.94 (2H, m, CH*H*N & CHN), 4.25 (1H, d, J=9.6 Hz, C*H*HN), 3.84 (3H, s, N-CH_3), 2.77 (3H, s, CH_3).). (λ_{max}/ nm, toluene): 703, 432, 326 . MALDI-TOF-MS (Terthiophene) m/z calcd for $C_{71}H_{13}NO_2$ 911.09 obsd 910.61

Synthesis of [*p*-7'-apo-7'-(4-aminophenyl)-β-carotenobenzoate]-[*p*--(N-methyl-3',4'-fulleropyrrodin-2'-yl)benzoate](2,9,16,23-tetra-*tert*-butylphthalocyaninato)silicon 17

Dyad **16** (23 mg, 0.015 mmol), C_{60} (54 mg, 0.07 mmol), and sarcosine (42 mg, 0.471 mmol) in anhydrous toluene (20 mL) were stirred at 105 ^oC under argon atmosphere for 24 hrs. The mixture was then cooled and the solvent removed under reduced pressure. The crude was purified on silica gel (toluene) yielding 21 mg (62%) of triad **17**.

^{1}H NMR (400 MHz, $CDCl_3$) δ 9.68 (m, 8H, Pc-Ar-H), 8.36-8.34 (m, 4H, Pc-Ar-H), 7.00-6.98 (d, 2H, *J*=8, Ph-Ar-H), 6.72-6.43 (m, 10H, vinyl H, Ph-Ar-H), 6.30-6.03 (m, 8H, vinyl H, Ph-Ar-H), 5.75-5.72 (d, 2H, *J*=12, Ph-Ar-H), 5.18-5.16 (br, d, 2H, Ph-Ar-H), 4.96-4.94 (d, 2H, *J*=8, Ph-Ar-H), 4.63-4.62 (d, 1H, *J*=4, C*H*HN), 4.28 (br s, 1H, CHN), 3.85-3.83 (d, 1H, *J*=8, C*H*HN), 2.17 (s, 3H, N-CH_3), 1.97-1.88 (m, 14H, CH_3-18C, CH_3-20C, CH_3-19'C, CH_3-20'C, CH_2-4C), 1.75-1.65 (m, 36H, 4× $(CH_3)_3$), 1.57-1.53 (m, 3H, CH_3-19C), 1.41-1.38 (m, 4H, CH_2-2C, CH_2-3C), 0.97-0.96 (m, 6H, CH_3-16 and CH_3-17C)

UV/Vis (λ_{max}/nm, CH_2Cl_2): 693, 663, 623, 508 (sh), 479, 455 (sh), 360, 329.

MALDI-TOF-MS (Terthiophene) m/z calcd for $C_{162}H_{108}N_{10}O_4Si$ 2284.83 obsd 2284.50

2.3 Design and Synthesis of Ferrocene-Silicon Phthalocyanine-Fullerene triad

The design, synthesis and study of artificial photosynthetic reaction center molecular models utilizing SiPc-C_{60} dyad was investigated further by incorporating an easily oxidizable molecule, ferrocene, as the secondary electron donor in the triad in place of the carotenoid moiety. Ferrocene (Fc)-porphyrin (P)-C_{60} triads[90,93-95] have been shown to have a long-lived charge separated ($Fc^{\bullet+}$-P-$C_{60}^{\bullet-}$) state. A Fc-P-C_{60} (figure 31) in which the chromophores are separated by short linkers was reported to have the longest charge-separated lifetime, 630 µs, ever reported for triads at room temperature.[95]

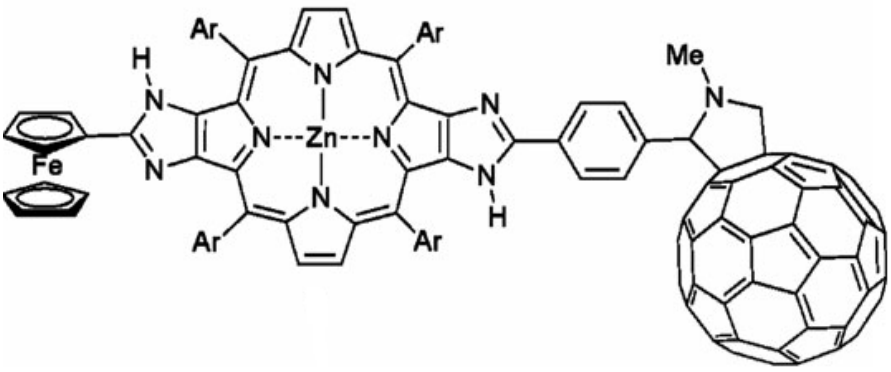

Figure 31: Ferrocene-Zinc porphyrin-fullerene triad.[95]

Due to the superior light harvesting and optical properties of axially substituted silicon phthalocyanine over porphyrins, it was thought that attaching ferrocene as a secondary donor to SiPc-C_{60} dyad will afford fast forward electron transfer and a long-lived CS state, towards this goal, a ferrocene (Fc)-silicon phthalocyanine (SiPc)-fullerene (C_{60}) triad (figure 32) was synthesized and the photophysical properties were studied.

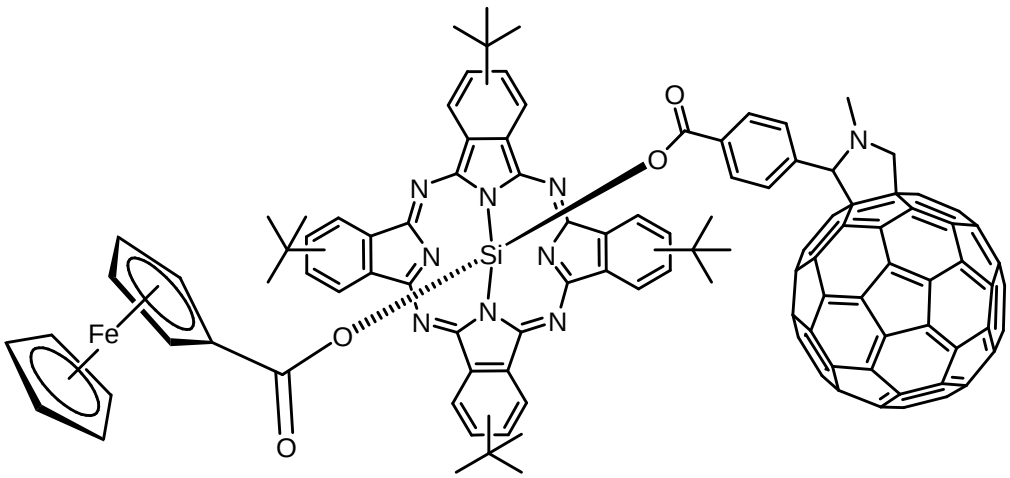

Figure 32: Molecular structure of proposed ferrocene-silicon phthalocyanine-fullerene (Fc-SiPc-C_{60}) triad.

The short linkers between the components are expected to provide better coupling between adjacent chromophores which will enhance a fast forward electron transfer. The excellent electron accepting ability of C_{60} is expected to favor forward electron transfer from the excited state SiPc and on the other hand its low reorganization, λ is expected to retard CR and consequently favoring hole transfer to the Fc moiety. Sequential electron transfer is expected to be achieved by initial electron transfer from an excited phthalocyanine to the C_{60} (Fc-^{1}*SiPc-C_{60}→ Fc-SiPc$^{\bullet+}$-$C_{60}^{\bullet-}$) and followed by charge shift to obtain the final charge separated state (Fc-SiPc$^{\bullet+}$-$C_{60}^{\bullet-}$ → Fc$^{\bullet+}$-SiPc-$C_{60}^{\bullet-}$).

Results and Discussions

Synthesis

Reaction between the commercially available tetra-*tert*-butylphthalocyanine silicon dihydroxide, ferrocene carboxylic acid and 4-formylbenzoic acid (scheme 19) yielded a

statistical mixture of products. Silica column purification (hexane/dichloromethane 3:7) afforded Fc-SiPc dyad **22**, a 22% yield

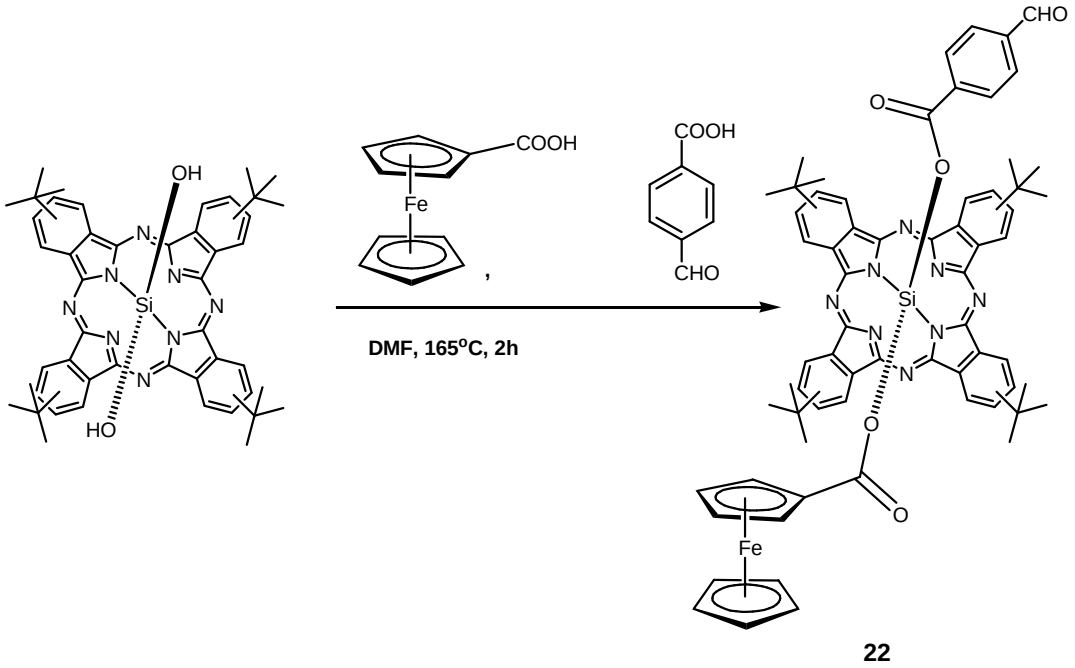

Scheme 19 : Synthesis of Fc-SiPc dyad **22**.

A Prato-type reaction between compound **22**, sarcosine and C_{60} in *o*-DCB as the solvent was used to obtain the triad **23.** The reaction crude was purified on silica column with toluene:EtOAc (49:1) as the solvent to obtain ferrocene-silicon phthalocyanine-fullerene triad **23**, a 65% yield. MALDI-TOF (Terthiophene matrix) showed a single peak at m/z: 1889.47 which matched the target triad. No peaks representing fragments were observed.

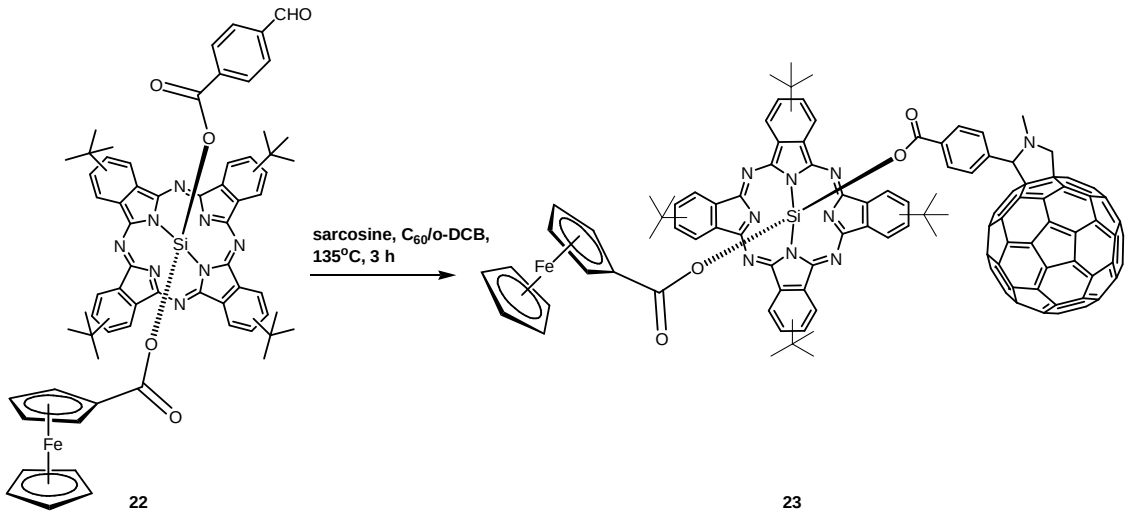

Scheme 20: Synthesis of ferrocene-silicon phthalocyanine-fullerene triad **23**

^{1}H NMR spectrum was measured in $CDCl_3$ solvent. On attachment of the ferrocene carboxylic acid, the resonance signals of the phthalocyanine moiety did not change significantly from that of phthalocyanine model **18.** The SiPc signals shifted from 9.75-9.55 ppm and 8.43-8.41 ppm in the model SiPc **18** to 9.70-9.52 ppm and 8.40-8.37 ppm in the Fc-SiPc dyad **22**. This is an indicator of some slight shielding of the Pc protons by the Fc. The formyl proton of Fc-SiPc dyad **22** appears as a singlet at 9.32 ppm which is also slightly up field from 9.37 ppm of SiPc **19.** The nine Fc protons appeared as three distinct broad peaks at 3.17 ppm (2H), 2.75 ppm (5H) and 2.17 ppm (2H).

In the final Fc-SiPc-C_{60} triad **23**, no shift in the resonance of the Pc protons were observed from that of Fc-SiPc dyad **22**. The phenyl aromatic protons between the SiPc and the C_{60} became broader due to the effect of the latter. The protons of the fulleropyrrolidine moiety in the triad **23** were shifted upfield when compared to those of the C_{60} model **21**. The pyrrolidine

and the N-CH_3 protons were shifted from 4.97, 4.95, 4.25 and 2.78 ppm in C_{60} model **21** to 4.57, 4.21, 3.80 and 2.13 ppm in the triad **23,** respectively. This means that the fulleropyrrolidine is close enough to have its protons shielded by the π-cloud of the phthalocyanine moiety.

Steady-state Absorption

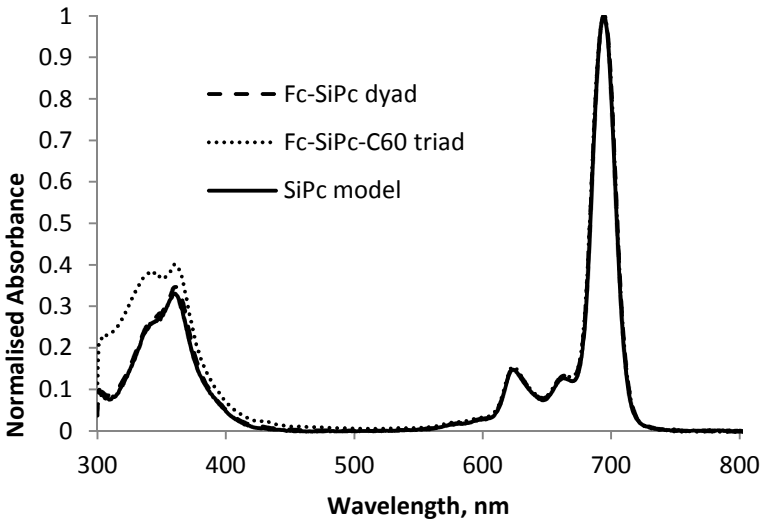

Figure 33: Normalized UV/Vis spectra (dichloromethane) of SiPc model **18** (solid line), Fc-SiPc dyad **22** (- - dashed line), and Fc-SiPc-C_{60} triad **23** (··· dotted line).

From figure 33, it can be seen that no shift in the Q-band of the SiPc chromophores occurs after the attachment of ferrocene and C_{60} which supports the notion that there are no ground state interactions among the chromophores. The small absorption at 431 nm and the band at 343 nm in the spectrum of triad **23** is a characteristic peak for [6, 6] fulleropyrrolidine and Soret band of fullerene, respectively.

Electrochemistry

Table 7: First reduction potentials of SiPc model **18**, C_{60} model **21**, and C_{60}-SiPc-Fc triad **23**

Molecule	E_{red}^{1}
18	**-0.47**
21	**-0.56**
23	**-0.55**

Table 8: Oxidation potentials of SiPc model **18**, C_{60} model **21**, SiPc-Fc dyad **22** and C_{60}-SiPc-Fc triad **23**

Molecule	Eox^{1}	Eox^{2}	Eox^{3}
18		0.93	
21			1.48 (irr)
22	0.74	1.19	
23	0.71	1.14	1.54 (irr)

The reduction potential of the C_{60} moiety in the triad **23** did not change significantly from that of the model C_{60} **21**, this confirms that C_{60} is a superior electron acceptor, a property it retains even in the triad. The first oxidation potential of the SiPc-Fc dyad **22** did not change much after coupling to form triad **23**; however the oxidation potential of SiPc changed from 0.93 V vs SCE in the model SiPc **18** to 1.19 V vs. SCE and 1.14 V vs SCE in the SiPc-Fc dyad **22** and triad **23,** respectively. This anodic shift in the oxidation potential of the SiPc moiety in the dyad and the triad can be attributed to the fact that, in these two molecules, SiPc oxidation is the 2nd

oxidation potential of the molecule and the presence of the neighboring oxidized ferrocene may make the Pc macrocycle less electron rich hence the observed reduced ease of oxidation. The observed irreversible oxidation peak at 1.48 V in the model C_{60} **21** and 1.54 V in the triad **23** has been reported in similar molecules and is due to the oxidation of the nitrogen atom in the fulleropyrrolidine.[96]

The electrochemistry data above supports the conclusion made from the absorption spectra data that at ambient condition there is no much ground state chromophoric interactions between the components of the triad.

Time-resolved absorption

The decay-associated spectra of Fc-SiPc dyad **22** and Fc-SiPc-C_{60} triad **23** dissolved in benzonitrile and subjected to 100 fs laser pulse at 695 nm is shown in figure 34. There is a very fast (with ~200 fs) formation of $Fc^{\cdot+}$-$Pc^{\cdot-}$ CS state in both dyad and triad. The CS state decays in 1.2 ps.

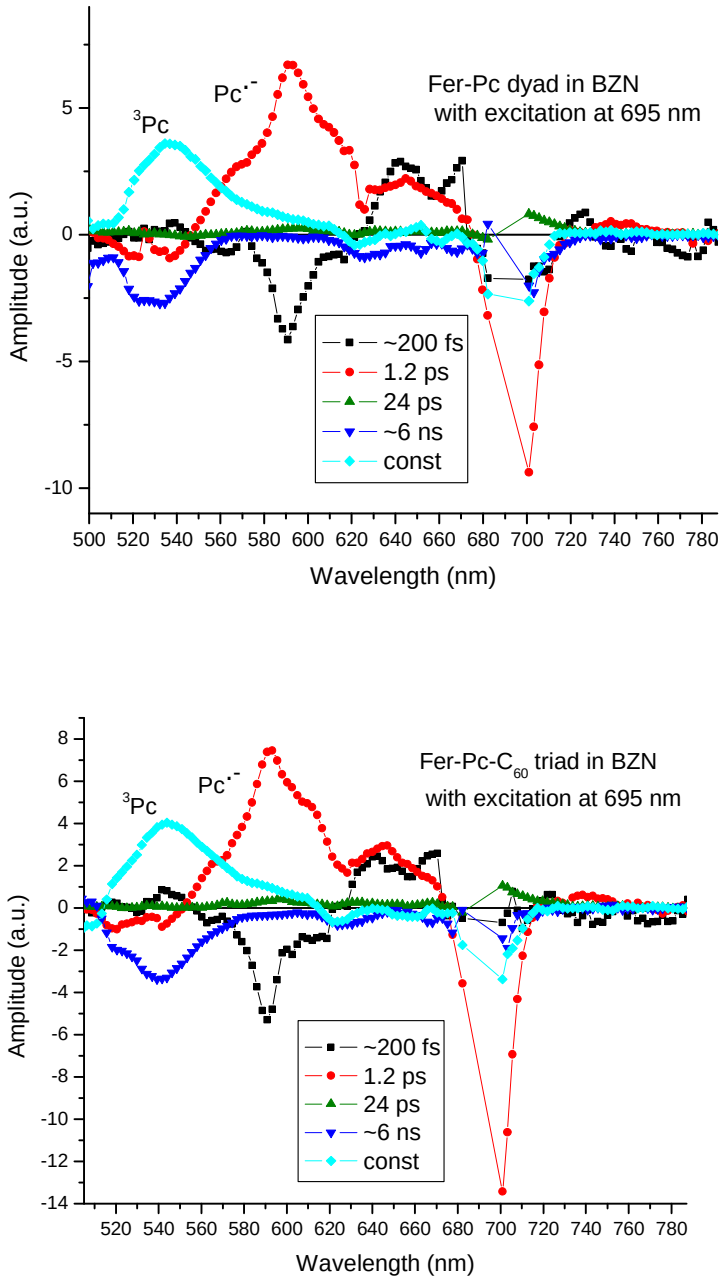

Figure 34: Femtosecond transient absorption spectra of Fc-SiPc dyad **22** (top) and Fc-SiPc-C_{60} triad **23** (bottom) in deaerated benzonitrile after laser excitation at 695 nm

There is some impurity or most likely decomposition product [fluorescence SPC does not show impurity, <5% (data not shown)] of Pc whose singlet excited state decays in 6.4 ns forming triplet excited state. The 24 ps component is most likely solvation of Pc excited singlet state. Absence of characteristic transients of $SiPc^{\bullet+}$ (~880 nm) and $C_{60}^{\bullet-}$(1000 nm) rules out formation of Fc-$SiPc^{\bullet+}$-$C_{60}^{\bullet-}$ CS state.

The dominant factor that determines formation of respective CS state is the thermodynamic driving force, and this is what seems to be favoring the formation of $Fc^{\bullet+}$-$SiPc^{\bullet-}$-C_{60} ($-\Delta G_{CS}$=0.56 eV) over Fc-$SiPc^{\bullet+}$-$C_{60}^{\bullet-}$ ($-\Delta G_{CS}$=0.29 eV). The shorter distance between the SiPc and the Fc could also explain the ultra fast charge separation and recombination between these two moieties. The ultrafast charge-recombination in $Fc^{\bullet+}$-$SiPc^{\bullet-}$-C_{60} is also due to the enhanced coupling between the ion radical pair as a result of a short linker and short distance.

Experimental Section

Synthesis of ferrocene- silicon phthalocyanine dyad 22

A mixture of $(^tBu)_4SiPc(OH)_2$ (46 mg, 0.0576 mmol), 4-formylbenzoic acid (75 mg, 0.5 mmol), and ferrocene carboxylic acid (115 mg, 0.5 mmol) in DMF (10 mL) was stirred and warmed to 160 ^oC under argon atmosphere for 3 hrs. Stirring was stopped, the mixture was cooled to room temperature and the solvent removed under reduced pressure. The crude was purified by silica column chromatography (hexane: DCM 3:7) and three greenish blue bands were observed. The middle band which was the target dyad **22** was isolated and solvent removed to obtain a greenish blue solid Fc-SiPc dyad **22,** with a 22% yield. ^1H NMR (400 MHz, $CDCl_3$) δ 9.70-9.52 (m, 8H, Pc-Ar-H), 9.32 (s, 1H, CHO), 8.39-8.37 (m, 4H, Pc-Ar-H), 6.69-6.67 (d, 2H,

J=8, Ph-Ar-H), 5.23-5.20 (d, 2H, *J*=8.4, Ph-Ar-H), 3.17 (br s, 2H, Fc-H), 2.75 (br s, 5H, Fc-H), 2.20-2.10 (m, 2H, Fc-H), 1.75-1.74 (m, 36H, 4× $(CH_3)_3$). UV/Vis ($\lambda_{max/}$nm, dichloromethane): 694, 663, 624, 361

MALDI-TOF-MS (Terthiophene) m/z calcd for $C_{67}H_{62}FeN_8O_5Si$ 1142.43 obsd 1142.31.

Synthesis of ferrocene-silicon phthalocyanine-fullerene triad 23

To a mixture of ferrocene-silicon phthalocyanine dyad **22** (14 mg, 0.0123 mmol), C_{60} (22 mg, 0.0305 mmol), and sarcosine (12 mg, 0.135 mmol), *o*-DCB (5 mL) anhydrous was added. The resulting mixture was stirred and heated to reflux under argon atmosphere. The reaction progress was monitored by TLC and after three hrs all the dyad **22** starting material has been consumed and the stirring and refluxing was stopped and the reaction mixture cooled to room temperature. The solvent was removed under reduced pressure and the crude was purified by silica gel column chromatography (toluene: EtOAc 49:1) to obtain a blue compound, triad **23**, 65% yield.

^{1}H NMR (400 MHz, $CDCl_3$) δ 9.70-9.50 (m, 8H, Pc-Ar-H), 8.36-8.34 (m, 4H, Pc-Ar-H), 6.63 (br s, 2H, Ph-Ar-H), 5.16-5.14 (d, 2H, *J*=6.8 Hz, Ph-Ar-H), 4.58-4.56 (d, 1H, *J*=9.2 Hz, C*H*HN), 4.21(br s, 1H, CHN), 3.81-3.79 (d, 1H, *J*=9.2 Hz, C*H*HN), 3.26 (br s, 4H, Fc-H), 2.88-2.75 (m, 5H, Fc-H), 2.13 (s, 3H, NCH_3), 1.74-1.73 (m, 36H, 4× $(CH_3)_3$).

UV/Vis ($\lambda_{max/}$nm, CH_2Cl_2): 694, 664, 624, 431, 360, 343.

MALDI-TOF-MS (Terthiophene) m/z calcd for $C_{129}H_{67}FeN_9O_4Si$ 1889.48 obsd 1889.47.

3. Regioselective oxidative synthesis of meso-β fused diporphyrin

Introduction

Extending the conjugated aromatic system of porphyrins leads to a significant change in optical and electrochemical properties, and such changes finds use in a wide range of fields[97] that includes technology and medicine[98] which utilizes the linear and non-linear optical properties of the π-extended porphyrinoids systems. Also, owing to their rigid shape and conjugated electronic system as evidenced by their absorption bands that extend into the NIR, these arrays have potential use as a molecular wires.[99] There are several methods of extending porphyrin and one of them is the oxidative dimerization.[100] Oxidative aromatic coupling is a favored method for the extension of the π system of the porphyrin chromophores as it gives the most significant red shift of absorption.[97] Osuka and coworkers have reported a number of agents for one electron oxidation of porphyrin rings. The most popular oxidants are tris(4-bromophenyl)aminium hexachloroantimonate (BAHA)[99], $AgPF_6$[101], and combinations of 2,3-dichloro-5,6-dicyano-1,4-benzoquinone (DDQ) and scandium trifluoromethanesulfonate ($Sc(OTf)_3$)[102]. Although these reagents have been shown to be effective in generating extended porphyrins, BAHA has been observed to cause β chlorination of porphyrins[99,102] while the other reagents are expensive. In an effort to suppress halogenation, our group has utilized copper (II) perchlorate and tetrafluoroborate salts in acetonitrile[103]. This method was effective because no chlorination of porphyrins were observed, however it lacked regioselectivity, the products were mixtures of β,β triply-connected and meso-β doubly connected dimers. These posed a purification challenge such that a series of chromatographic column separations were required.

A method that can give a regioselective oxidative porphyrin dimerization without causing unwanted halogenation and a high yield is desirable. In pursuit of this, we utilized Cu^{2+} as an oxidizing agent in the solvent nitromethane to selectively form meso-β doubly-connected fused porphyrin dimer in almost quantitative yield with only a short flash column required for purification[100]. Just like in acetonitrile, Cu^{2+} is a strong oxidizer in nitromethane, with an oxidation potential of 1.0 V vs SCE. [104,105] Unlike the other oxidation reactions, using Cu^{2+} in acetonitrile allowed us to obtain the pure meso-β doubly connected dimer [100]. Removal of the copper metal from the macrocycle to obtain the free base dimer allows for exchange of metals and provides a route to a wider range of metalloporphyrin dimers.

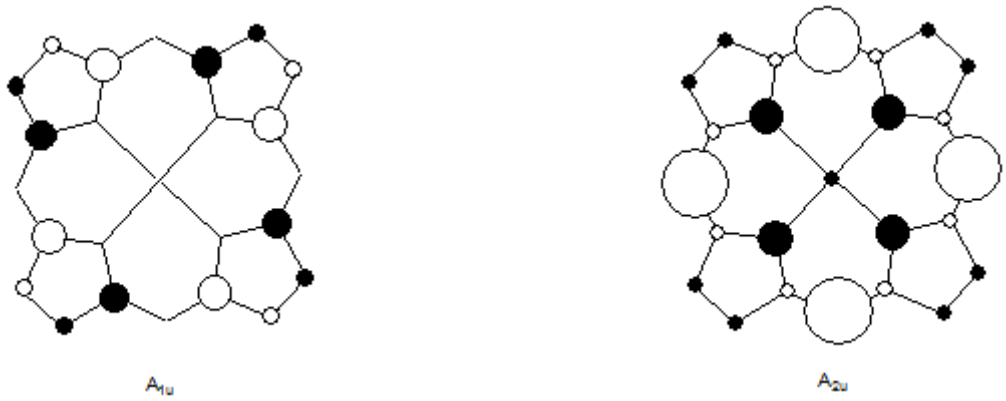

Figure 35: Schematic representation of the two HOMO orbitals of the D_{4h} porphyrin ring.[99]

The regioselectivity of Cu porphyrin to give exclusively a meso-β doubly linked diporphyrins could be due to the A_{1u} HOMO orbital characters of Cu^{II} which has nodal planes through the meso positions and a higher electron density at the β position {(figure 35 (A_{1u})}[106].

Results and Discussions

Synthesis

Dimerization of pyrrole was achieved by using a well-known protocol that employs paraformaldehyde, $InCl_3$ and NaOH[107]. The unreacted pyrrole during the first reaction was distilled off and taken through the reaction process one more time, the crude from the two reactions were combined and purified over flash column to yield an overall 3% yield.

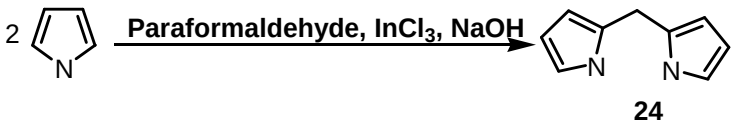

24

Scheme 21: Synthesis of dipyrromethane **24**.

Porphyrin **25** was synthesized by a $BF_3 \bullet OEt_2$ catalyzed condensation of dipyrromethane **24** with mesityl aldeyde followed by DDQ oxidation and neutralization by triethyl amine.[108] Silica column purification afforded 26% of pure compound **25.**

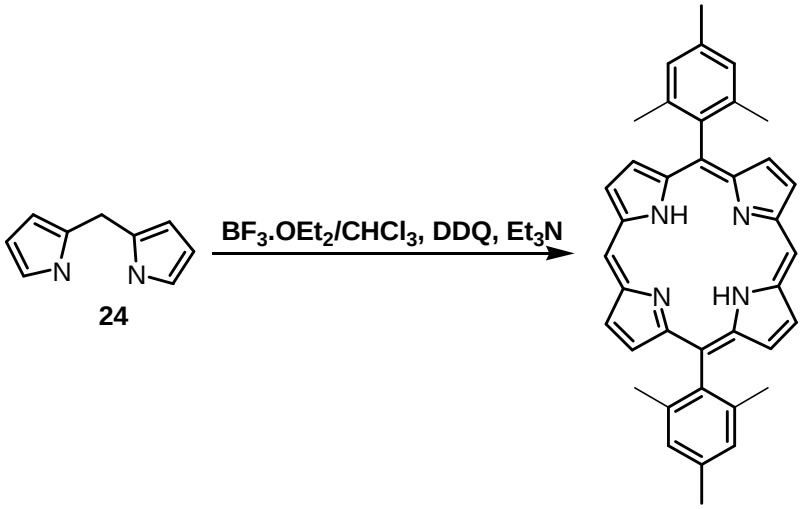

24 **25**

Scheme 22: Synthesis of porphyrin **25**

The brominating agent N-bromosuccinimide was used to carry out monobromination of the *meso* position of porphyrin **25**.[109] The HBr generated was neutralized with pyridine. The reaction was very fast and it was monitored by TLC and MALDI-TOF and it was stopped as soon as the dibromo product appeared. Lower temperature favored the monobromo product and to optimize the yield of the monobrominated porphyrin the reaction was carried out at below 0^{o}C temperature.

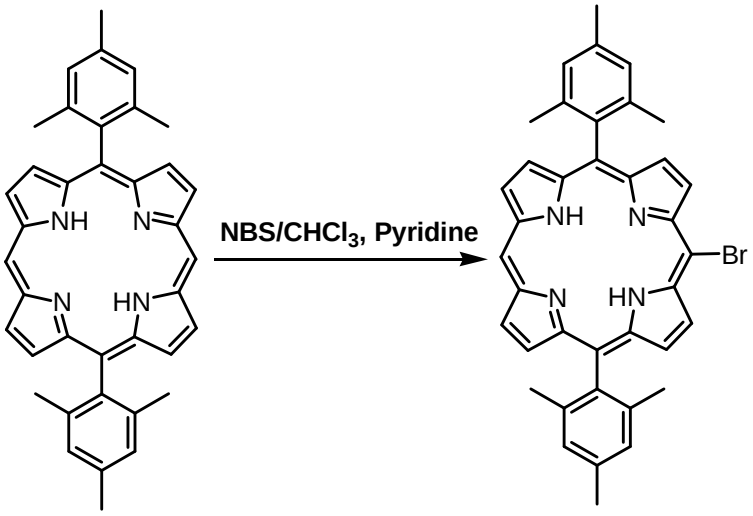

25 **26**

Scheme 23: Synthesis of porphyrin **26**

A yield of 50% was obtained and an unfragmented molecular ion peak, m/z = 624.3 that correspond to the target monobrominated porphyrin were observed.

Porphyin **27** (scheme 24) was synthesized by Suzuki coupling reaction between tolyl boronic acid and monobromo pophyrin **26.** Under a reflux condition in presence of heterogeneous solvent mixture of toluene/water/methanol, a high yield of 72% of porphyrin **27** was realized. In MALDI-TOF a single peak at m/z = 636.6 was observed.

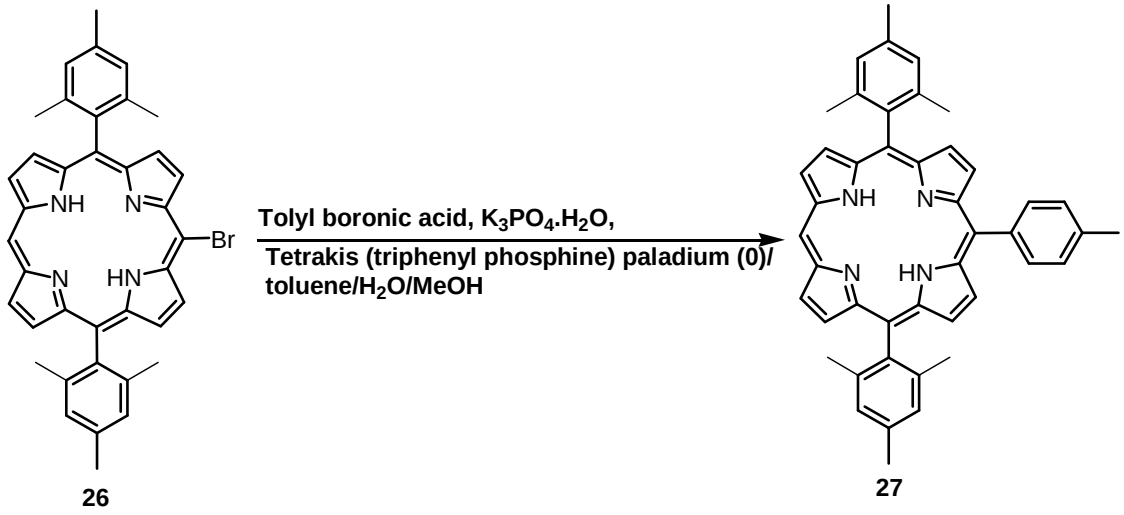

26 **27**

Scheme 24: Synthesis of porphyrin **27**

As shown in scheme 25, stirring of porphyrin **27** with Cu(II) acetate monohydrate in methanol at room temperature gave a quantitative yield of Cu(II) porphyrin **28** which was easily isolated by washing with water and brine without need for a chromatographic purification. MALDI-TOF gave a single peak at m/z = 697.5 indicating that the Cu (II) is tightly held in the macrocycle under the MALDI condition.

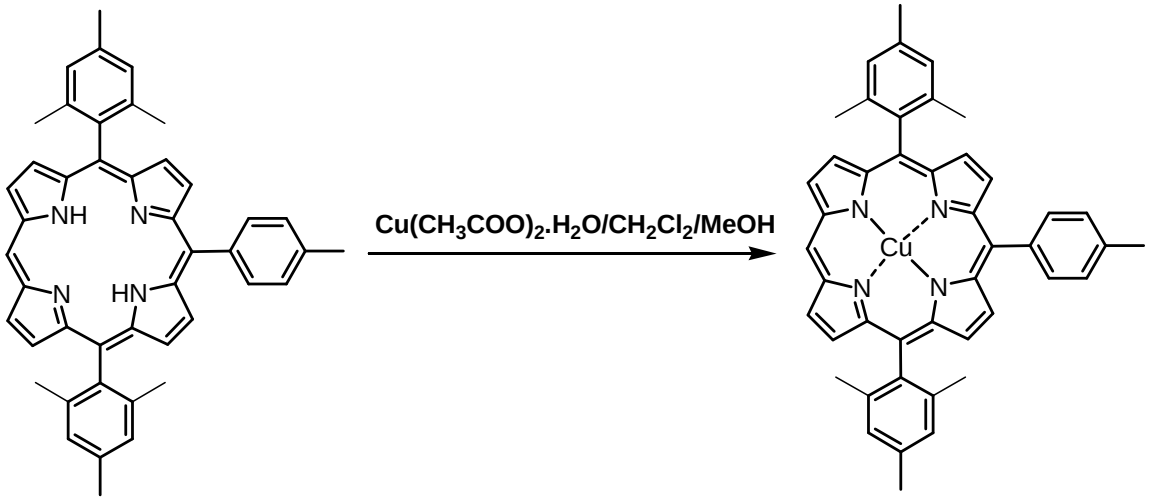

27 **28**

Scheme 25 : Synthesis of porphyrin **28**

The porphyrin dimer **29** was obtained by a selective one electron oxidative coupling of porphyrin **28** using Cu(II) tetrafluoroborate in nitromethane solvent. By treating porphyrin **28** with 3.3 equivalents of Cu(II) tetrafluoroborate in nitromethane at room temperature for 3 hours all starting materials were consumed and the reaction mixture was quenched with aqueous potassium ferrocyanide so as to reduce any remaining Cu(II) and unreacted oxidized porphyrin (scheme 26).[100]

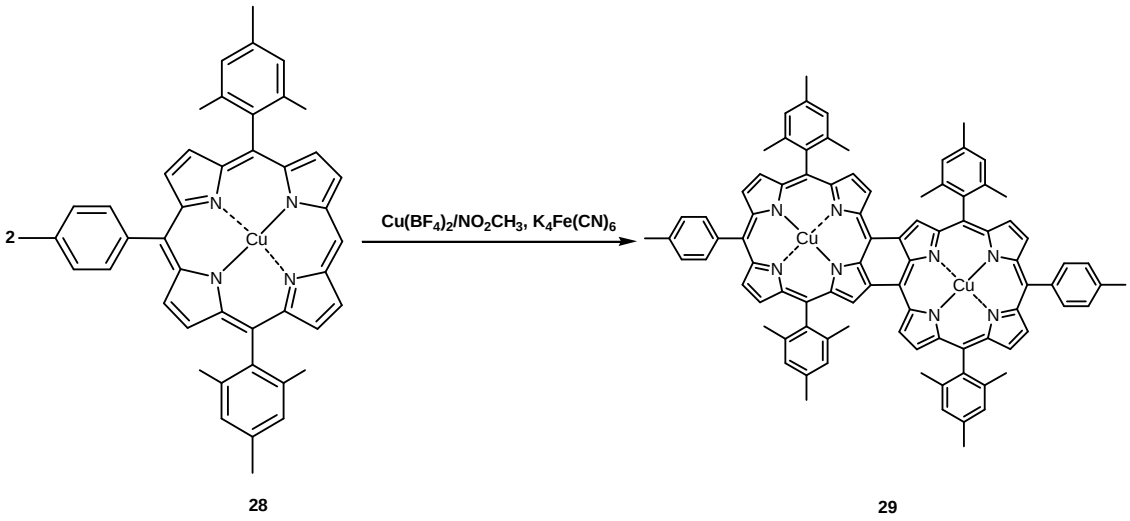

Scheme 26: Synthesis of compound **29**

A short and a quick silica gel column were used to obtain a pure compound **29** with almost quantitative yield of 90%. MALDI-TOF result of the crude mixture also showed only a single peak at m/z = 1393.0 which matches the calculated mass of the target porphyrin dimer **29**.

Stirring compound **29** in a mixture of trifluoroacetic acid and concentrated sulfuric acid (1:10 v/v) at ambient temperature yielded compound **30** after only 20 minutes. Only a single product was obtained as evidenced by a single peak observed in MALDI-TOF, m/z = 1267.0 and a single spot on TLC. A short silica column was run to obtain a pure compound **30**, 85% yield; there was no trace of the starting material on the column.

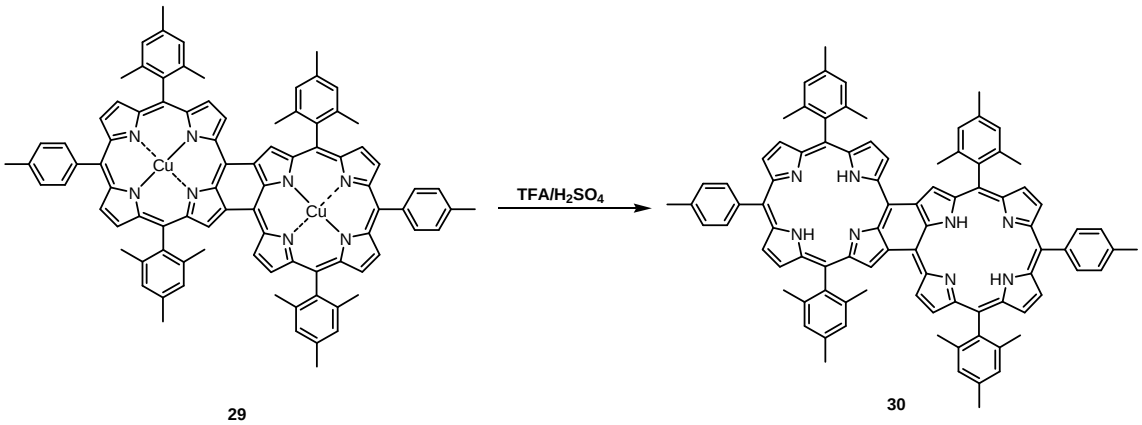

Scheme 27: Synthesis of compound **30**

The ease of demetallating compound **29** to produce a free base dimer **30** opens up a possibility of producing a wider range of metallodiporphyrins.

^{1}H NMR ($CDCl_3$) spectroscopy was used to characterize the copper free intermediates and the final product. The aromaticity of the electronic π system of porphyrins can be deduced from the chemical shift of the β-protons and the inner N-H. In the monomer porphyrin **27**, the β-protons appear at 8.71-9.26 ppm and the inner N-H protons appear at -2.89 ppm in $CDCl_3$. The ^{1}H NMR spectrum of the *meso*-β doubling linked fused diporphyin **30** shows upfield shifts of the β-protons to 8.16-9.24 ppm and downfield shift of the inner N-H protons at 0.72 ppm. The upfield shifts of the β-protons are an indicator that the aromatic ring current is decreased probably as a result of increased conjugation over the diporphyrin. The dramatic downshift of the inner N-H chemical resonance of the diporphyrin **30** relative to that of the monomer **28** is a further evidence that aromaticity, as measured by ring-current effects, is reduced in the doubly fused porphyrin as opposed to the monoporphyrins.

Steady-state Absorption

The UV/Vis/NIR absorption spectra shows a broad and bathochromically shifted three major bands (bands I, II and III) as shown in figure 36. The shift in the major bands towards red is understood to be as a result of extensive conjugation over the diporphyrin π-electronic systems. The positions of band I (414-423 nm) of the diporphyrins are similar to those of the Soret bands of the monomers, only slight red-shift were observed, Soret band of Cu porphyrin dimer **29** is at 414 nm while the Soret of the corresponding monomer **27** is at 410 nm. On the other hand, the Soret band of free base porphyrin dimer **30** is at 423 nm and that of the corresponding monomer **27** is at 412 nm.

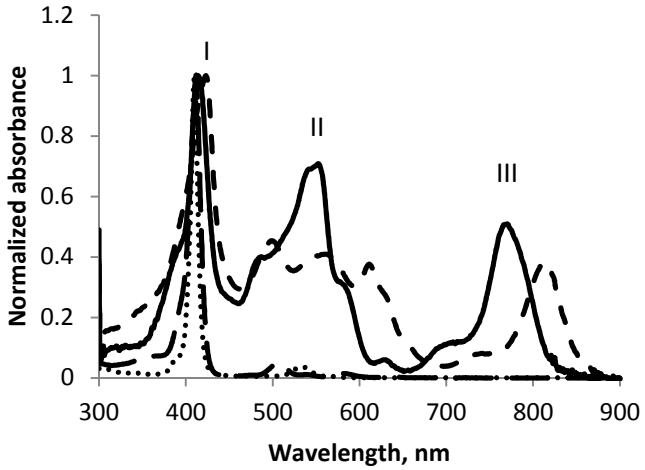

Figure 36: UV-visible-NIR of **27** (broken), **28** (dots), **29** (solid) and **30** (dashed) in dichloromethane.

The spectra was normalized at the highest absorbance peak.

Band II are not only red-shifted and their intensities magnified, but they are also more broad and complicated. This is an indication of presence of interactions in the ground state and

first excited state. The most red-shifted band is band III and it is dramatically intensified when compared to the Q-bands of the porphyrin monomers. There is a difference in the position of bands, particularly band III between the free-base diporphyrin **30** and Cu^{II} diporphyrin **29**. Band III of Cu^{II} diporphyrin **29** is observed at high-energy 770 nm and free-base diporphyrin **30** is observed at low-energy position 814 nm., this mean that the HOMO-LUMO gap is narrower in the latter diporphyrin when compared to the former.

Experimental Section

General procedure for metallation of porphyrin.

Metalation of porphyrins was performed by adding porphyrin and 5-10 equivalents of Cu(II) acetate to a 5:1 solution of dichloromethane / methanol. The solution was heated for 30 min and then allowed to stir overnight under a nitrogen atmosphere. The organic layer was washed with distilled water, saturated aqueous sodium bicarbonate, and again with distilled water, and the solvent removed under reduced pressure. All reactions went to completion.

Synthesis of di(1H-pyrrol-2-yl)methane 24

Undistilled pyrrole was passed through a short alumina column to obtain a clear pyrrole. To the clear pyrrole (205 g, 3.06 mol), paraformaldeyde (0.92 g, 30.6 mmol) was added, and the mixture degassed for 30 min while stirring. The mixture was then warmed at 50 ^{o}C in an oil bath for 1 hr followed by addition of $InCl_3$ (0.68 g, 3.07 mmol), and then the resulting mixture was stirred for another 3 hr after which NaOH (3.63 g, 90.75 mmol) was added and stirring continued for another 1.5 hr at room temperature. The crude was passed through celite and the filtrate was

taken through distillation. The dark oily residue was stored while the pyrrole (169 g, 2.5 mol) distillate was taken through the procedure described above with paraformaldedye (0.76 g, 25.3 mmol), $InCl_3$ (0.56 g, 2.53 mmol), and NaOH (0.297 g, 7.43 mmol). The crude from the two reactions were combined and silica column chromatography was run with dichloromethane/hexane 7:3 to obtain a snow white fluffy solid dipyrromethane **24**, 3.2 g, 3%.

^{1}H NMR (400 MHz, $CDCl_3$) δppm 7.80 (2H, br s, N-H), 6.64-6.63 (2H, m, β-H), 6.15-6.13 (2H,m, β-H), 6.03 (2H, br s, β-H , 3.96 (2H, s, meso).

Synthesis of 5, 15-dimesitylporphyrin 25

A solution of dipyrromethane **24** (0.2 g, 1.37 mmol) and mesityl aldehyde (0.23 g, 1.54 mmol) in $CHCl_3$ (140 mL) was purged with argon for 15 minutes, and then $BF_3 \bullet OEt_2$ (0.14 g, 0.972 mmol) was added and the mixture stirred at room temperature. After 6 hr, DDQ (0.467, 2.06 mmol) was added. After a total of 8 hr, the reaction mixture was neutralized by adding 2 mL of triethylamine. The crude mixture was filtered through a pad of basic alumina and the filtrate was evaporated under a reduced pressure. Purification was carried out by silica column chromatography (hexane: CH_2Cl_2- 3:7) to afford 5, 15-dimesitylporphyrin **25,** 98.5 mg, 26% yield.

^{1}H NMR (400 MHz, $CDCl_3$) δppm 10.21 (2H, s, meso), 9.32 (4H, d, *J*=4 Hz, β-H), 8.88 (4H, d, *J*=5 Hz, β-H), 7.33 (4H, s, Ar-H) , 2.66 (6H, s, Ar-CH_3), 1.85 (12H, s, Ar-CH_3), -3.05 (2H, s, N-H). MALDI-TOF-MS m/z calcd for $C_{38}H_{34}N_4$ 546.3 obsd 546.4.

Synthesis of 10-Bromo-5, 15-dimesitylporphyrin 26

85 mg (0.156 mmol) of 5, 15-dimesitylporphyrin **25** was dissolved in $CHCl_3$ (40 mL) and the mixture cooled to below -20 ^oC by immersing the round-bottom flask in dry ice bath cooled with isopropyl alcohol. To the mixture, NBS (29 mg, 0.163 mmol) and pyridine (0.196 g, 2.48 mmol) were added and the resulting mixture was stirred under argon atmosphere for 20 minutes after which stirring was stopped and acetone was added to the crude mixture. Solvent was removed under a reduced pressure and the resulting crude was purified on a short flash silica gel column (hexane/toluene 1:1) to obtain 10-Bromo-5, 15-dimesitylporphyrin **26,** 48.5 mg, 50% yield.

^1H NMR (400 MHz, $CDCl_3$) δ 10.07 (1H, s, *meso*), 9.65 (2H, d, *J*=4 Hz, β-H), 9.21 (2H, d, *J*=4 Hz, β-H), 8.77 (4H, d, *J*=5 Hz, β-H), 7.29 (4H, s, Ar-H) , 2.64 (6H, s, Ar-CH_3), 1.84 (12H, s, Ar-CH_3), -2.88 (2H, s, N-H). MALDI-TOF-MS m/z calcd for $C_{38}H_{33}BrN_4$ 624.2 obsd 624.3

Synthesis of 5,15-dimesityl-10-tolylporphyrin 27.

A solution of 48 mg (7.69×10^{-5} mol) of **26**, 30 mg (2.24×10^{-4} mol) of tolyl boronic acid, and 54 mg of potassium phosphate hydrate in 11 mL of toluene/water/methanol (27:1.5:1.5) was degassed for 40 minutes and then 14.4 mg (1.21×10^{-5} mol) of tetrakis (triphenyl phosphine) palladium (0) was added and the resulting mixture refluxed under argon atmosphere for 10 hrs. The crude mixture was filtered through celite and washed with 50 mL diethyl ether. The filtrate was successively washed with saturated sodium bicarbonate, water and brine. The organic layer was dried over anhydrous magnesium sulfate and the solvent removed. The purplish residue was purified on a silica gel column using a mixture of hexane/dichloromethane (2:1), to obtain a pure

porphyrin **26** (35mg, 72%) . ^{1}H NMR (400 MHz, $CDCl_3$) δ 10.10 (1H, s, meso), 9.26 (2H, d, J=4 Hz, β-H), 8.85-8.81 (4H, m, β-H), 8.72 (2H, d, J=5 Hz, β-H), 8.10 (2H, d, J= 8Hz, Ar-H), 7.53 (2H, d, J= 8Hz, Ar-H), 7.30 (4H, s, Ar-H) , 2.67 (3H, s, Ar-CH_3), 2.64 (6H, s, Ar-H), 1.84 (12H, s, Ar-H), -2.89 (2H, s, N-H). MALDI-TOF-MS m/z calcd for $C_{45}H_{40}N_4$ 636.3 obsd 636.6; UV-visible ($\lambda_{max,}$ CH_2Cl_2) 412, 507, 538, 582, 637 nm.

Synthesis of Cu (II) 5,15-dimesityl-10-tolylporphyrin porphyrin 28

This material was prepared from **27** as specified by the general procedure for porphyrin metalation to obtain a quantitative yield. MALDI-TOF-MS m/z calcd for $C_{45}H_{38}CuN_4$ 697.2, obsd 697.5; UV-visible-NIR ($\lambda_{max,}$ CH_2Cl_2) 533, 410 nm

Synthesis of Cu^{II} diporphyrin 29

Thirty-nine mg (5.59×10^{-5} mol) of **28** in 20 mL nitromethane was sonicated for 30 minutes and then degassed and then transferred to a round bottom flask containing 63 mg (1.83×10^{-4} mol) of $Cu(BF_4)_2$•6 H_2O in 15 mL nitromethane which has previously been sonicated until all salt has dissolved followed by degassing. The color of the mixture immediately turned to dark purple. Stirring at room temperature under argon atmosphere for 2 hrs was continued. The reaction mixture was quenched with potassium ferrocyanide in 50 mL water followed by addition of 50 mL chloroform. Organic layer was dried over anhydrous sodium sulfate and filtered. Solvent was removed to obtain purplish crude. The purplish residue was purified on a silica column using a mixture of hexane/dichloromethane (4:1), to obtain copper (II) diporphyrin **29** (35 mg, 90%)**.** MALDI-TOF-MS m/z calcd for $C_{90}H_{76}Cu_2N_8$ 1392.5, obsd 1392.7;

UV/Visible/NIR ($\lambda_{max,}$ CH_2Cl_2): 414, 487 (sh), 552, 628, 702 (sh), 770 nm.

Synthesis of free base diporhyrin 30

A solution of 35 mg (2.51×10^{-5} mol) of copper (II) diporhyrin **29** in 15 mL H_2SO_4/TFA (1:10 v/v) was stirred at room temperature under argon atmosphere for 20 min when all the starting material were gone by TLC using hexane/dichloromethane (1:2) mixture. The reaction mixture was quenched by adding excess ice. The product was extracted with dichloromethane and the organic phase was washed with aqueous NaOH (20%, w/w) water, brine and dried over anhydrous Na_2SO_4. The resulting crude was purified on a short silica gel column using hexane/dichloromethane (1:2) to obtain free base diporphyrin **30** (27 mg, 85%). ^{1}H NMR (400 MHz, $CDCl_3$) δ_H 9.23 (2H, d, *J*= 5Hz, β-H), 8.90 (2H, s, β-H), 8.42 (2H, d, *J*=5 Hz, β-H), 8.36 (2H, d, *J*=5 Hz, β-H), 8.31 (2H, d, *J*=4 Hz, β-H), 8.20 (2H, d, *J*= 5Hz, β-H), 8.16 (2H, d, *J*= 5Hz, β-H), 7.95 (4H, d, *J*= 8Hz, Ar-H), 7.49 (4H, d, *J*=13 Hz, Ar-H), 7.29 (4H, s, Ar-H), 7.23 (4H, s, Ar-H), 2.64 (12H, d, *J*= 4Hz, Ar-CH_3), 2.60 (6H, s, Ar-CH_3), 2.07 (12H, s, Ar-CH_3), 1.94 (12H, s, Ar-CH_3), 0.72 (4H, br, s, N-H). MALDI-TOF-MS m/z calcd for $C_{90}H_{76}N_8$ 1269.6, obsd 1484.2; UV-visible-NIR ($\lambda_{max,}$ CH_2Cl_2) 423, 499, 560, 611, 737(sh), 814 nm. [39]

4. Expedient synthesis of bacteriopurpurin: A red-absorbing dye for potential application in hydrogen production

Introduction

Dye-sensitized solar cells (DSCC) based on TiO_2 using Ruthenium (Ru) dyes with efficiencies of up to 11% has been reported.[110] However, the cost and the environmental issues associated with ruthenium dyes demands for discovery of cheaper and safer organic dyes.[111] Some of the advantages of organic dyes include, diversity, ease of modification of their molecular structures and their intense absorption.[112]

Porphyrin (figure 37) sensitizers make good candidates for this purpose owing to their intense absorption in Soret and Q bands to harvest solar energy efficiently in a broad spectral region.[113] However, porphyrin-sensitized TiO_2 cells have poor light harvesting properties relative to Ru dyes at 450-500 nm and 650-900 nm due to the existence of a gap between the Soret and Q bands and this is a major limitation. One possible way to overcome this problem is to modulate the electronic structures of porphyrins so that we can match the light-harvesting properties with the energy distribution on the earth[110] particularly in the visible and NIR regions.

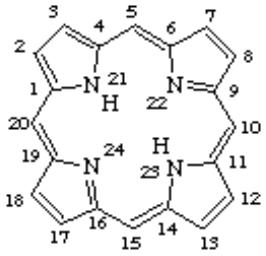

Figure 37: Porphyrin 1-24 numbering system

These types of dyes can be used to replace Ru dyes as TiO_2 sensitizers and coupled to water splitting catalytic center to produce hydrogen. Figure 38 shows a working of water splitting DSSC.

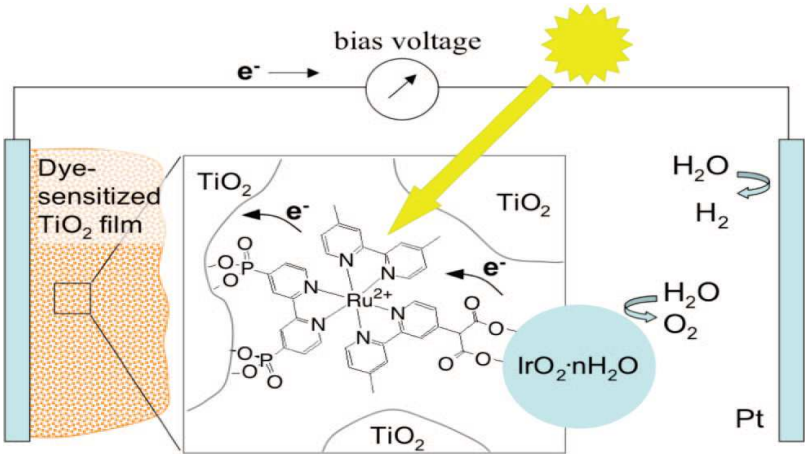

Figure 38: Schematic diagram of the water splitting dye sensitized solar cell[114].

The electrons injected by the sensitizer are conducted through the wire to the cathode, where protons are reduced to hydrogen. The net result is solar production of hydrogen gas and molecular oxygen. Towards the goal of developing a dye with the right absorption spectra and redox properties, bacteriopurpurin **31** was synthesized.

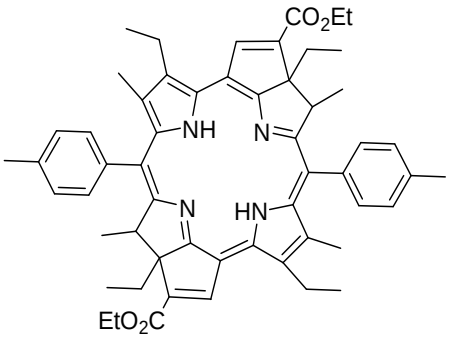

Bacteriopurpurin 31

Bacteriopurpurins possesses two annelated cyclopentyl rings which are opposite to each other. The reduction of the pyrrolic rings in the porphyrin macrocycle has a significant effect on the absorption spectrum of the reduced compounds.[115]

Results and Discussions

Synthesis

Synthesis of bacteriopurpurin **31** was started from metalation of Porphyrin **32** (obtained from Dr. Paul Liddell) as shown in scheme 28.[116]

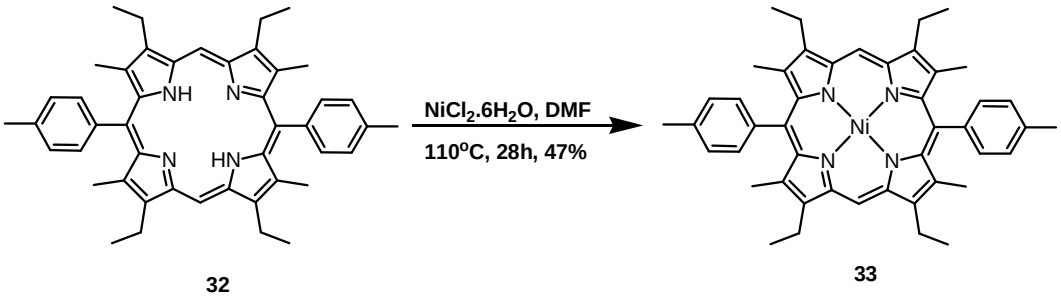

Scheme 28: Nicklyation of porphyrin **32**

The yield was not very good, and also it was also observed that the percent yield decreased when scaling up was attempted. This may have been due to the HCl formed displacing Ni from the product and reforming the starting material. Different reagents and reaction conditions were used to obtain a better yield of **33.** Reaction between compound **32** and Ni (II) acetylacetone hydrate in refluxing toluene for 24 hours afforded compound **33** in a near quantitative yield, 92% yield (scheme 29)

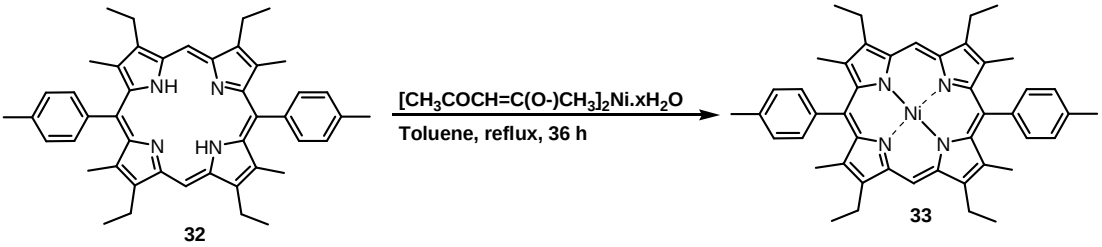

Scheme 29: Nickel 5, 15-bis(tolyl)-2,8,12,18-tetraethyl-3,7,13,17-tetramethylporphyrin **33**

Monoformylation of **33** using Vilsmeier formylation protocol with (chloromethylene)dimethyl ammonium chloride yielded a deep green compound **34** as shown in scheme 30.[115] The diformyl product was a tiny slow moving band on the silica gel column and separation was easily achieved.

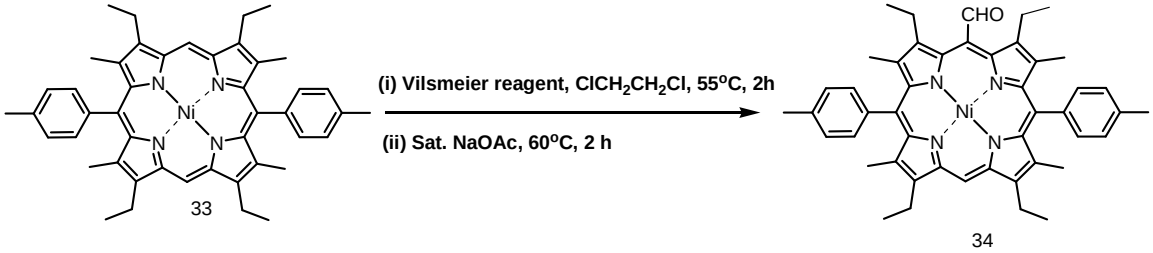

Scheme 30: Nickel 10-meso-formyl- 5, 15-bis(tolyl)-2,8,12,18-tetraethyl-3,7,13,17-tetramethylporphyrin **34**

A Wittig type reaction between compound **34** and (carboethoxymethylene) triphenyl phosphorane afforded compound **35** (scheme 31). Compound **35** was purified by flash chromatography on silica column (dichloromethane: hexane 3:1) followed by recrystallization in methanol: dichloromethane to obtain a small dark green crystals[117] to obtain high yield, 84%.

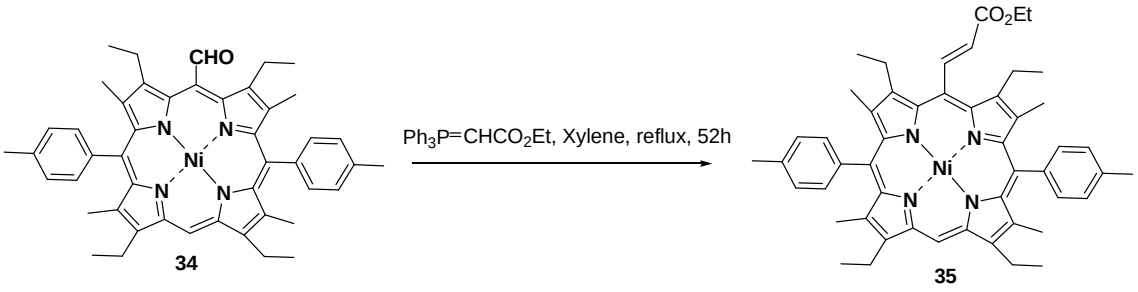

Scheme 31: Synthesis of porphyrin **35**

Several attempts to formylate position 20 (figure 37) of compound **35** using the method used by Robinson[115] were not successful. Although it has been reported by Morgan et al[118] that nickel porphyrin undergo only monoformylation, diformylation of Ni (II) porphyrin **33** was realized by modifying the method used in scheme 30. Using an excess of a freshly prepared Vilsmeier reagent obtained by drop wise addition of phosphorous oxychloride to DMF and running the reaction longer at higher temperature, the diformyl product, compound **36** was obtained as the major product. The diformyl product was separated from the monoformyl product on a silica flash column (dichloromethane: hexane 3:1) and obtained in 61% yield. Scheme 32 shows conversion of nickel porphyrin **33** to 10, 20-diformyl nickel porphyrin **36.**

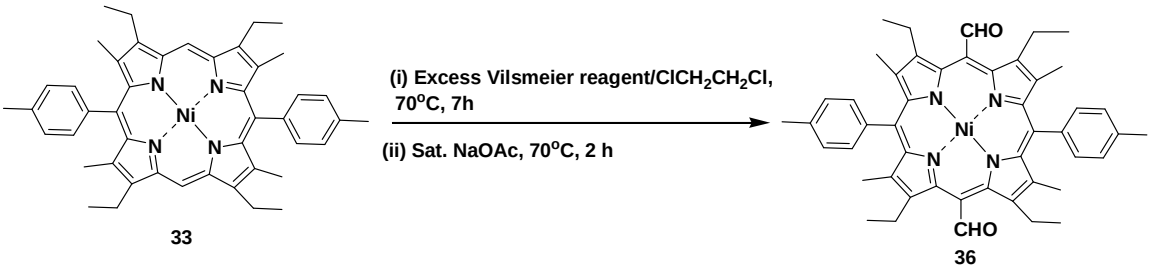

Scheme 32: Nickel 10,20-bis(meso-formyl)- 5, 15-bis(tolyl)-2,8,12,18-tetraethyl-3,7,13,17-tetramethylporphyrin **36**

Compound **36** was converted to compound **37** as shown in scheme 33, column purification afforded porphyrin **37**, 43% yield. The side product had one of the formyl group unreacted and it was separated from compound **37** on a silica flash column with dichloromethane as the mobile phase.

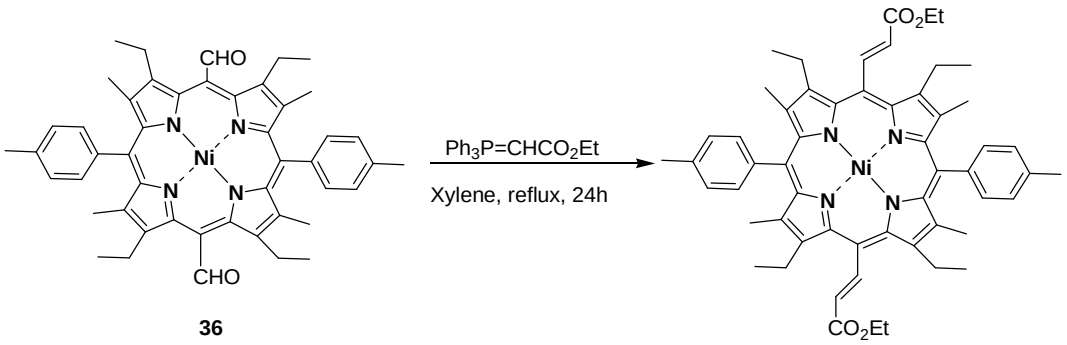

Scheme 33: Synthesis of nickel Porphyrin **37**

Demetalation of **37** was attempted following the method used by Robinson[115] which employed the use of concentrated sulfuric acid followed by neutralization with saturated sodium bicarbonate as shown in scheme 34.

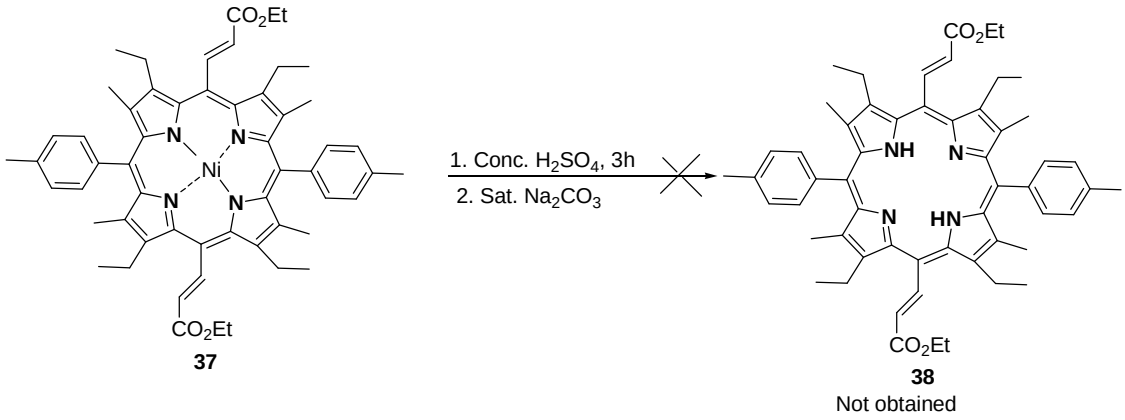

Scheme 34: Attempted synthesis of porphyrin **38**

Compound **38** was not obtained; from the MALDI-TOF results it was observed that the concentrated sulfuric acid used hydrolyzed the vinylic esters to the corresponding vinylic acids without removing nickel from the macrocycle.

We thought of a way of avoiding reactions involving concentrated sulfuric acid in presence of esters, an easily hydrolysable group, the only way to do that was to remove the nickel from 10, 20-diformyl nickel porphyrin **34,** generally aldehydes are known to be less susceptible to acid hydrolysis than esters. After all, the role of nickel was to facilitate formylation, a role it has served diligently and it is no longer needed in further steps.

Free base 10, 20- diformyl porphyrin **39** was obtained by reacting Ni (II) 10, 20-diformyl porphyrin **36** with concentrated sulfuric acid as shown in scheme 35. The progress of the reaction was monitored by TLC, and in less than 20 minutes all the starting material has been consumed. After neutralization with sodium bicarbonate the crude was purified on silica column to afford free base porphyrin **39**, 21% yield

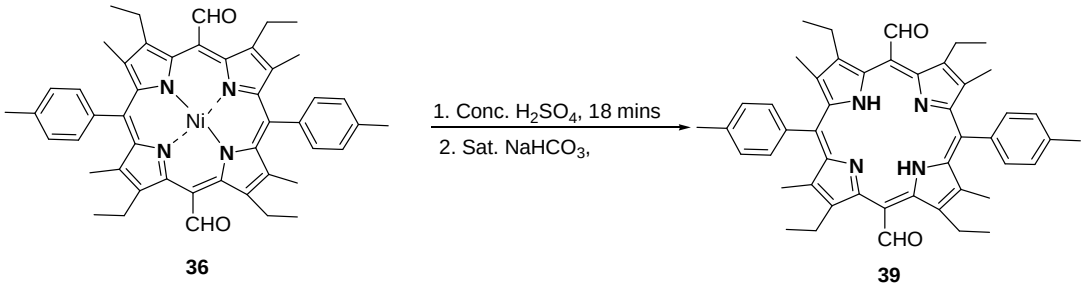

36 **39**

Scheme 35:10,20-bis(meso-formyl)- 5, 15-bis(tolyl)-2,8,12,18-tetraethyl-3,7,13,17-tetramethylporphyrin **39**

The low yield was attributed to high polarity of the product which made it stick to the silica flash column used, 4% methanol: dichloromethane was used to elute the compound from a short column.

Synthesis of 5,15-(3,7,13,17-tetraethyl-2,8,12,18-tetramethyl-10,20-ditolyl)bacteriopurpurin **31** was achieved by reacting free base porphyrin **39** with (carboethoxymethylene) triphenyl phosphorane in a refluxing xylene. Scheme 36 shows synthesis of bacteriopurpurin **31**. Column purification with dichloromethane as the eluent afforded bacteriopurpurpurin **31** as a lime green product, 31% yield.

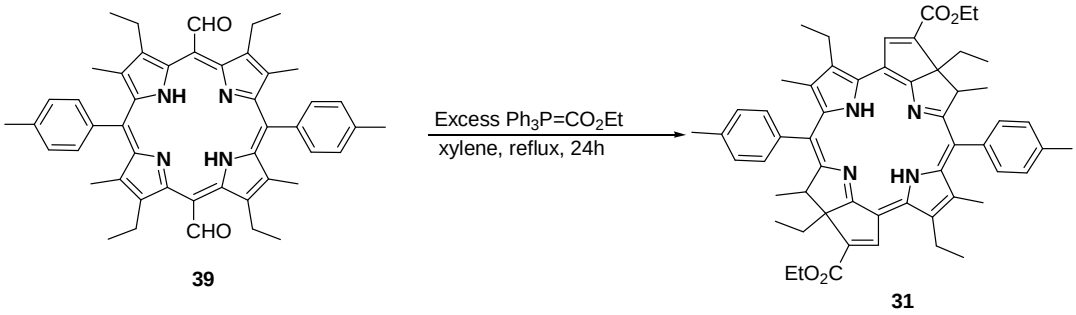

Scheme 36: 5,15-(3,7,13,17-tetraethyl-2,8,12,18-tetramethyl-10,20-ditolyl)bacteriopurpurin **31**

It important to note that the formation of *meso* diacrylate free base porphyrin and cyclization to bacteriopurpurin **31** occurred in one step without the use of non-nucleophic base such as DBU as used in the literature.

Steady-state Absorption

Bacteriopurpurin **31** dye shows a characteristic Soret band at 435 and Q-bands at 578, 611, 696 and 845 nm. Figure 39 shows UV-Vis-NIR absorption of bacteriopurpurin **31.**

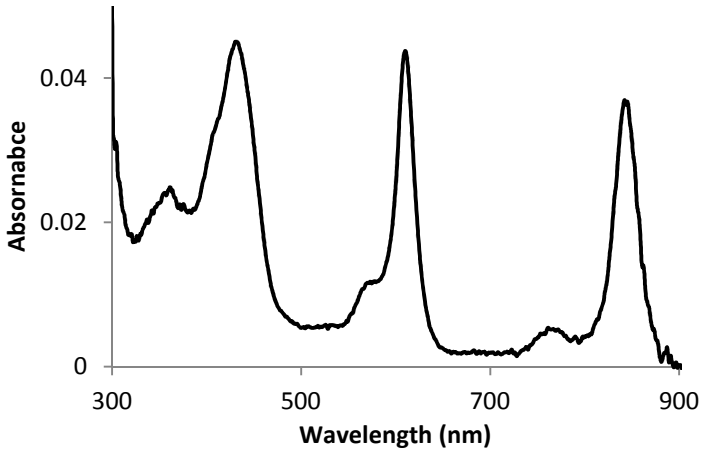

Figure 39: UV/Vis/NIR spectra absorption of Bacteriopurpurin **31** in dichloromethane.

The ability to absorb into the NIR makes it a good harvester of light across the electromagnetic spectrum.

Electrochemistry

Figure 40 show the CV scan of bacteriopurpurin **31** (Electrochemistry measurement was done by Dr. Ben Sherman)

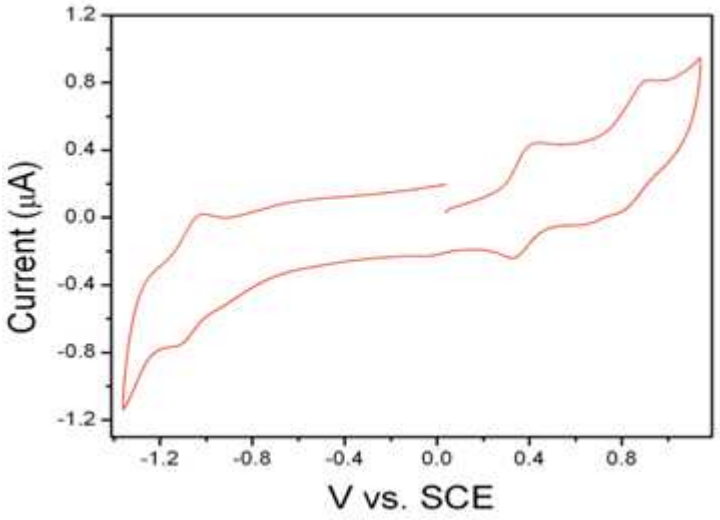

Figure 37 : CV scans of bacteriopurpurin **31**

The experiment was performed in dichloromethane with 0.1 M $TBAPF_6$, Pt working electrode, Ag^+/Ag quasi-reference calibrated to SCE with ferrocene (Fc^+/Fc 0.45 V vs SCE). Scans shown were measured at a rate of 100 mV/s.

As shown in figure 39 bacteriopurpurin **31** undergoes successive oxidations. First reversible single oxidation occurs at 0.38 V vs SCE and the second irreversible oxidation occurs at 0.92 V vs SCE. The first reduction potential of the excited state is -1.07 V vs SCE. Therefore, the synthesized bacteriopurpurin **31** is likely to be a good donor to TiO_2 (E^{red} = -0.85 V vs SCE) when incorporated onto a photocathode catalyst of a photoelectrochemical device for light driven H_2O splitting by reducing hydrogen ions (E^{red} = -0.6 5V vs SCE) [19] to produce hydrogen gas.

In conclusion, an expedient route to the synthesis of bacteriopurpurin has been developed. CV studies have shown that this dye has promising redox properties to be used as a TiO_2 sensitizer in a dye sensitized solar cells for the production of hydrogen. The molecule was found to be unstable in air due to oxidative decomposition.

Experimental Section

Nickel 5, 15-bis(β-tolyl)-2,8,12,18-tetraethyl-3,7,13,17-tetramethylporphyrin 33

A solution of 5, 15-bis(β-tolyl)-2,8,12,18-tetraethyl-3,7,13,17-tetramethylporphyrin **32** 0.208 g (0.313 mmol) and nickel (II) acetylacetone hydrate 1.241 g (4.8 mmol) in toluene (50 mL) was heated under reflux for 24 hrs. The resulting solution was cooled and the solvent was removed under reduced pressure. The resulting crude was dissolved in dichloromethane and washed with water several times. The organic layers were combined and solvent removed. Silica column chromatography of the crude product on silica with dichloromethane as eluent gave only one band, which was collected to yield **33** (0.206 g, 92 %) as a bright red solid.

^{1}H-NMR ($CDCl_3$, 400 MHz) δ_H 9.41 (s, 2H, meso-**H**), 7.69 (d, 4H, *J*=7.6 Hz, Ar-**H**), 7.41 (d, 4H, *J*=7.6 Hz, Ar-**H**), 3.71-3.66 (m, 8H, 4×C**H**$_2$), 2.63 (s, 6H, 2×Ar-C**H**$_3$), 2.26 (s, 12H, 4×C**H**$_3$), 1.62-1.58 (t, 12H, 4×CH_2C**H**$_3$)

UV/Vis (CH_2Cl_2): λ_{max} nm 562, 520, 400

Nickel 10,20-bis(meso-formyl) - 5, 15-bis(β-tolyl)-2,8,12,18-tetraethyl-3,7,13,17-tetramethylporphyrin 36

A 20-mL portion of Vilsmier reagent, prepared by a drop wise addition of $POCl_3$ (14 mL) to DMF (11 mL) at 0 ^{o}C and allowed to stand at room temperature for 1 hr during which the

solution turned pink was transferred to a round-bottom flask immersed in an oil bath heated to 70 ^{o}C. To this solution Nickel 5, 15-bis(β-tolyl)-2,8,12,18-tetraethyl-3,7,13,17-tetramethylporphyrin **33** (107 mg, 0.15 mmol) dissolved in anhydrous 1,2-dichloroethane (62 mL) was added drop wise. The reaction mixture was stirred for an additional 9 hr while maintaining at around 70 ^{o}C. A saturated solution of sodium acetate (200 mL) was then added, and stirring and heating were continued for 2 more hours. The organic and the aqueous phase were separated and the former was washed with dichloromethane three times. Organic layers were combined and the solvent removed under reduced pressure. The resulting crude was purified on silica flash column, the first red band was eluted with CH_2Cl_2/hexane 4:1 and the major green band eluted with CH_2Cl_2. On drying, the green band gave a bright green solid nickel 10,20-bis(meso-formyl)- 5, 15-bis(β-tolyl)-2,8,12,18-tetraethyl-3,7,13,17-tetramethylporphyrin **36** (95 mg, 82%).

^{1}H-NMR ($CDCl_3$, 400 MHz) δ_H 11.53 (s, 2H, 2×C**H**O), 7.55 (d, 4H, *J*= 8 Hz, Ar-**H**), 7.39 (d, 4H, *J*= 8 Hz, Ar-**H**), 3.39-3.35 (m, 8H, 4×C**H**$_2$), 2.58 (s,6H, 2×Ar-C**H**$_3$), 1.96 (s, 12H, 4×C**H**$_3$), 1.48-1.45 (t, 12H, 4×CH_2C**H**$_3$).

MALDI-TOF-MS m/z calcd for $C_{48}H_{48}N_4NiO_2$ 770.3 obsd 770.6

10,20-bis(meso-formyl)- 5, 15-bis(β-tolyl)-2,8,12,18-tetraethyl-3,7,13,17-tetramethylporphyrin 39

To a solution of nickel porphyrin **36** (110 mg, 0.1429 mmol) in dichloromethane (30 mL), concentrated sulfuric acid (0.4 mL) was added drop wise and the mixture stirred at room temperature for 6 minutes. The mixture was neutralized by addition of saturated aqueous sodium

hydrogen carbonate (30 mL) and the organic layer was collected, washed and dried. The solvent was removed under reduced pressure, and the crude product purified on a silica gel (CH_2Cl_2/MeOH 9.5:0.5) to yield a dark green solid **39** (61.7 mg, 60%).

^{1}H-NMR ($CDCl_3$, 400 MHz) δ_H 12.14 (s, 2H, 2×C**H**O), 7.98 (d, 4H, J= 8 Hz, Ar-**H**), 7.541 (d, 4H, J= 8 Hz, Ar-**H**), 3.02-2.99 35 (m, 8H, 4×C**H**$_2$), 2.66 (s,6H, 2×Ar-C**H**$_3$), 1.85 (s, 12H, 4×C**H**$_3$), 1.28-1.25 (t, 12H, 4×CH_2C**H**$_3$).

MALDI-TOF-MS m/z calcd for $C_{48}H_{50}N_4O_2$ 714.9 obsd 715.4

5, 15-Bis(β-tolyl)-2,8,12,18-tetraethyl-3,7,13,17-tetramethylbacteriopurpurin 31

(Carboethoxymethylene)triphenyl phosphorane (0.5955 g, 1.71 mmol) was added to a solution of porphyrin **39** (13 mg, 0.0182 mmol) in xylene (20 mL) and the mixture heated to reflux while stirring under argon atmosphere for 24 hrs. The mixture was cooled and solvent removed under reduced pressure. The crude was purified on silica gel chromatography (dichloromethane) and the only lime green band observed was collected to yield bacteriopurpurin **31** (4.8 mg, 31%).

^{1}H-NMR ($CDCl_3$, 400 MHz) δ_H 9.22 (s, 2H, 2× isocyclic ring **H**), 7.70-7.68 (m, 4H, Ar-**H**), 7.52-7.50 (m, 4H, Ar-**H**), 4.39-4.37 (m, 4H, 2×CO_2C**H**$_2$), 4.24-4.16 (m, 2×CHC**H**$_3$, 2×CH_2C**H**$_3$, 2×C**H**CH_3), 2.55 (s, 6H, 2×CH_3) , 2.34-2.69 (m, 4H, 2×CHC**H**$_2$), 2.02 (s, 6H, 2×CH_3), 1.71-1.62 (m, 6H, 2×CO_2CH_2C**H**$_3$), -0.26-0.3 (t, 6H, 2×$CHCH_2$C**H**$_3$).

MALDI-TOF-MS: M/z calcd.for $C_{56}H_{22}N_4O_4$ 854.5, obsd. 854.9.

Conclusions

An efficient synthesis of several organic molecular models of artificial photosynthetic reaction centers were realised and interesting and promising photophysical properties were observed. Both free base (H_2) phthalocyanine(Pc)-fullerene (C_{60}) and Zinc (Zn) Pc-C_{60} where the Pc and the C_{60} moeities are separated by a phenylethynyl linker was realised in high yields. While H_2Pc-C_{60} exhibited aggregation characteristics and was insoluble in most common organic solvents, ZnPc-C_{60} was soluble. While in non-polar solvents the fluorescence of the excited Pc chromophore is quenched mainly by singlet-singlet energy transfer to C_{60} in polar solvents both dyads exhibited a ultrafast electron transfer to the covalently-linked C_{60}. Transient absorption studies on ZnPc-C_{60} showed formation of a charge-separated (CS) with quantum yield of unit that had a lifetime of 94 ps. This is the longest life time reported for similir dyads with similar electron transfer driving force, it can be concluded that the unusually long-lived CS state achieved with the current dyad is as result of the phenylethynyl linker.

A novel non-aggregating silicon (Si)-Pc dyad where the Pc and the C_{60} are linked axially via the central Si was synthezied and lifetime of CS state of ~5 ns was observed. The lifetime for axially linked dyad's CS state is about 50 times that of the the peripherally linked dyads, an observation that can be used to infer that the lifetime of CS state is not only dependent on the type of linker separating the donor and the acceptor but also on the orientation, pheripheral or axial. Assymetrical diaxial substitution on the central Si in SiPc was achieved, and this presents a possibility of attaching different kind of ligands such as donor-acceptor, push-pull systems on the opposite plane of the SiPc chromophore through the central Si without the occurence of the

photoinactive aggregates in solution and this allow tuning of the optical and electrochemical properties of the phthalocyanine for efficient solar energy capture and other photochemical applications.

A carotenoid (Car) and a ferrocene (Fc) secondary electron donors were covalently attached to the SiPc-C_{60} through axial linkage to form Car-SiPc-C_{60} and Fc-SiPc-C_{60} triads respectively. A very fast charge separation and charge-recombination (CR) within Car-SiPc and Fc-SiPc dyads were observed. Lifetime of the CS states were 1.2 ps and 200 fs for Car-SiPc and Fc-SiPc dyads respectively. The ultra fast charge separation observed is favored by enhanced couplng afforded by the short linkers and a large driving force in the Car-SiPc and Fc-SiPc dyads. The driving force ($-\Delta G_{CS}$) for the formation of the CS state for $Car^{\bullet+}$-$SiPc^{\bullet-}$ and $Fc^{\bullet+}$-$SiPc^{\bullet-}$ are 0.81 eV and 0.56 eV respectively. In the Car-SiPc-C_{60} triad, the transfer of electrons to the C_{60} to form Car-$SiPc^{\bullet+}$-$C_{60}^{\bullet-}$ is a minor pathway for quenching of the SiPc fluorescence. This is because the slower electron transfer from SiPc to C_{60} gets outcompeted by the very fast electron transfer from the ground state carotenoid to the hole in the HOMO of the excited SiPc. Molecular orbital calculations has showed that the highest occupied molecular orbital (HOMO) of the C_{60} moeity is below those of both car and SiPc, and transfer of electrons from SiPc to C_{60} has been observed to occur after singlet-singlet energy transfer from excited state SiPc to the C_{60} followed by a hole transfer from the HOMO of the C_{60} to the energetically higher HOMO of SiPc. Currently, exclusive excitation of C_{60} chromophore so as to realise step wise hole transfer to the Car moeity to afford a long-lived $Car^{\bullet+}$-SiPc-$C_{60}^{\bullet-}$ is under investigation. Alternative approach that may favor formation of $Car^{\bullet+}$-SiPc-$C_{60}^{\bullet-}$ as the final state includes: Use of shorter

carotenoid to lower the HOMO of the Car moeity, so as to make it a poor donor to the excited state Pc, decoupling of the Car and SiPc dyad will also slower the rate of electron transfer between the Car to the SiPc, while introducing a shorter linker between the SiPc and the C_{60} will make the intramolecular electron transfer from the SiPc to the C_{60} faster hence enabling this step to be kinetically competitive to afford a charge-shift to the Car moeity. The above modifications between the respective dyads can also be applied to Fc-SiPc-C_{60} to give a long-lived $Fc^{\bullet+}$-SiPc-$C_{60}^{\bullet+}$ CS that will enable harnessing of the stored energy in the CS state.

An efficient route to meso-β doubly connected porphyrin dimer was developed. A near quantitative yield with minimal purification was obtained. Use of cheap Cu^{2+} oxidants and chloride free solvent ensured absence of β- chlorinated porphyrin impurities as was reported with use of tris(4-bromophenyl)aminium hexachloroantimonate (BAHA), 2,3-dichloro-5,6-dicyano-1,4-benzoquinone (DDQ) and trifluoromethanesulfonate. Unlike the lack of regioselectivity reported with use of copper (II) perchlorate and tetrafluoroborate salts in acetonitrile, use of Cu^{2+} salt as the oxidant in nitromethane afforded *meso*-β doubly-connected fused porphyrin dimer exclusively. Stirring the copper (II) porphyrin dimer in H_2SO_4/TFA mixture easily converted it into free base porphyrin dimer in 20 mins with a high yield of 85 %. The optical and the electrochemical properties of the porphyrin dimer can be tuned by inserting different metals or combinations of metals into the macrocycles. The interesting photophysical properties and the low band gap of the porphyrin dimer find applications not only in solar energy conversion but in other fields of technology and medicine.

An efficient and expedient route to bacteriopurpurin, a red-absorbing dye was developed. Due to the presence of stereocenters and two annelated cyclopentyl rings, synthesis of bacteriopurpurin has been reported to be a synthetically challenging task. Starting with a quantitative nicklyation of porphyrin **32** by nickel (II) acetylacetone hydrate, one-step 10,20-diformylation of porphyrin **33** was achieved by using a freshly prepared Vilsmaer reagent as opposed to the commercially available one which only yields monoformyl product. Use of (Carboethoxymethylene)triphenyl phosphorane, Wittig reagent, to synthesize *meso*-diacrylate product and stereoselective cyclization to afford bacteriopurpurin **31** occurred in a single step without the need for additional reagents. Overall the seven steps from porphyrin to bacteriopurpurin reported in literature were reduced to four and still with a higher yield of the final product.

The bacteriopurpurin obtained was observed to have interesting electrochemical and optical properties, reduction potential (-0.85 V vs SCE) and λ_{max}: 845 nm. These properties makes it an ideal candidate for use as a dye to sensitize TiO_2 which can be coupled to the H^+ reduction side of the water splitting catalytic center to produce H_2, a clean source of energy.

General Experimental Methods

Materials: Unless noted all reagents and solvents were obtained from commercials sources which are referenced where applicable. Toluene, dichloromethane and hexanes were distilled prior to use. Silica gel chromatorgraphy was carried out using 230-400 silica gel (Silicyale, Siliflas F60).

General analytical methods

Stead-state spectroscopy

UV-Visible-NIR spectroscopy was performed using a Shimadzu UV-3101PC UV-Visible spectrophotometer or Shimadzu UV-2550 UV-Visible spectrophotometer. Excitation was provided by a 75 W xenon-arc lamp and single grating monochromator. Fluorescence was detected at 90˚ to the excitation beam via a single grating monochromator and an R928 photomultiplier tube having S-20 spectral response and operating in the single photon counting mode.

Time-resolved fluorescence

Fluorescence decay measurements were performed on optically dilute (ca. 1×10^{-5} M) samples by the time-correlated single-photon-counting method. Two different systems were employed. Excitation source for the first system was a mode-locked Ti:Sapphire laser (Spectra Physics, Millennia-pumped Tsunami) with a 130-fs pulse duration operating at 80 MHz. The laser output was sent through a frequency doubler and pulse selector (Spectra Physics Model 3980) to obtain 370-450 nm pulses at 4 MHz. Fluorescence emissions was detected at the magic angle using a double grating monochromator (Jobin Yvon Gemini-180) and a microchannel plate photomultiplier tube (Hamamatsu R3809U-50). The instrument response function was 35-55 ps. The spectrometer was controlled by software based on the LabView programming language and data acquisition was done using a single photon counting card (Becker-Hickl, SPC-830).

Excitation source for the second system was a fiber supercontinuum laser based on a passive modelocked fiber laser and a high-nonlinearity photonic crystal fiber supercontinuum

generator (Fianium SC450). The laser provides 6-ps pulses at a repetition rate variable between 0.1 – 40 MHz. The laser output was sent through an Acousto-Optical Tunable Filer (Fianium AOTF) to obtain excitation pulses at desired wavelength. Fluorescence emission was detected at the magic angle using a double grating monochromator (Jobin Yvon Gemini-180) and a microchannel plate photomultiplier tube (Hamamatsu R3809U-50). The instrument response function was 35-55 ps. The spectrometer was controlled by software based on the LabView programming language and data acquisition was done using a single photon counting card (Becker-Hickl, SPC-830).

Transient absorption

The femtosecond transient absorption apparatus consisted of a kilohertz pulsed laser source and a pump-probe optical setup. Laser pulses of 100 fs at 800 nm were generated from an amplified, mode-locked Titanium Sapphire kilohertz laser system (Millennia/Tsunami/Spitfire, Spectra Physics). Part of the laser pulse energy was sent through an optical delay line and focused on to a 3 mm sapphire plate to generate a white light continuum for the probe beam. The remainder of the pulse energy was used to pump an optical parametric amplifier (Spectra Physics) to generate excitation pulses, which were selected using a mechanical chopper. The white light generated was then compressed by prism pairs (CVI) before passing through the sample. The polarization of pump beam was set to the magic angle (54.7°) relative to the probe beam and its intensity adjusted using a continuously variable neutral density filter. The white light probe is dispersed by a spectrograph (300 line grating) onto a charge-coupled device (CCD)

camera (DU420, Andor Tech.). The final spectral resolution was about 2.3 nm for over a nearly 300 nm spectral region. The instrument response function was ca. 150 fs.

The nanosecond-millisecond transient absorption measurements were made with excitation from an optical parametric oscillator driven by the third harmonic of a Nd:YAG laser (Ekspla NT342B). The pulse width was ~4-5 ns, and the repetition rate was 10 Hz. The detection portion of the spectrometer (Proteus) was manufactured by Ultrafast Systems. The instrument response function was ca. 4.8 ns.

Data analysis

Data analysis was carried out using locally written software (ASUFIT) developed under a MATLAB environment (Mathworks Inc.). Decay-associated spectra (DAS) were obtained by fitting the transient absorption or fluorescence change curves over a selected wavelength region simultaneously as described by Eq 1 (parallel kinetic model),

$$\Delta A(\lambda,t) = \sum_{i=1}^{n} A_i(\lambda)\exp(-t/\tau_i) \qquad (1)$$

where $\Delta A(\lambda,t)$ is the observed absorption (or fluorescence) change at a given wavelength at time delay t and n is the number of kinetic components used in the fitting. A plot of $A_i(\lambda)$ versus wavelength is called a decay-associated spectrum, and represents the amplitude spectrum of the i^{th} kinetic component, which has a lifetime of τ_i.

The global analysis procedures described here have been extensively reviewed in literature.[119] Random errors associated with the reported lifetimes obtained from fluorescence and transient absorption measurements were typically ≤ 5%.

Mass spectrometry was performed using the MALDI-TOF method using a Voyager DE STR from Applied Biosytems in reflector mode for all molecules. Commonly used matrices were terthiophene, dithranol and trans-2-[3-(4-tert-butylphenyl)-2-methyl-2-propenylidene]-malononitrile.

^{1}H NMR spectra for the molecules were obtained in deuterated solvents using a Varian 400 MHz instrument with tetramethysilane as internal reference. Proton assigments were by the use of COSY and NOESY experiments.

Electrochemical measurements were performed using a CH instruments 650C or 760D electrochemical workstation using a standard 3-electrode cell setup. Counter and reference electrodes were platinum gauze and pseudo Ag/AgCl. Working glassy electrodes and electrolytes were specific for each experiment. Potentials were referenced to SCE using the ferrocene/ferrocenium redox couple as an internal standard, with values depending on the solvent.[120]

References

1. UN DESA: United Nations Department of Economic and Social Affairs. *https://www.un.org/en/development/desa/index.html* (accessed 2/10/2014, 2014).

2. IEA - Publication:- Key World Energy Statistics 2013. *http://www.iea.org/publications/freepublications/publication/name,31287,en.html* (accessed 2/10/2014, 2014).

3. Hoffert, M. I.; Caldeira, K.; Jain, A. K.; Haites, E. F.; Harvey, L. D. D.; Potter, S. D.; Schlesinger, M. E.; Schneider, S. H.; Watts, R. G.; Wigley, T. M. L.; Wuebbles, D. J. Energy implications of future stabilization of atmospheric CO2 content. *Nature* **1998**, *395*, 881-884.

4. Emissions Scenarios. *http://www.ipcc.ch/ipccreports/sres/emission/index.php?idp=116#531* (accessed 2/10/2014, 2014).

5. Lewis, N. S.; Nocera, D. G. Powering the planet: Chemical challenges in solar energy utilization. *Proceedings of the National Academy of Sciences* **2006**, *103*, 15729-15735.

6. Barber, J.; Tran, P. D. From natural to artificial photosynthesis. *Journal of the Royal Society, Interface / the Royal Society JID - 101217269* **0705**.

7. Wigley, T. M. L.; Richels, R.; Edmonds, J. A. Economic and environmental choices in the stabilization of atmospheric CO2 concentrations. *Nature* **1996**, *379*, 240-243.

8. Shaheen, S. E.; Ginley, D. S.; Jabbour, G. E. Organic-Based Photovoltaics: Toward Low-Cost Power Generation. *MRS Bull* **2005**, *30*, 10-19.

9. Hagberg, D. P.; Yum, J.; Lee, H.; De Angelis, F.; Marinado, T.; Karlsson, K. M.; Humphry-Baker, R.; Sun, L.; Hagfeldt, A.; Gratzel, M.; Nazeeruddin, M. K. Molecular Engineering of Organic Sensitizers for Dye-Sensitized Solar Cell Applications. *J. Am. Chem. Soc.* **2008**, *130*, 6259-6266.

10. Swanson, R. M. A vision for crystalline silicon photovoltaics. *Prog Photovoltaics Res Appl* **2006**, *14*, 443-453.

11. Artificial photosynthesis. http://en.wikipedia.org/wiki/Photosynthesis. Accessed on 10/2/2014

12. Barber, J.; Andersson, B. Revealing the blueprint of photosynthesis. *Nature* **1994**, *370*, 31-34.

13. Gust, D.; Moore, T. A.; Moore, A. L. Realizing artificial photosynthesis. *Faraday Discuss.* **2012**, *155*, 9-26.

14. Kodis, G.; Liddell, P. A.; Moore, A. L.; Moore, T. A.; Gust, D. Synthesis and photochemistry of a carotene-porphyrin-fullerene model photosynthetic reaction center. *Journal of Physical Organic Chemistry* **2004**, *17*, 724-734.

15. Gust, D.; Moore, T. A.; Moore, A. L. Solar Fuels via Artificial Photosynthesis. *Acc. Chem. Res.* **2009**, *42*, 1890-1898.

16. Liddell, P. A.; Kuciauskas, D.; Sumida, J. P.; Nash, B.; Nguyen, D.; Moore, A. L.; Moore, T. A.; Gust, D. Photoinduced Charge Separation and Charge Recombination to a Triplet State in a Carotene-Porphyrin-Fullerene Triad. *J. Am. Chem. Soc.* **1997**, *119*, 1400-1405.

17. Lombardi, J. L.; Chuchawin, C. Fabrics Comprising a Photocatalyst to Produce Singlet Oxygen from Ambient Oxygen. **2012**.

18. Bertini, I. *Biological inorganic chemistry: structure and reactivity;* University Science Books: Sausalito, Calif., 2007; , pp 739.

19. Martinez-Diaz, M. V.; de la Torre, G.; Torres, T. Lighting porphyrins and phthalocyanines for molecular photovoltaics. *Chem. Commun. (Camb)* **2010**, *46*, 7090-7108.

20. Photosynthesis. *http://bioenergy.asu.edu/photosyn/education/photointro.html* (accessed 2/13/2014, 2014).

21. Gust, D.; Moore, T. A.; Moore, A. L.; Krasnovsky, A. A.; Liddell, P. A.; Nicodem, D.; DeGraziano, J. M.; Kerrigan, P.; Makings, L. R.; Pessiki, P. J. Mimicking the photosynthetic triplet energy-transfer relay. *J. Am. Chem. Soc.* **1993**, *115*, 5684-5691.

22. Moore, T.; Moore, A.; Gust, D. In *Novel and Biomimetic Functions of Carotenoids in Artificial Photosynthesis;* Frank, H., Young, A., Britton, G. and Cogdell, R., Eds.; Springer Netherlands: 1999; Vol. 8, pp 327-339.

23. Centi, G.; Perathoner, S. CO2-based energy vectors for the storage of solar energy. *Greenhouse Gases: Science and Technology* **2011**, *1*, 21-35.

24. Centi, G.; Perathoner, S. Towards Solar Fuels from Water and CO2. *ChemSusChem* **2010**, *3*, 195-208.

25. Bensaid, S.; Centi, G.; Garrone, E.; Perathoner, S.; Saracco, G. Towards Artificial Leaves for Solar Hydrogen and Fuels from Carbon Dioxide. *ChemSusChem* **2012**, *5*, 500-521.

26. Centi, G. In Carbon□Neutral Fuels and Energy Carriers; 2011; pp 291-323.

27. El-Khouly, M.; Ito, O.; Smith, P. M.; DΓÇÖSouza, F. Intermolecular and supramolecular photoinduced electron transfer processes of fullereneΓÇôporphyrin/phthalocyanine systems. *Journal of Photochemistry and Photobiology C: Photochemistry Reviews* **2004**, *5*, 79-104.

28. Barigelletti, F.; Flamigni, L. Photoactive molecular wires based on metal complexes. *Chem. Soc. Rev.* **2000**, *29*, 1-12.

29. Scholes, G. D. LONG-RANGE RESONANCE ENERGY TRANSFER IN MOLECULAR SYSTEMS. *Annu. Rev. Phys. Chem.* **2003**, *54*, 57-87.

30. Ceroni, P.; Balzani, V. In *Photoinduced Energy and Electron Transfer Processes;* Ceroni, P., Ed.; Springer Netherlands: 2012; Vol. 78, pp 21-38.

31. Förster, T. Zwischenmolekulare Energiewanderung und Fluoreszenz. *Annalen der Physik* **1948**, *437*, 55-75.

32. Pullerits, T.; Sundstrom, V. Photosynthetic Light-Harvesting Pigment-Protein Complexes: Toward Understanding How and Why. *Acc. Chem. Res.* **1996**, *29*, 381-389.

33. Dexter, D. L. A Theory of Sensitized Luminescence in Solids. *J. Chem. Phys.* **1953**, *21*, 836-850.

34. Scandola, F.; Balzani, V. Energy-transfer processes of excited states of coordination compounds. *J. Chem. Educ.* **1983**, *60*, 814.

35. Marcus, R. A. On the Theory of Oxidation-Reduction Reactions Involving Electron Transfer. I. *J. Chem. Phys.* **1956**, *24*, 966-978.

36. Hush, N. S. Adiabatic Rate Processes at Electrodes. I. Energy-Charge Relationships. *J. Chem. Phys.* **1958**, *28*, 962-963-972.

37. Levich, V. G.; Dogonadze, R. R. **Adiabatic theory of electron-processes in solution**. *Collect.Czech.Chem.Commun.* **1961**, *26*, 193-214.

38. Jortner, J. Temperature dependent activation energy for electron transfer between biological molecules. *J. Chem. Phys.* **62**, *12*, 4860-4867.

39. Closs, G. L.; Miller, J. R. Intramolecular Long-Distance Electron Transfer in Organic Molecules. *Science* **1988**, *240*, 440-447.

40. **Electron Transfer in Proteins**. *http://www.ictinike.org/cnk/thesis/ch1/chapter-1.html* (accessed 2/17, 2014).

41. Balzani, V.; Venturi, M.; Credi, A. ***Molecular Devices and Machines: Concepts and Perspectives for the Nanoworld;*** Wiley-VCH: Weinheim, 2008; , pp 588.

42. Guldi, D. M.; Prato, M. Excited-State Properties of C60 Fullerene Derivatives. *Acc. Chem. Res.* **2000**, *33*, 695-703.

43. Iwaki, M.; Kumazaki, S.; Yoshihara, K.; Erabi, T.; Itoh, S. ΔG^0 Dependence of the Electron Transfer Rate in the Photosynthetic Reaction Center of Plant Photosystem I:ΓÇë Natural Optimization of Reaction between Chlorophyll *a* (A_0) and Quinone. *J. Phys. Chem.* **1996**, *100*, 10802-10809.

44. Gust, D.; Moore, T. A.; Moore, A. L. Mimicking Photosynthetic Solar Energy Transduction. *Acc. Chem. Res.* **2001**, *34*, 40-48.

45. Kroto, H. W.; Heath, J. R.; O'Brien, S. C.; Curl, R. F.; Smalley, R. E. C_{60}: Buckminsterfullerene. *Nature* **1985**, *318*, 162-163.

46. Guldi, D. M.; Martin, N. *Fullerenes: from synthesis to optoelectronic properties;* Developments in fullerene science; Kluwer Academic Publishers: Boston, 2002; Vol. 4, pp 440.

47. Echegoyen, L.; Diederich, F.; Echegoyen, L. E. In *Electrochemistry of Fullerenes;* Ruoff, R. S., Ed.; Fullerenes: Chemistry, Physics, and Technology; John Wiley & Sons, Inc.: New York, 2000; pp 1-51.

48. Imahori, H.; Sakata, Y. Fullerenes as Novel Acceptors in Photosynthetic Electron Transfer. *European Journal of Organic Chemistry* **1999**, *1999*, 2445-2457.

49. Gust, D.; Moore, T. A.; Moore, A. L. Mimicking Photosynthetic Solar Energy Transduction. *Acc. Chem. Res.* **2001**, *34*, 40-48.

50. Imahori, H.; Sakata, Y. Donor-Linked Fullerenes: Photoinduced electron transfer and its potential application. *Adv Mater* **1997**, *9*, 537-546.

51. Lever, A. B. P. The phthalocyanines. *Advances in inorganic and Radiochemistry* **1965**, *27*, 27-114.
52. Prahl, S. Phthalocyanine. *http://omlc.ogi.edu/spectra/PhotochemCAD/html/074.html* (accessed 3/30, 2014).

53. McKeown, N. B. *Phthalocyanine materials :synthesis, structure, and function;* Chemistry of solid state materials; Cambridge University Press: Cambridge, U.K.; New York, 1998; Vol. 6, pp 193.

54. Gouterman, M. In *Optical spectra and electronic structure of porphyrins and related macrocyles;* Dolphin, D., Ed.; The Porphyrins; Academic Press: New York, 1977; Vol. 3, pp 1-157.

55. Stillman, M. J.; Nyokong, T. In *Absorption and magnetic circular dichroism spectral properties of phthalocyanines. Part 1. Complexes of the Pc2- dianion;* Leznoff, C. C., Lever, A. B. P., Eds.; Phthalocyanines: Properties and Applications; VCH: New York, 1989; Vol. 1, pp 133-257.

56. Cook, M. J.; Dunn, A. J.; Howe, S. D.; Thomson, A. J.; Harrison, K. J. Octa-alkoxy phthalocyanine and naphthalocyanine derivatives: dyes with Q-band absorption in the far red or near infrared. *J. Chem. Soc. , Perkin Trans. 1* **1988**, 2453-2458.

57. Kobayashi, N.; Nakajima, S.; Osa, T. Spectroscopic comparison of tetra-tert-butylated tetraazaporphyrin, phthalocyanine, naphthalocyanine and anthracocyanine cobalt complexes. *Inorg. Chim. Acta* **1993**, *210*, 131-133.

58. Taylor, R.; Walton, D. R. M. The chemistry of fullerenes. *Nature* **1993**, *363*, 685-693.

59. Tkachenko, N. V.; Efimov, A.; Lemmetyinen, H. Covalent phthalocyanine-fullerene dyads: synthesis, electron transfer in solutions and molecular films. *J. Porphyrins Phthalocyanines* **2011**, *15*, 780-790.

60. Isosomppi, M.; Tkachenko, N. V.; Efimov, A.; Vahasalo, H.; Jukola, J.; Vainiotalo, P.; Lemmetyinen, H. Photoinduced electron transfer of double-bridged phthalocyanine–fullerene dyads. *Chemical Physics Letters* **2006**, *430*, 36-40.

61. Quintiliani, M.; Kahnt, A.; Wölfle, T.; Hieringer, W.; Vázquez, P.; Görling, A.; Guldi, D.; Torres, T. Synthesis and Photoinduced Electron-Transfer Properties of Phthalocyanine-[60]Fullerene Conjugates. *Chemistry: A European Journal* **2008**, *14*, 3765-3775.

62. Lemmetyinen, H.; Kumpulainen, T.; Niemi, M.; Efimov, A.; Ranta, J.; Stranius, K.; Tkachenko, N. V. Independence and inverted dependence on temperature of rates of photoinduced electron transfer in double-linked phthalocyanine-fullerene dyads. *Photochem. Photobiol. Sci.* **2010**, *9*, 949-959.
63. Fukuda, T.; Hashimoto, N.; Araki, Y.; El-Khouly, M.; Ito, O.; Kobayashi, N. Phthalocyanine-C_{60} Fused Conjugates Exhibiting Molecular Orbital Interactions Depending on the Solvent Polarity. *Chemistry: An Asian Journal* **2009**, *4*, 1678-1686.

64. Quintiliani, M.; Kahnt, A.; Wölfle, T.; Hieringer, W.; Vázquez, P.; Görling, A.; Guldi, D.; Torres, T. Synthesis and Photoinduced Electron-Transfer Properties of Phthalocyanine?[60]Fullerene Conjugates. *Chemistry ? A European Journal* **2008**, *14*, 3765-3775.

65. Ince, M.; Martinez-Diaz, M.; Barbera, J.; Torres, T. Liquid crystalline phthalocyanine-fullerene dyads. *J. Mater. Chem.* **2011**, *21*, 1531-1536.

66. Bahr, J. L.; Kuciauskas, D.; Liddell, P. A.; Moore, A. L.; Moore, T. A.; Gust, D. Driving Force and Electronic Coupling Effects on Photoinduced Electron Transfer in a Fullerene-based Molecular Triad. *Photochem. Photobiol.* **2000**, *72*, 598-611.

67. Gust, D.; Moore, T. A.; Moore, A. L.; Kang, H. K.; DeGraziano, J. M.; Liddell, P. A.; Seely, G. R. Effect of coordinated ligands on interporphyrin photoinduced-electron-transfer rates. *J. Phys. Chem.* **1993**, *97*, 13637-13642.

68. Guldi, D. M.; Zilbermann, I.; Gouloumis, A.; Vazquez, P.; Torres, T. Metallophthalocyanines: Versatile Electron-Donating Building Blocks for Fullerene Dyads. *J Phys Chem B* **2004**, *108*, 18485-18494.

69. Quintiliani, M.; Kahnt, A.; Wölfle, T.; Hieringer, W.; Vázquez, P.; Görling, A.; Guldi, D.; Torres, T. Synthesis and Photoinduced Electron-Transfer Properties of Phthalocyanine-[60]Fullerene Conjugates. *Chemistry: A European Journal* **2008**, *14*, 3765-3775.

70. Martin-Gomis, L.; Ohkubo, K.; Fernandez-Lazaro, F.; Fukuzumi, S.; Sastre-Santos, A. Adiabatic Photoinduced Electron Transfer and Back Electron Transfer in a Series of Axially Substituted Silicon Phthalocyanine Triads. *J. Phys. Chem. C* **2008**, *112*, 17694-17701.

71. Cheng, G.; Peng, X.; Hao, G.; Kennedy, V. O.; Ivanov, I. N.; Knappenberger, K.; Hill, T. J.; Rodgers, M. A. J.; Kenney, M. E. Synthesis, Photochemistry, and Electrochemistry of a Series of Phthalocyanines with Graded Steric Hindrance *J Phys Chem A* **2003**, *107*, 3503-3514.

72. Kim, K. N.; Choi, C. S.; Kay, K. A novel phthalocyanine with two axial fullerene substituents. *Tetrahedron Lett.* **2005**, *46*, 6791-6795.

73. Martin-Gomis, L.; Ohkubo, K.; Fernandez-Lazaro, F.; Fukuzumi, S.; Sastre-Santos, A. Synthesis and photophysical studies of a new nonaggregated C60-silicon phthalocyanine-C60 triad. *Org. Lett.* **2007**, *9*, 3441-3444.

74. Martin-Gomis, L.; Ohkubo, K.; Fernandez-Lazaro, F.; Fukuzumi, S.; Sastre-Santos, A. Adiabatic Photoinduced Electron Transfer and Back Electron Transfer in a Series of Axially Substituted Silicon Phthalocyanine Triads. *J. Phys. Chem. C* **2008**, *112*, 17694-17701.

75. El-Khouly, M.; Kim, J.; Kay, K.; Choi, C.; Ito, O.; Fukuzumi, S. Synthesis and Photoinduced Intramolecular Processes of Light-Harvesting Silicon Phthalocyanine-Naphthalenediimide-Fullerene Connected Systems. *Chemistry: A European Journal* **2009**, *15*, 5301-5310.

76. Moore, T. A.; Gust, D.; Mathis, P.; Mialocq, J.; Chachaty, C.; Bensasson, R. V.; Land, E. J.; Doizi, D.; Liddell, P. A.; Lehman, W. R.; Nemeth, G. A.; Moore, A. L. Photodriven charge separation in a carotenoporphyrin-quinone triad. *Nature* **1984**, *307*, 630-632.

77. Ritz, T.; Damjanoviç, A.; Schulten, K.; Zhang, J.; Koyama, Y. Efficient light harvesting through carotenoids. *Photosynthesis Res.* **2000**, *66*, 125-144.

78. Wasielewski, M. R.; Liddell, P. A.; Barrett, D.; Moore, T. A.; Gust, D. Ultrafast carotenoid to pheophorbide energy transfer in a biomimetic model for antenna function in photosynthesis. *Nature* **1986**, *322*, 570-572.

79. DeRosa, M. C.; Crutchley, R. J. Photosensitized singlet oxygen and its applications. *Coord. Chem. Rev.* **2002**, *233–234*, 351-371.

80. Cardona, T.; Sedoud, A.; Cox, N.; Rutherford, A. W. Charge separation in Photosystem II: A comparative and evolutionary overview. *Biochimica et Biophysica Acta (BBA) - Bioenergetics* **2012**, *1817*, 26-43.

81. Polivka, T.; Frank, H. A. Molecular Factors Controlling Photosynthetic Light Harvesting by Carotenoids. *Acc. Chem. Res.* **2010**, *43*, 1125-1134.

82. Tracewell, C. A.; Vrettos, J. S.; Bautista, J. A.; Frank, H. A.; Brudvig, G. W. Carotenoid Photooxidation in Photosystem II. *Arch. Biochem. Biophys.* **2001**, *385*, 61-69.

83. Bergkamp, J. J.; Sherman, B. D.; Mariño-Ochoa, E.; Palacios, R. E.; Cosa, G.; Moore, T. A.; Gust, D.; Moore, A. L. Synthesis and characterization of silicon phthalocyanines bearing

axial phenoxyl groups for attachment to semiconducting metal oxides. *J. Porphyrins Phthalocyanines* **2011**, *15*, 943-950.

84. Gust, D.; Moore, T. A.; Moore, A. L.; Liddell, P. A. In *[10] Synthesis of carotenoporphyrin models for photosynthetic energy and electron transfer;* Methods in Enzymology; Academic Press: Vol. Volume 213, pp 87-100.

85. Kodis, G.; Herrero, C.; Palacios, R.; Marino-Ochoa, E.; Gould, S.; de, l. G.; van Grondelle, R.; Gust, D.; Moore, T. A.; Moore, A. L.; Kennis, J. T. M. Light Harvesting and Photoprotective Functions of Carotenoids in Compact Artificial Photosynthetic Antenna Designs. *J Phys Chem B* **2004**, *108*, 414-425.

86. Kuciauskas, D.; Liddell, P. A.; Lin, S.; Stone, S. G.; Moore, A. L.; Moore, T. A.; Gust, D. Photoinduced Electron Transfer in Carotenoporphyrin-Fullerene Triads: Temperature and Solvent Effects. *J Phys Chem B* **2000**, *104*, 4307-4321.

87. Closs, G. L.; Miller, J. R. Intramolecular Long-Distance Electron Transfer in Organic Molecules. *Science* **1988**, *240*, 440-447.

88. El-Khouly, M.; Kang, E.; Kay, K.; Choi, C.; Aaraki, Y.; Ito, O. Silicon-Phthalocyanine-Cored Fullerene Dendrimers: Synthesis and Prolonged Charge-Separated States with Dendrimer Generations. *Chem. Eur. J.* **2007**, *13*, 2854-2863.

89. Silver, J.; Sosa-Sanchez, J.; Frampton, C. S. Structure, Electrochemistry, and Properties of Bis(ferrocenecarboxylato)(phthalocyaninato)silicon(IV) and Its Implications for (Si(Pc)O)n Polymer Chemistry. *Inorg. Chem.* **1998**, *37*, 411-417.

90. Imahori, H.; Tamaki, K.; Guldi, D. M.; Luo, C.; Fujitsuka, M.; Ito, O.; Sakata, Y.; Fukuzumi, S. Modulating Charge Separation and Charge Recombination Dynamics in Porphyrin-Fullerene Linked Dyads and Triads: Marcus-Normal versus Inverted Region. *J. Am. Chem. Soc.* **2001**, *123*, 2607-2617.

91. Imahori, H.; Guldi, D. M.; Tamaki, K.; Yoshida, Y.; Luo, C.; Sakata, Y.; Fukuzumi, S. Charge Separation in a Novel Artificial Photosynthetic Reaction Center Lives 380 ms. *J. Am. Chem. Soc.* **2001**, *123*, 6617-6628.

92. Mariño-Ochoa, E.; Palacios, R.; Kodis, G.; Macpherson, A. N.; Gillbro, T.; Gust, D.; Moore, T. A.; Moore, A. L. High-efficiency Energy Transfer from Carotenoids to a Phthalocyanine in an Artificial Photosynthetic Antenna. *Photochem. Photobiol.* **2002**, *76*, 116-121.

93. Imahori, H.; Yamada, H.; Nishimura, Y.; Yamazaki, I.; Sakata, Y. Vectorial Multistep Electron Transfer at the Gold Electrodes Modified with Self-Assembled Monolayers of Ferrocene-Porphyrin-Fullerene Triads. *J Phys Chem B* **2000**, *104*, 2099-2108.

94. Imahori, H.; Tamaki, K.; Yamada, H.; Yamada, K.; Sakata, Y.; Nishimura, Y.; Yamazaki, I.; Fujitsuka, M.; Ito, O. Photosynthetic electron transfer using fullerenes as novel acceptors. *Carbon* **2000**, *38*, 1599-1605.

95. Curiel, D.; Ohkubo, K.; Reimers, J. R.; Fukuzumi, S.; Crossley, M. J. Photoinduced electron transfer in a small beta],small beta]prime or minute]-pyrrolic fused ferrocene-(zinc porphyrin)-fullerene. *Phys. Chem. Chem. Phys.* **2007**, *9*, 5260-5266.

96. Gouloumis, A.; Liu, S.; Sastre, Á; Vázquez, P.; Echegoyen, L.; Torres, T. Synthesis and Electrochemical Properties of Phthalocyanine-Fullerene Hybrids. *Chemistry : A European Journal* **2000**, *6*, 3600-3607.

97. Lewtak, J. P.; Gryko, D. T. Synthesis of small pi-extended porphyrins via intramolecular oxidative coupling. *Chem. Commun.* **2012**, *48*, 10069-10086.

98. Collins, H. A.; Khurana, M.; Moriyama, E. H.; Mariampillai, A.; Dahlstedt, E.; Balaz, M.; Kuimova, M. K.; Drobizhev, M.; YangVictor, X. D.; Phillips, D.; Rebane, A.; Wilson, B. C.; Anderson, H. L. Blood-vessel closure using photosensitizers engineered for two-photon excitation. *Nat Photon* **2008**, *2*, 420-424.

99. Tsuda, A.; Furuta, H.; Osuka, A. Syntheses, structural characterizations, and optical and electrochemical properties of directly fused diporphyrins. *J. Am. Chem. Soc.* **2001**, *123*, 10304-10321.

100. Brennan, B. J.; Arero, J.; Liddell, P. A.; Moore, T. A.; Moore, A. L.; Gust, D. Selective oxidative synthesis of meso-beta fused porphyrin dimers. *J. Porphyrins Phthalocyanines* **2013**, *17*, 247-251.

101. Osuka, A.; Shimidzu, H. meso, meso-Linked Porphyrin Arrays. *Angewandte Chemie International Edition in English* **1997**, *36*, 135-137.

102. Tsuda, A.; Osuka, A. Fully conjugated porphyrin tapes with electronic absorption bands that reach into infrared. *Science* **2001**, *293*, 79-82.

103. Brennan, B. J.; Kenney, M. J.; Liddell, P. A.; Cherry, B. R.; Li, J.; Moore, A. L.; Moore, T. A.; Gust, D. Oxidative coupling of porphyrins using copper(ii) salts. *Chem. Commun.* **2011**, *47*, 10034-10036.

104. Badoz-Lambling, J.; Bardin, J. C. Solvatation des ions par le nitromethane. *Electrochim. Acta* **1974**, *19*, 725-731.

105.The Decamethylferrocenium/Decamethylferrocene Redox Couple: A Superior Redox Standard to the Ferrocenium/Ferrocene Redox Couple for Studying Solvent Effects on the Thermodynamics of Electron Transfer. - *J. Phys. Chem. B*, - 6713.

106. Dolphin, D. *The Porphyrins;* Academic Press: New York, 1978; .

107.A Scalable Synthesis of Meso-Substituted Dipyrromethanes. - *Org. Process Res. Dev.*, - 799.

108. Takanami, T.; Wakita, A.; Sawaizumi, A.; Iso, K.; Onodera, H.; Suda, K. One-Pot Synthesis of meso-Formylporphyrins by SNAr Reaction of 5,15-Disubstituted Porphyrins with (2-Pyridyldimethylsilyl)methyllithium. *Org. Lett.* **2008**, *10*, 685-687.

109. Vinogradova, E. V.; Enakieva, Y. Y.; Gorbunova, Y. G.; Tsivadze, A. Y. Synthesis of meso-substituted porphyrins as precursors in creating highly ordered electroluminescent polymer materials. *Protection of Metals and Physical Chemistry of Surfaces* **2009**, *45*, 529-534.

110. Hayashi, S.; Tanaka, M.; Hayashi, H.; Eu, S.; Umeyama, T.; Matano, Y.; Araki, Y.; Imahori, H. Naphthyl-Fused Π-Elongated Porphyrins for Dye-Sensitized TiO_2 Cells. *J. Phys. Chem. C* **2008**, *112*, 15576-15585.

111. Campbell, W. M.; Jolley, K. W.; Wagner, P.; Wagner, K.; Walsh, P. J.; Gordon, K. C.; Schmidt-Mende, L.; Nazeeruddin, M. K.; Wang, Q.; Gr├ñtzel, M.; Officer, D. L. Highly Efficient Porphyrin Sensitizers for Dye-Sensitized Solar Cells. *J. Phys. Chem. C* **2007**, *111*, 11760-11762.

112. Mai, C.; Huang, W.; Lu, H.; Lee, C.; Chiu, C.; Liang, Y.; Diau, E. W.; Yeh, C. Synthesis and characterization of diporphyrin sensitizers for dye-sensitized solar cells. *Chem. Commun.* **2010**, *46*, 809-811.

113. Imahori, H.; Umeyama, T.; Ito, S. Large Π-Aromatic Molecules as Potential Sensitizers for Highly Efficient Dye-Sensitized Solar Cells. *Acc. Chem. Res.* **2009**, *42*, 1809-1818.

114. Youngblood, W. J.; Lee, S. A.; Kobayashi, Y.; Hernandez-Pagan, E.; Hoertz, P. G.; Moore, T. A.; Moore, A. L.; Gust, D.; Mallouk, T. E. Photoassisted Overall Water Splitting in a Visible Light-Absorbing Dye-Sensitized Photoelectrochemical Cell. *J. Am. Chem. Soc.* **2009**, *131*, 926-927.

115. Robinson, B. C. Bacteriopurpurins: Synthesis from meso-Diacrylate Substituted Porphyrins. *Tetrahedron* **2000**, *56*, 6005-6014.

116. Grigg, R.; Shelton, G.; Sweeney, A.; Johnson, A. W. N-methylation and electrophilic substitution reactions of octa-alkyl-porphins, octaethylchlorin, and metalloporphins. *J. Chem. Soc. , Perkin Trans. 1* **1972**, 1789-1799.

117. Morgan, A. R.; Tertel, N. C. Observations on the synthesis and spectroscopic characteristics of purpurins. *J. Org. Chem.* **1986**, *51*, 1347-1350.

118. Morgan, A. R.; Garbo, G. M.; Keck, R. W.; Selman, S. H.; Skalkos, D. Synthesis and in vivo photodynamic activity of some bacteriochlorin derivatives against bladder tumors in rodents. *J. Med. Chem.* **1991**, *34*, 2126-2133.

119. Van Stokkum, I. H. M.; Larsen, D. S.; van Grondelle, R. Global and target analysis of time-resolved spectra. *Biochimica et Biophysica Acta (BBA) - Bioenergetics* **2004**, *1657*, 82-104.

120. Noviandri, I.; Brown, K. N.; Fleming, D. S.; Gulyas, P. T.; Lay, P. A.; Masters, A. F.; Phillips, L. The Decamethylferrocenium/Decamethylferrocene Redox Couple:ΓÇë A Superior Redox Standard to the Ferrocenium/Ferrocene Redox Couple for Studying Solvent Effects on the Thermodynamics of Electron Transfer. *J Phys Chem B* **1999**, *103*, 6713-6722.